Higher order unfitted isoparametric space-time FEM on moving domains

Master's thesis

by:

Janosch Preuß

Supervisor:

Jun.-Prof. Dr. Christoph Lehrenfeld

Second Assessor:

Prof. Dr. Gert Lube

prepared at the

Institute for Numerical and Applied Mathematics

University of Göttingen

Version as of 28.02.2018 (including minor corrections)

Hiermit erkläre ich, dass ich die vorliegende Arbeit selbstständig verfasst und keine anderen als die angegebenen Quellen und Hilfsmittel verwendet habe.

Göttingen, den 31. Januar 2018

Acknowledgments

First of all, I would like to express my gratitude to my supervisor Jun.-Prof. Dr. Christoph Lehrenfeld for proposing such an exciting topic for my thesis and guiding my work throughout its preparation with great commitment. I feel grateful for having a supervisor who is willing to discuss open problems and provide insightful answers to my questions at nearly any time of the day. His enthusiasm and support have been immensely motivating throughout the last year.

I would also like to thank Prof. Dr. Gert Lube for kindling my interest in numerics of partial differential equations. My Bachelor's thesis, that I prepared under his supervision, introduced me to advanced finite element methods and paved the way for the thesis at hand. I also appreciate that he examines this thesis as a second assessor.

The numerical experiments in this thesis have been performed with the finite element software `Netgen/NGSolve` and its Add-On `ngsxfem` for unfitted discretizations. I would like to take the oppurtunity to thank all people who have contributed to developing this software. In particular, I would like to point out Fabian Heimann who is working on extensions of the numerical integration in `ngsxfem`. His work forms the backbone for the numerical realization of the method presented in this thesis.

At last, I would like to sincerely thank my family for their support and encouragement during my studies.

Contents

Chapter 1

Introduction

1.1 Motivation

Solving partial differential equations (PDE) on evolving geometries is a challenging and useful task. The geometry that has to be treated in applications is often quite complicated. This is for example the case in the simulation of two-phase flows. Here the interface that separates the two fluids may undergo large deformations. Even topology changes are possible when droplets emerge. The efficient and accurate simulation of such phenomena requires the development of novel numerical techniques.

The standard finite element method (FEM) employs a mesh that is fitted to the geometry. Keeping the mesh conforming to a moving and deforming geometry may require substantial efforts. Thus, it is interesting to consider unfitted finite element methods where the mesh is independent of the geometry on which the PDE has to be solved. Since remeshing procedures are avoided, this approach seems to be a promising basis for constructing efficient numerical techniques.

Using an unfitted method entails new challenges. Often one chooses to model the geometry by means of a level set function. This provides a highly accurate, yet implicit description of the domains on which the integrals arising in the variational formulation of the PDE have to be calculated. Since the mesh is not fitted to the geometry, an implementation of such methods thus requires to evaluate integrals on cut elements. The cut is described only implicitly as the zero set of the level set function. If linear finite elements are used, then it suffices to compute these integrals with second order accuracy in order to preserve the accuracy of the whole method. Since this task can be solved robustly by established methods, most research so far has concentrated on linear finite elements. However, the extension to higher order elements is not straightforward and requires new ideas.

In [Leh16] and [LR17], a new approach for high order unfitted finite element methods has been proposed and analyzed for stationary problems. It is based on a parametric mapping of the underlying mesh. On simplicial meshes, the image of a piecewise planar representation of the geometry under this mapping yields a high order accurate description of the geometry. The resulting isoparametric unfitted finite element method has been shown to allow for error bounds of optimal order.

In this thesis, we start to extend this approach to evolving geometries.

1.2 Outline of the thesis

As a model problem, we consider a convection diffusion equation on a moving domain. The first six chapters deal with the development of a higher order isoparametric FEM for this problem. The main part of the thesis consists of an a priori error analysis for the derived method (under the assumption of exact geometry handling) and numerical experiments. In the end, we also outline how the method can be applied to mass transport problems in two-phase flows and present results of numerical experiments.

The outline of the thesis is as follows:

- In chapter 2 a space-time discretization for the moving domain problem is derived. For the time stepping we use a discontinuous Galerkin method [Tho97] applied in an unfitted setting. Here, the space-time domain is partitioned into time slabs. We define a finite element space on these time slabs and derive a variational formulation which allows to solve the problem time slab per time slab.

  In this chapter it is assumed that all the arising integrals can be calculated exactly. A description how we achieve higher order geometrical accuracy in practice will be given in chapter 4.

- In chapter 3 an a priori error analysis for the method from chapter 2, which assumes exact geometry handling, is carried out. We combine stability, consistency and continuity to derive a Céa-like result. The formulation of the method involves a finite element space on the time slabs. For proving an a priori error estimate a suitable interpolation operator into these spaces is constructed. Making use of the interpolation results we arrive at an error estimate in a discrete norm which is anisotropic in the time step and the spatial mesh width.

- The previous two chapters assumed an exact handling of the geometry, which is unattainable in practice. Thus, chapter 4 deals with the extension of the isoparametric method from [LR17] to the instationary case. We derive a space-time version of the parametric mapping from [LR17]. Then it is shown how the finite element spaces and the variational formulation on the time slabs need to be adapted in order to benefit from the higher order accurate geometry description provided by the parametric mapping. This results in an isoparametric unfitted space-time discretization.

- Some aspects regarding the implementation of the method are discussed in chapter 5. One of them is how the integration on space-time domains that are implicitely described by a level set function is carried out. The higher order accurate, isoparametric method for stationary problems from [LR17] allows to reduce all the arising integrals to a reference configuration which is described by a piecewise linear approximation of the level set function. The situation for the extension to the space-time case is similar.

- In chapter 6 the method is tested for two different moving domains. The results of the numerical experiments are compared to the a priori error estimate derived in chapter 3. The observed rates are better than guaranteed by the derived error estimate.

- Chapter 7 illustrates how the method can be applied to mass transport problems in two-phase flows. The conditions at the fluid interface are imposed by means of the Nitsche technique (see [Nit71],[HH02] and [RN09]). We derive the method but do not provide an analysis.
- In chapter 8 numerical experiments for two-phase interface problems are presented. As test cases a moving plane and a moving circle are considered.
- We conclude in chapter 9 with a summary of the thesis. Open problems will be discussed and we propose directions for further research.

Chapter 2

Space-time discretization for a moving domain problem assuming exact geometry handling

This chapter starts by introducing the main model problem which is considered in this thesis. Then we derive a variational formulation for this problem. Time and space variables are treated similarly in this formulation. Moreover, our method is unfitted, i.e. the geometry does not fit to the mesh. We assume an exact handling of the geometry in this chapter. This includes that all the arising integrals can be calculated exactly. This assumption will be dropped in chapter 4, where it is described how we achieve higher order geometrical accuracy in practice. To this end, we use an isoparametric finite element method and an adapted variational formulation. These aspects will be introduced later in chapter 4.

2.1 Model problem

Let $\Omega(t) \subset \mathbb{R}^d$ for $d \in \{1, 2, 3\}$ be a time-dependent domain whose evolution is driven by a divergence-free convection field $\mathbf{w}$ (see Figure 2.1). This domain $\Omega(t)$ contains a quantity whose concentration is modelled by a scalar field $u(x, t)$. We assume that the concentration fulfills a convection-diffusion equation inside $\Omega(t)$. Moreover, we suppose that the quantity contained inside the time-dependent domain does not flow out over the boundary, $\nabla u \cdot \mathbf{n}_{\partial\Omega(t)} = 0$, where $\mathbf{n}_{\partial\Omega(t)}$ denotes the outer normal vector to $\Omega(t)$. Given the evolution of the domain $\Omega(t)$ and the initial concentration $u_0(x)$ at $t = 0$ the task is then to compute the concentration $u(x, t)$ for $t > 0$. So the problem is:

$$\begin{aligned} \partial_t u - \Delta u + \mathbf{w} \cdot \nabla u &= f && \text{in } \Omega(t), && t \in [0, T], \\ \nabla \cdot \mathbf{w} &= 0 && \text{in } \Omega(t), && t \in [0, T], \\ \nabla u \cdot \mathbf{n}_{\partial\Omega} &= 0 && \text{on } \partial\Omega(t), && t \in [0, T], \\ u(\cdot, t = 0) &= u_0 && \text{in } \Omega(t = 0). \end{aligned} \tag{2.1}$$

Remark 1. *In principle it is possible that the quantity contained inside $\Omega(t)$ exerts a pressure on $\partial\Omega(t)$. Furthermore, one could take the surface tension as a counteracting force into account. This is for example the case in an osmotic cell swelling problem, where the evolution of the cell is determined by these two forces. In this thesis we neglect*

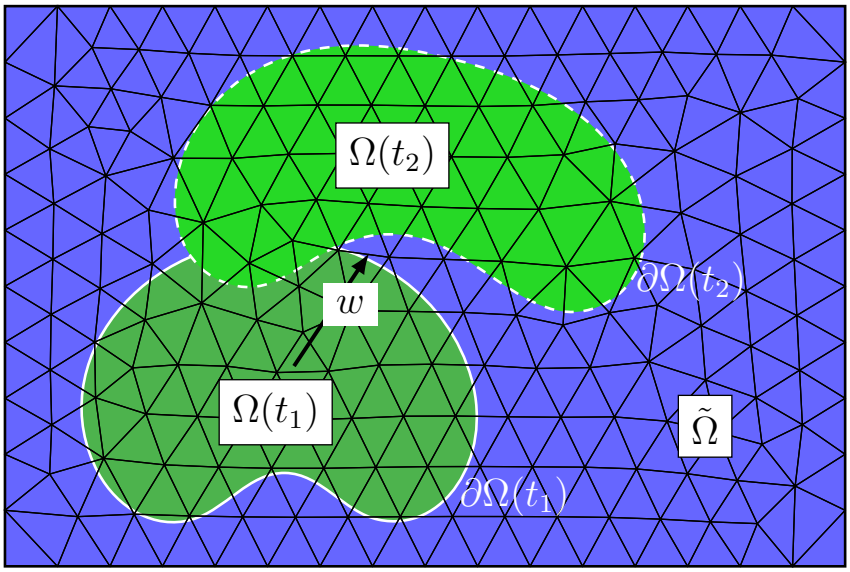

Figure 2.1: The domain moving from t_1 to t_2 with $t_2 > t_1$.

these complications and assume that the velocity of the boundary in normal direction $\mathcal{V}_n$ is solely determined by the given convection field, that is $\mathcal{V}_n = \mathbf{w} \cdot \mathbf{n}$.

2.2 Space-time discretization

The problem will be treated by an unfitted space-time DG method. In order to avoid $d+1$-dimensional complexity for the arising algebraic systems, the space-time domain will be divided into so called time slabs. To this end, let $0 < t_1 < \ldots < t_{N-1} < t_N$ be a partition of the time domain into time intervals $I_n = (t_{n-1}, t_n]$. For simplicity of presentation, the time intervals are of constant size $\Delta t = t_n - t_{n-1}$. We introduce the time slab $Q^n := \cup_{t \in I_n} \Omega(t) \times \{t\}$. The whole space-time domain is then given by the union over the time slabs $Q = \cup_{n=1}^N Q^n$. The spatial domain at a fixed time $\Omega(t_n)$ will sometimes be abbreviated by $\Omega^n = \Omega(t_n)$. Further, we define the space-time boundary $\Gamma_* := \cup_{t \in (0,T]} \partial\Omega(t) \times \{t\}$ and its restriction to the time slab $\Gamma_*^n := \cup_{t \in I_n} \partial\Omega(t) \times \{t\}$.

Next we will derive a variational formulation on the time slabs Q^n which allows to solve the problem time slab per time slab. This leads to the variational structure of a time-stepping scheme. This requires a finite element space W_n on the time slabs Q^n. To define this space some preparations are necessary.

Let $\tilde{\Omega}$ be a larger, time independent, polygonal background domain that contains $\Omega(t)$ for all times t. The time slabs Q^n are then contained in $\tilde{Q}^n = \tilde{\Omega} \times I_n$ and Q is a subset of $\tilde{Q} = \cup_{n=1}^N \tilde{Q}^n$. Let $\tilde{\mathcal{T}_h}^n$ be a shape-regular triangulation of the background domain $\tilde{\Omega}$. In this thesis we will only work with simplicial meshes. The index n indicates that the triangulation is in principle allowed to change between the time slabs. However, for ease of presentation, we restrict here to the case of a fixed triangulation $\tilde{\mathcal{T}_h}^n = \tilde{\mathcal{T}_h}$ on every time slab $n = 1, \ldots, N$. The extension to non-matching triangulations poses no major difficulties. The elements T of the spatial mesh and the time interval I_n form the space-time prisms $Q_T^n = T \times I_n$. Let $V_h^{k_s}$ be a standard finite element space of order k_s on the mesh $\tilde{\mathcal{T}_h}$, i.e.

$$V_h^{k_s} := \{v \in H^1(\tilde{\Omega}) \mid v_{|T} \in \mathcal{P}^{k_s}(T) \; \forall \, T \in \tilde{\mathcal{T}_h}\},$$

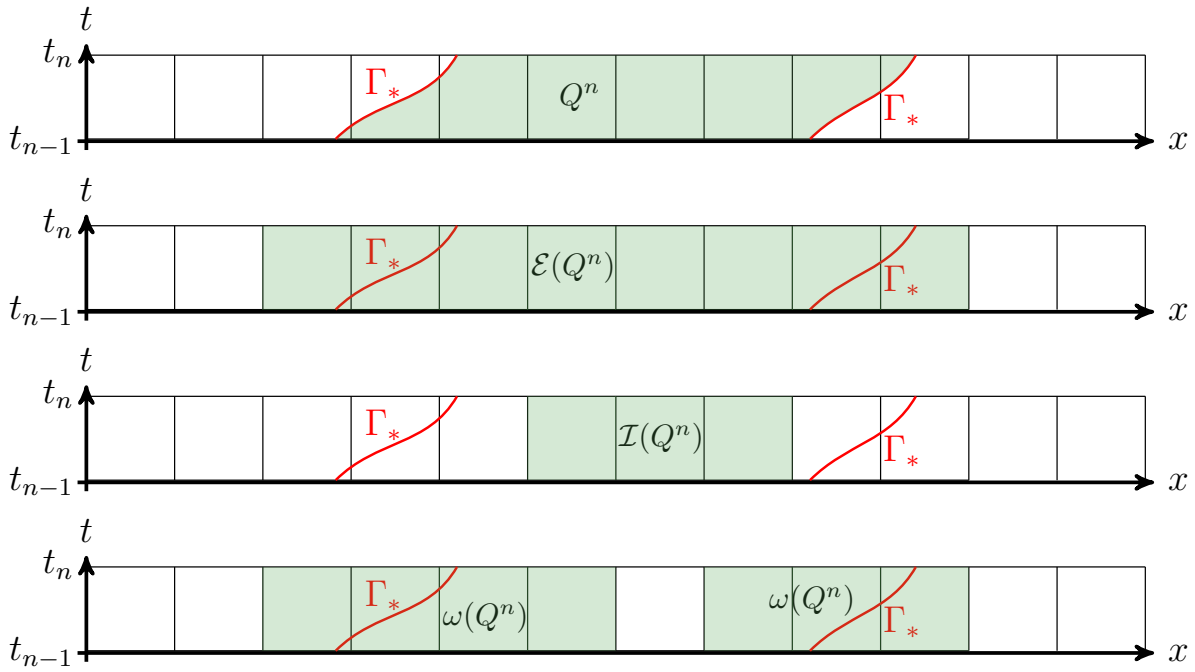

Figure 2.2: Sketch of different domains on the time slab: Here we denote by $\omega(Q^n)$ the space-time prisms that are involved in the stabilization term, i.e. $\omega(Q^n) = \cup_{F \in \mathcal{F}_R^{*,n}} \omega_F \times I_n$.

where $\mathcal{P}^{k_s}(T)$ denotes the space of polynomials up to degree k_s on the simplex T.

We define an extension operator $\mathcal{E}$ that extends the domain Q^n onto a domain with a tensor product structure within each time slab

$$\mathcal{E}(Q^n) \coloneqq \{x \in T \text{ for some } T \in \tilde{\mathcal{T}}_h \text{ with } Q_T^n \cap Q^n \neq \emptyset\}. \tag{2.2}$$

Let then $\mathcal{E}(Q) = \cup_{n=1}^N (\mathcal{E}(Q^n))$.

We further introduce an operator which restricts the domain Q^n onto a domain with a tensor product structure within each time slab

$$\mathcal{I}(Q^n) \coloneqq Q^n \setminus \mathcal{E}((\tilde{Q} \times I_n) \setminus Q^n).$$

Then we introduce purely spatial counterparts

$$\mathcal{I}(\Omega^n) \text{ such that } \mathcal{I}(\Omega^n) \times I_n = \mathcal{I}(Q^n),$$

$$\mathcal{E}(\Omega^n) \text{ such that } \mathcal{E}(\Omega^n) \times I_n = \mathcal{E}(Q^n).$$

Here $\mathcal{E}(\Omega^n)$ might extend into regions where elements are not touched by Ω^n at time t_n. The different domains on the time slab are sketched in Figure 2.2 for the spatially one-dimensional case. Figure 2.4 provides an illustration of $\mathcal{E}(\Omega^n)$ for two spatial dimensions.

Now we define the ansatz space $W_h = \{v : \mathcal{E}(Q) \to \mathbb{R} \mid v_{|\mathcal{E}(Q^n)} \in W_n\}$ with W_n defined as

$$W_n \coloneqq \{v : \mathcal{E}(Q^n) \to \mathbb{R} \mid v(x,t) = \sum_{m=0}^{k_t} t^m \phi_m,\ \phi_m \in V_h^{k_s}(\mathcal{E}(\Omega^n))\}. \tag{2.3}$$

Here $V_h^{k_s}(\mathcal{E}(\Omega^n))$ denotes the restriction of $V_h^{k_s}$ to the so called active mesh $\mathcal{E}(\Omega^n)$. Note that W_h contains functions that may be discontinuous between the time slabs.

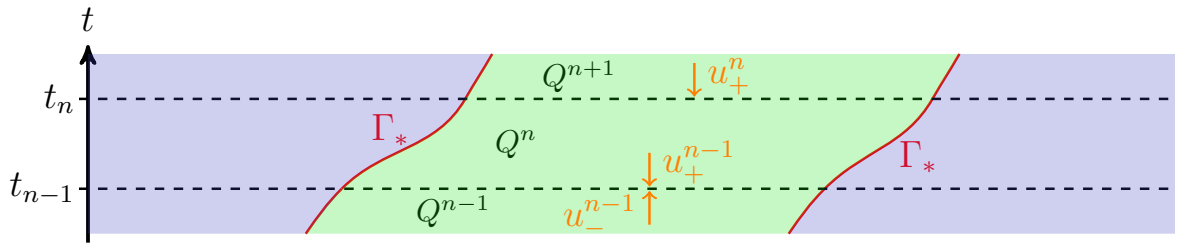

Figure 2.3: DG in time: The functions in W_h may be discontinuous between the time slabs. This means that the limit u_-^{n-1} coming from below might not agree with the limit u_+^{n-1} coming above on Ω^{n-1}.

To derive the variational formulation, we multiply the PDE with a function $v \in W_n$ and integrate over Q^n. Due to homogeneous Neumann boundary conditions an integration by parts of the diffusion term then leads to:

$$(\partial_t u + \mathbf{w} \cdot \nabla u, v)_{Q^n} + (\nabla u, \nabla v)_{Q^n} = (f, v)_{Q^n}.$$

This equation, posed for all $v \in W_n$, is not sufficient to specify the solution on the time slab since it does not involve an initial condition. There are different ways to include information from the previous time slab. One of them is to recognize that the time derivative acts as a convection term in the space-time domain Q^n. In this sense $\Omega^{n-1} \times \{t_{n-1}\}$ is the inflow boundary of Q^n where inflow information has to be provided. Here one adds upwind stabilization to impose weak continuity in time : $\left([\![u]\!]^{n-1}, v_+^{n-1}\right)_{\Omega^{n-1}}$. The terms $v_\pm^{n-1}$ are defined as the limits in time from above respectively below $v_\pm^{n-1} := \lim_{s\to 0} v(\cdot, t_{n-1} \pm s)$. An illustration is given in Figure 2.3. The bracket denotes the jump over the time boundary $[\![u]\!]^{n-1} := u_+^{n-1} - u_-^{n-1}$. The term u_-^{n-1} is known from the previous time slab and can be shifted to the right hand side. This leads to the variational formulation:

Find $u \in W_n$ such that

$$(\partial_t u + \mathbf{w} \cdot \nabla u, v)_{Q^n} + (\nabla u, \nabla v)_{Q^n} + \left(u_+^{n-1}, v_+^{n-1}\right)_{\Omega^{n-1}} = (f, v)_{Q^n} + \left(u_-^{n-1}, v_+^{n-1}\right)_{\Omega^{n-1}} \quad (2.4)$$

for all $v \in W_n$ holds.

The equation will be treated by an unfitted method. That is, the mesh is not fitted to $\partial\Omega(t)$. A major advantage of this approach is that one can work with a simple background mesh that does not need to be changed during the time evolution. In particular, possibly expensive remeshing procedures are avoided.

Unfortunately, the unfitted approach also gives rise to some difficulties. One of them is how to control the norm of the solution on the elements which are cut by the boundary $\partial\Omega(t)$. Certain inverse inequalities that are known from the fitted case are not valid anymore in this situation. In order to resolve this difficulty we will add a stabilization term $j_h^n(u, v)$ to the variational formulation. It will allow us to regain control of the solution on the whole computational domain and essentially carry over the inverse inequalities from the fitted case. To this end, it is necessary to introduce some further notation.

Let $\mathcal{F} = \{F\}$ be the set of spatial facets of $\tilde{\mathcal{T}}_h$. The relevant facets for the stabilization are then given by

$$\mathcal{F}_R^{*,n} := \{F \in \mathcal{F} \ : \ F = T_1 \cap T_2,\ T_1 \in \mathcal{E}(\Omega^n) \setminus \mathcal{I}(\Omega^n),\ T_2 \in \mathcal{E}(\Omega^n)\}.$$

The corresponding facet-patches are defined as

$$\omega_F \coloneqq T_1 \cup T_2,\ F \subset \partial T_i,\ i = 1, 2. \tag{2.5}$$

An illustration is given in Figure 2.2 for $d = 1$ and in Figure 2.4 for $d = 2$.

Then, we define the stabilization term

$$j_h^n(u, v) \coloneqq \int_{t_{n-1}}^{t_n} \tilde{\gamma}_J(\Delta t, h) \sum_{F \in \mathcal{F}_R^{*,n}} \int_{\omega_F} \frac{1}{h^2} [\![u]\!]_{\omega_F} [\![v]\!]_{\omega_F} \, dx \, dt, \tag{2.6}$$

for discrete functions $u, v \in W_h$. Here, $[\![u]\!]_{\omega_F}$ is used to denote the jump on the facet patch and is defined in the following way: Let $\omega_F = T_1 \cup T_2$ and denote by u_i the restriction of u to the element T_i for $i = 1, 2$. These polynomials have a canonical extension to the neighboring elements, e.g. the polynomial $u_1(x)$ can be evaluated at $x \in T_2$. This allows to define

$$[\![u]\!]_{\omega_F}(x) \coloneqq v_1(x) - v_2(x) \text{ for } x \in \omega_F.$$

The scaling factor $\tilde{\gamma}_J(\Delta t, h) \coloneqq \gamma_J \cdot \left(1 + \frac{\Delta t}{h}\right)$ will be motivated in chapter 3. Its main function is to compensate for an anisotropic choice of the spatial mesh width and the time step. For $\Delta t \sim h$ we have $\tilde{\gamma}_J(\Delta t, h) = \mathcal{O}(1)$.

Remark 2 (Relation of stabilization term to literature)**.** *There are (at least) two ways discussed in the literature on unfitted methods to gain control of the norm on cut elements. The most popular one is a stabilization based on penalizing jumps of normal derivatives over element facets (e.g. [BH12]). The relation between this stabilization and the one used here will be discussed in Remark 6. Another option is a local projection type stabilization which goes back to [BB01] for the fitted case. In the context of unfitted methods it is for example applied in [Bur10] (section 4) and [BH14]. This stabilization consists of a sum of integrals over patches ω_l (not necessarily associated to a facet) of the form*

$$\int_{\omega_l} h_{\omega_l}^{-2} (u - P_{\omega_l} u) v \, dx$$

for discrete functions u and v. Here, $P_{\omega_l} u$ is an L^2- projection onto a polynomial on the patch ω_l and $h_{\omega_l} \approx \mathcal{O}(h)$ the diameter of the patch. The stabilization used in this thesis is similar because it also involves integrals over (facet) patches. However, we do not compare the functions to their projection, but rather there restrictions to the individual elements which form the facet patch. Nevertheless, an L^2 projection onto the facet patch will show up later in the analysis while bounding the approximation error of our stabilization (see Proposition 3.26).

The discrete variational problem on the whole space-time domain is obtained by summing up over the time slabs:

Find $u \in W_h$ such that for all $v \in W_h$ there holds

$$B(u, v) + J(u, v) = f(v) \tag{2.7}$$

with

$$\begin{aligned} B(u, v) \coloneqq & \sum_{n=1}^{N} \left(\partial_t u + \mathbf{w} \cdot \nabla u, v\right)_{Q^n} + \sum_{n=1}^{N} \left(\nabla u, \nabla v\right)_{Q^n} \\ & + \sum_{n=1}^{N-1} \left([\![u]\!]^n, v_+^n\right)_{\Omega^n} + \left(u_+^0, v_+^0\right)_{\Omega^0}, \end{aligned} \tag{2.8}$$

$$J(u,v) \coloneqq \sum_{n=1}^{N} j_h^n(u,v),$$

and

$$f(v) \coloneqq \sum_{n=1}^{N} (f,v)_{Q^n} + \left(u_0, v_+^0\right)_{\Omega^0}.$$

It is useful to define the abbreviations

$$\begin{aligned} d(u,v) &\coloneqq \sum_{n=1}^{N} (\partial_t u + \mathbf{w}\cdot\nabla u, v)_{Q^n}, \\ b(u,v) &\coloneqq \sum_{n=1}^{N-1} \left([\![u]\!]^n, v_+^n\right)_{\Omega^n} + \left(u_+^0, v_+^0\right)_{\Omega^0}, \\ a(u,v) &\coloneqq \sum_{n=1}^{N} (\nabla u, \nabla v)_{Q^n}. \end{aligned}$$

We also introduce variants which we will use later

$$\begin{aligned} d'(u,v) &\coloneqq \sum_{n=1}^{N} (u, -\partial_t v - \mathbf{w}\cdot\nabla v)_{Q^n}, \\ b'(u,v) &\coloneqq -\sum_{n=1}^{N-1} \left(u_-^n, [\![v]\!]^n\right)_{\Omega^n} + \left(u_-^N, v_-^N\right)_{\Omega^N}. \end{aligned}$$

Lemma 2.1 (Rewriting the bilinear form)**.** *For $u, v \in W_h + H^1(Q)$ there holds*

$$d(u,v) + b(u,v) = d'(u,v) + b'(u,v)$$

and thus

$$B(u,v) = d'(u,v) + b'(u,v) + a(u,v). \tag{2.9}$$

Proof. The alternative representation of the bilinear form is derived by integration by parts of the space-time convection (∇, ∂_t).

For the time derivative one obtains

$$(\partial_t u, v)_{Q^n} = -(u, \partial_t v)_{Q^n} + \left(u_-^n, v_-^n\right)_{\Omega^n} - \left(u_+^{n-1}, v_+^{n-1}\right)_{\Omega^{n-1}} - \int_{t_{n-1}}^{t_n} \int_{\partial\Omega(t)} \mathcal{V}_n uv \, ds dt,$$

where $\mathcal{V}_n$ denotes the velocity of the boundary in normal direction.

For the convection term one has

$$\begin{aligned} (\mathbf{w}\cdot\nabla u, v)_{Q^n} &= -(u, \nabla\cdot(\mathbf{w}v))_{Q^n} + \int_{t_{n-1}}^{t_n} \int_{\partial\Omega(t)} \mathbf{w}\cdot\mathbf{n} uv \, ds dt \\ &= -(u, \mathbf{w}\cdot\nabla v)_{Q^n} + \int_{t_{n-1}}^{t_n} \int_{\partial\Omega(t)} \mathbf{w}\cdot\mathbf{n} uv \, ds dt, \end{aligned}$$

where it was used that $\nabla \cdot (\mathbf{w}v) = v\nabla \cdot \mathbf{w} + \mathbf{w} \cdot \nabla v = \mathbf{w} \cdot \nabla v$ since $\mathbf{w}$ is divergence free.

Now one has that the velocity of the boundary in normal direction coincides with the convection field: $\mathbf{w} \cdot \mathbf{n} - \mathcal{V}_n = 0$, cf. Remark 1. So these two terms cancel and we obtain:

$$(\partial_t u + \mathbf{w} \cdot \nabla u, v)_{Q^n} = (u, -\partial_t v - \mathbf{w} \cdot \nabla v)_{Q^n} + \left(u_-^n, v_-^n\right)_{\Omega^n} - \left(u_+^{n-1}, v_+^{n-1}\right)_{\Omega^{n-1}}.$$

Summation over $n = 1, \ldots, N$ leads to

$$d(u, v) = \sum_{n=1}^{N} \{\left(u_-^n, v_-^n\right)_{\Omega^n} - \left(u_+^{n-1}, v_+^{n-1}\right)_{\Omega^{n-1}}\} + d'(u, v).$$

Writing

$$\begin{aligned} b(u, v) &= \sum_{n=1}^{N-1} \left(u_+^n - u_-^n, v_+^n\right)_{\Omega^n} + \left(u_+^0, v_+^0\right)_{\Omega^0} \\ &= \sum_{n=1}^{N} \left(u_+^{n-1}, v_+^{n-1}\right)_{\Omega^{n-1}} - \sum_{n=1}^{N-1} \left(u_-^n, v_+^n\right)_{\Omega^n} \end{aligned}$$

and adding this to the expression for $d(u, v)$ from above yields:

$$\begin{aligned} b(u, v) + d(u, v) &= -\sum_{n=1}^{N-1} \left(u_-^n, v_+^n - v_-^n\right)_{\Omega^n} + \left(u_-^N, v_-^N\right)_{\Omega^N} + d'(u, v) \\ &= b'(u, v) + d'(u, v). \end{aligned}$$

□

Remark 3 (Mass conservation)**.** *Lemma 2.1 can be employed to show that the space-time DG method is globally mass conserving. Using the characterization of B from (2.9) and testing with $v = 1$ in the variational formulation yields:*

$$\int_{\Omega^N} u_-(\cdot, t_N)\, dx = \int_{\Omega^0} u_0\, dx + \int_{Q} f\, dx. \tag{2.10}$$

A local version of this mass balance on each time slab is obtained by testing with a function v that is constant on the time slab Q^n and vanishes everywhere else:

$$\int_{\Omega^n} u_-(\cdot, t_n)\, dx = \int_{\Omega^{n-1}} u_-(\cdot, t_{n-1})\, dx + \int_{Q^n} f\, dx. \tag{2.11}$$

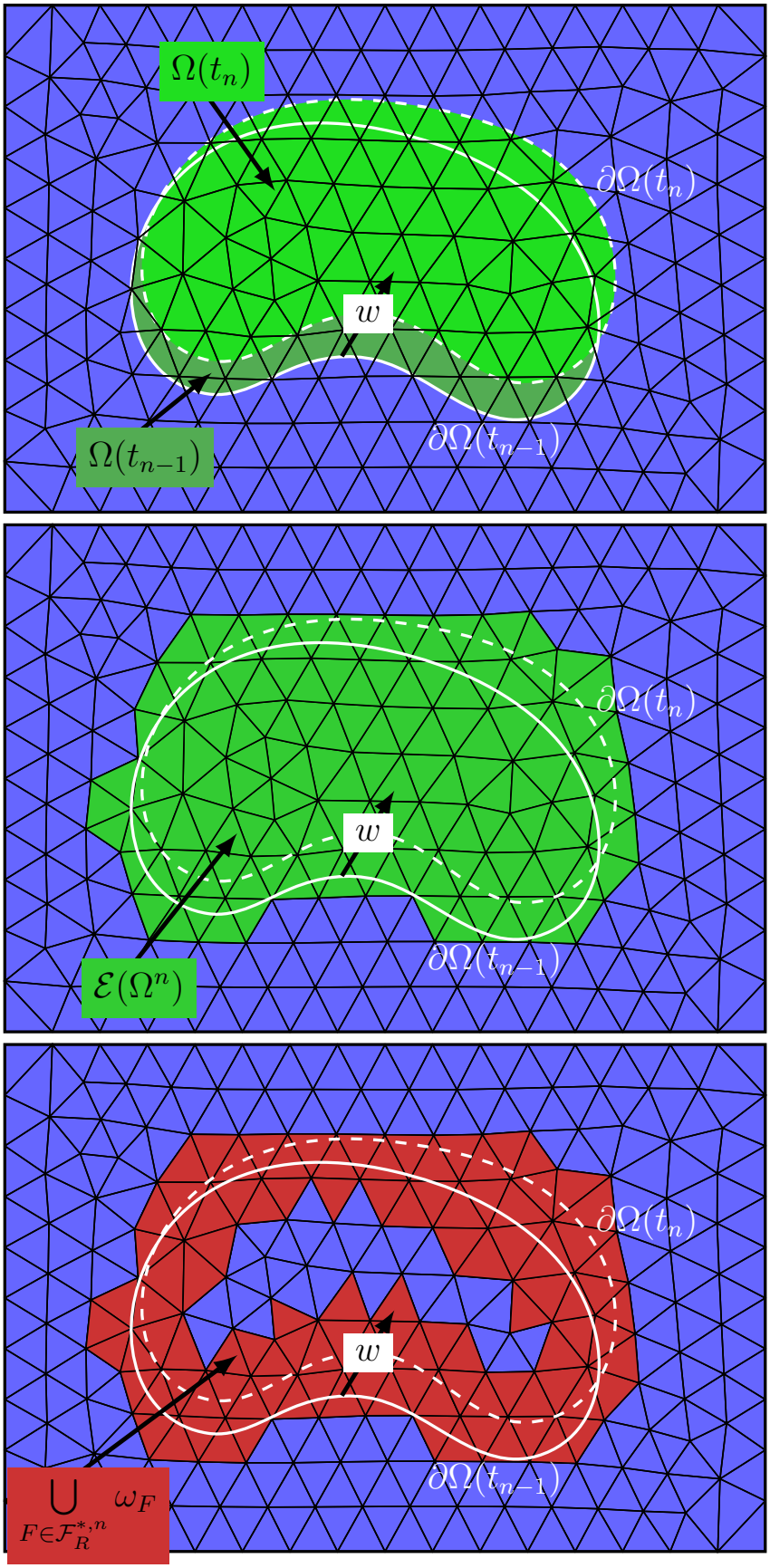

Figure 2.4: The topmost sketch shows the domain $\Omega(t)$ at times $t = t_{n-1}$ and $t = t_n$. In the middle, one can see the spatial domain $\mathcal{E}(\Omega^n)$ which forms the extended time slab $\mathcal{E}(\Omega^n) \times I_n = \mathcal{E}(Q^n)$. The facet patches involved in the stabilization term j_h^n are shown in the lowermost sketch.

Chapter 3

Error analysis of a space-time discretization for a moving domain problem assuming exact geometry handling

This chapter contains an error analysis for a modified version of the method introduced in chapter 2. It is assumed that all the arising integrals can be calculated exactly.

The analysis proceeds by an approach that is similar to the error analysis of DG schemes for linear transport equations. See for example the procedure for the linear model problem arising from DG methods described in section 1.3 of [DPE12]. First we define discrete norms. Then we calculate the consistency error and show boundedness and (discrete) stability. To this end, we need certain inverse estimates that are not automatically guaranteed for unfitted problems. At this point the ghost penalty stabilization comes into play. It basically allows to carry over the inverse estimates that are known for the discretization of PDEs on fitted tensor product domains.

Based on the derived properties of the bilinear form we prove a Céa-like result. In order to carry on, we need to bound the best approximation error of the solution in the employed space-time finite element spaces. This requires suitable interpolation operators. We construct these and derive their stability and approximation properties. The approximation results are then applied to prove an error bound for the method that is anisotropic in the time step and spatial mesh width as well as the spatial and temporal polynomial degrees.

3.1 Notation and assumptions

The analysis is based on assumptions A1-A5 which will now be introduced. The first assumption A1 is related to the use of an unfitted discretization. In order to accomodate for this assumption, the set of facet patches $\{\omega_F \mid F \in \mathcal{F}_R^{*,n}\}$ that are used for the stabilization needs to be expanded. We will first state the assumption and then provide some explanation in a subsequent remark.

A.1 There exists a mapping (between elements) $\mathcal{B} : \mathcal{E}(\Omega^n) \to \mathcal{I}(\Omega^n)$ such that:

- The number of elements $T \in \mathcal{E}(\Omega^n)$ that map to a specific element $T_0 \in \mathcal{I}(\Omega^n)$ can be bounded independently of h and Δt, i.e. $\#(\mathcal{B}^{-1}(T_0)) \leq C$.

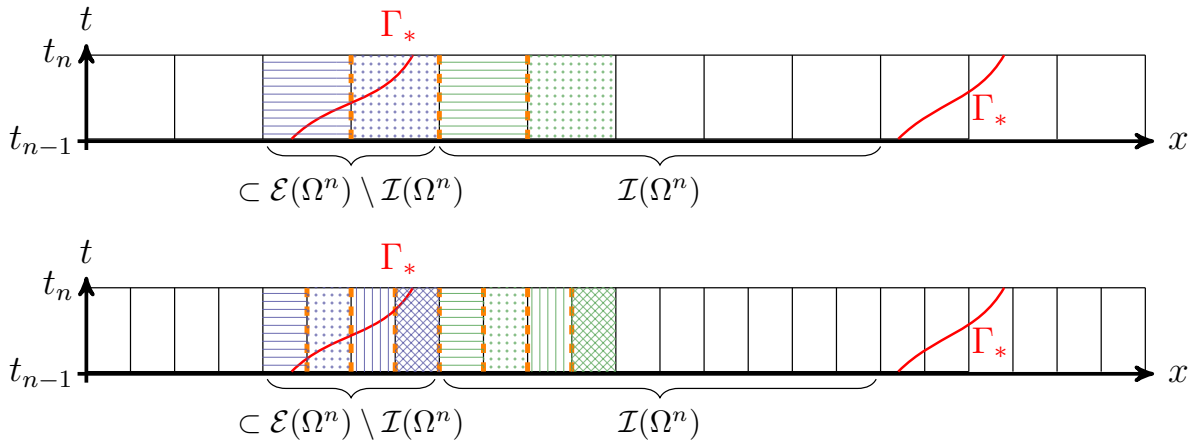

Figure 3.1: Illustration of assumption A.1: The upper sketch shows a basic mesh while the lower one features a spatial refinement. Elements with the same pattern are mapped to each other under $\mathcal{B} : \mathcal{E}(\Omega^n) \setminus \mathcal{I}(\Omega^n) \to \mathcal{I}(\Omega^n)$. The facets for the stabilization term are marked in orange.

- For $T \in \mathcal{E}(\Omega^n) \setminus \mathcal{I}(\Omega^n)$ let $\{T_i\}_{i=0}^M$ be the set of elements that need to be crossed in order to traverse from $T_M = T$ to $T_0 = \mathcal{B}(T)$. Then the facets $\{T_i \cap T_j \mid i, j = 1, \dots, M;\ i \neq j\}$ are contained in $\mathcal{F}_R^{*,n}$. That is, the stabilization encompasses all facets that are passed while walking from T to T_0.
- The thickness of the layer of cut elements is bounded as

$$\#\{T \in \mathcal{E}(\Omega^n) \setminus \mathcal{I}(\Omega^n)\} \leq C_{\mathrm{B}} \left(1 + \frac{\Delta t}{h}\right) \tag{3.1}$$

  with C_{B} independent of h and Δt.

Remark 4. *This assumption arises because we use an unfitted discretization. Here one needs to control the norm on cut elements $T \in \mathcal{E}(\Omega^n) \setminus \mathcal{I}(\Omega^n)$. Combining this assumption with the employed stabilization will allow us to bound the norm on a cut element T against the norm on an uncut element $\mathcal{B}(T) = T_0 \in \mathcal{I}(\Omega^n)$ plus stabilization terms. The stabilization needs to be applied on all the facet patches that need to be crossed in order to traverse from T to T_0.*

In the analysis, we need bounds on the number of elements $\#(\mathcal{B}^{-1}(T_0))$ that map to an element $T_0 \in \mathcal{I}(\Omega^n)$ and on the thickness of the layer of cut elements $\#\{T \in \mathcal{E}(\Omega^n) \setminus \mathcal{I}(\Omega^n)\}$. These assumptions are illustrated in Figure 3.1: The upper sketch shows a given cut situation on a coarse mesh while the lower sketch illustrates the behavior under mesh refinement. With respect to assumption A.1 the following two observations can be made:

- *On the coarse mesh the boundary Γ_* on the left cuts through the two elements with a blue pattern. But on the finer mesh the number of elements that are cut by this part of the boundary has increased to four. Hence, it is not plausible to impose a uniform bound on the number of elements that are cut by the boundary. Requesting a bound of the form (3.1), which imlies an increase with shrinking mesh size, is a more realistic assumption.*

– *On the other hand, we require a uniform bound on the number of elements that map under* $\mathcal{B} : \mathcal{E}(\Omega^n) \setminus \mathcal{I}(\Omega^n) \to \mathcal{I}(\Omega^n)$ *to the same element* $T_0 \in \mathcal{I}(\Omega^n)$*. This assumption is also illustrated in Figure 3.1. Here, the elements* $T \in \mathcal{E}(\Omega^n) \setminus \mathcal{I}(\Omega^n)$ *and their images* $\mathcal{B}(T) \in \mathcal{I}(\Omega^n)$ *have been drawn with the same pattern. For example, the element with the blue dots, which is cut by* Γ_**, on the coarse mesh maps to the element with the green dots in* $\mathcal{I}(\Omega^n)$*. Both on the coarse and the fine mesh the Figure shows a one-to-one correspondence between cut elements and their images in* $\mathcal{I}(\Omega^n)$*. This illustrates that the assumption* $\#(\mathcal{B}^{-1}(T_0)) \leq C$ *for* $T_0 \in \mathcal{I}(\Omega^n)$ *is not unrealistic. As mentioned above, this assumption will be used to bound the norm on a cut element* $T \in \mathcal{E}(\Omega^n) \setminus \mathcal{I}(\Omega^n)$ *against the norm on* $\mathcal{B}(T) \in \mathcal{I}(\Omega^n)$*. In order to realize this bound, we need to take into account all the facets that have to be crossed to walk from* T *to* $\mathcal{B}(T)$ *and collect the corresponding stabilization terms. Hoewever, these facets are not necessarily included in the original definition of the set* $\mathcal{F}_R^{*,n}$ *given in Chapter 2. For example, on the coarse mesh, only the facet between the element with the blue dots and the element with the green horizontal lines would be included in* $\mathcal{F}_R^{*,n}$*, not the one between the element with the green horizontal lines and its right neighbor. In practice, this means that we have to expand the stabilization to a small band inside the domain which includes approximately as many elements as are cut by the boundary in order to realize assumption A.1. With respect to the numerical experiments in Chapter 6, we already mention that this enrichment of* $\mathcal{F}_R^{*,n}$ *has not been applied. Instead we stick to the original definition of* $\mathcal{F}_R^{*,n}$ *given in Chapter 2 for all numerical computations.*

Finally, we define the scaling factor $\tilde{\gamma}_J(\Delta t, h)$ *in equation (2.6) as* $\tilde{\gamma}_J(\Delta t, h) = \gamma_J \left(1 + \frac{\Delta t}{h}\right)$ *with* $\gamma_J > 0$ *independent of* Δt *and* h*. This accounts for the factor obtained by the bound (3.1).*

A.2 We assume $\|\mathbf{w}\|_\infty$ is bounded.

A.3 There exists a constant $C_{\mathrm{G}} > 0$ such that $\frac{h^2}{\Delta t} \leq C_{\mathrm{G}}$.

A.4 The time step is bounded by a constant $\Delta t \leq C_{\mathrm{o}}$.

A.5 The domain $\Omega(t)$ for all times t and accordingly the space-time domain Q^n are sufficiently smooth, so that a linear continuous Soobolev extension operator

$$E^n : H^k(Q^n) \to H^k(\mathcal{E}(Q^n)),\ k \in \mathbb{N},$$

exists.

Remark 5. *In view of the fact that the spatial triangulation is required to be sufficiently fine to resolve the moving domain, the assumption A.3 appears to be rather mild. A reasonable choice for the constant in A.4 is* $C_o = 1$*.*

In the analysis below, we labelled some constants, which we would like to keep track of, according to the Lemma in which they originate. For example, $C_{3.3}$ is the constant corresponding to Lemma 3.3.

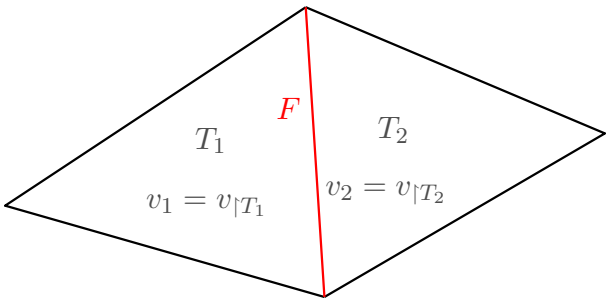

Figure 3.2: Sketch of the macro element $\bar{T} = T_1 \cup T_2$.

3.2 Near best-approximation in a discrete norm

3.2.1 Norms and inverse estimates

We introduce discrete norms. The first norm is

$$|||u|||^2 \coloneqq \sum_{n=1}^{N} \Delta t(\partial_t u, \partial_t u)_{Q^n} + [\![u]\!]^2 + \sum_{n=1}^{N} (\nabla u, \nabla u)_{Q^n}$$

with

$$[\![u]\!]^2 \coloneqq \sum_{n=1}^{N-1} ([\![u]\!]^n, [\![u]\!]^n)_{\Omega^n} + \left(u_+^0, u_+^0\right)_{\Omega^0} + \left(u_-^N, u_-^N\right)_{\Omega^N}.$$

Let $\|u\|_J^2 \coloneqq J(u,u)$ be the semi-norm induced by the ghost penalty term. Then we define the norm

$$|||u|||_j^2 \coloneqq |||u|||^2 + \|u\|_J^2,$$

which offers additional control on the ghost penalty term.This norm is mainly used. For continuity we will also consider another discrete norm:

$$|||u|||_*^2 \coloneqq \sum_{n=1}^{N} \left(\frac{1}{\Delta t} u, u\right)_{Q^n} + [\![u]\!]_*^2 + \sum_{n=1}^{N} (\nabla u, \nabla u)_{Q^n}$$

with

$$[\![u]\!]_*^2 \coloneqq \sum_{n=1}^{N} \left(u_-^n, u_-^n\right)_{\Omega^n}.$$

Also for this norm there is a corresponding version which includes the ghost penalty term:

$$|||u|||_{*,j}^2 \coloneqq |||u|||_*^2 + \|u\|_J^2.$$

The following Lemma shows the main mechanism behind the stabilizing effect of the ghost penalty terms. It is a modification of the classical ghost penalty result found in Lemma 5.1 of [MLLR14].

Lemma 3.1 (Ghost penalty mechanism)**.** *Let $T_1, T_2 \in \tilde{\mathcal{T}}_h$ be two elements sharing a common face F (illustrated in Figure 3.2). Moreover, assume that v is a piecewise polynomial function of degree at most $k_s \in \mathbb{N}$, possibly discontinuous and defined relative to the macro element $\bar{T} = T_1 \cup T_2$. Denote by v_i the restriction of v to T_i for $i = 1, 2$.*

Then there is a constant $C > 0$ which only depends on the shape regularity of $\tilde{\mathcal{T}}_h$ and the polynomial order of v such that:

$$\|v\|_{T_1}^2 \leq C \left(\|[\![v]\!]_{\omega_F}\|_{T_1}^2 + \|v\|_{T_2}^2 \right) \tag{3.2}$$

holds true.

Proof. Consider a point $x \in T_1$. We have

$$v_1(x) = (v_1 - v_2)(x) + v_2(x) = [\![v]\!]_{\omega_F}(x) + v_2(x),$$

where v_2 is the canonical extension of the polynomial defined on T_2 to T_1. Integrating over T_1 yields:

$$\|v_1\|_{T_1}^2 \leq 2 \left(\|[\![v]\!]_{\omega_F}\|_{T_1}^2 + \|v_2\|_{T_1}^2 \right).$$

Due to shape regularity the norms $\|\cdot\|_{T_1}$ and $\|\cdot\|_{T_2}$ are equivalent: $\|v_2\|_{T_1} \leq C \|v_2\|_{T_2}$. Thus,

$$\|v_1\|_{T_1}^2 \leq C \left(\|[\![v]\!]_{\omega_F}\|_{T_1}^2 + \|v_2\|_{T_2}^2 \right)$$

which completes the proof. □

Remark 6 (Comparison with 'derivative-jump'-based ghost penalty)**.** *Let us investigate the proof of Lemma 5.1 from [MLLR14] while keeping the notation from the proof of Lemma 3.1 above. The authors proceed in this proof by writing the polynomials $v_i(x)$ at a point $x \in T_1$ in terms of their Taylor series around x_F. Here, x_F denotes the normal projection of x onto the plane defined by the face F. This yields*

$$v_i(x) = \sum_{|\alpha| \leq k_s} \frac{D^\alpha v_i(x_F)}{\alpha!} \left(\|x - x_F\| \, \mathbf{n} \right)^\alpha,$$

where $\alpha = (\alpha_1, \ldots, \alpha_d)$ is a multiindex and $\mathbf{n}^\alpha = n_1^{\alpha_1} \cdot n_2^{\alpha_2} \cdot \ldots \cdot n_d^{\alpha_d}$ with $\mathbf{n} = (x - x_F)/\|x - x_F\|$ being the normal vector of the face F pointing towards T_1. Then the two Taylor expansions are subtracted which gives

$$v_1(x) = v_2(x) + \sum_{|\alpha| \leq k_s} \frac{[\![D^\alpha v(x_F)]\!]}{\alpha!} \left(\|x - x_F\| \, \mathbf{n} \right)^\alpha, \tag{3.3}$$

where $[\![D^\alpha v(x_F)]\!] = D^\alpha v_1(x_F) - D^\alpha v_2(x_F)$ denotes the jump over the facet F. Now an integration over T_1 with respect to x is performed, the expressions are squared and the Cauchy-Schwarz inequality is used:

$$\|v_1\|_{T_1}^2 \leq C \left(\|v_2\|_{T_1}^2 + + \sum_{|\alpha| \leq k_s} \int_{T_1} \left([\![D^\alpha v(x_F(x))]\!] \mathbf{n}^\alpha \right)^2 h^{2|\alpha|} \, dx \right).$$

After a change of variables and an application of shape regularity the authors arrive at

$$\|v_1\|_{T_1}^2 \leq C \left(\|v_2\|_{T_1}^2 + \sum_{j \leq k_s} \int_F [\![\partial_{\mathbf{n}}^j v(y)]\!]^2 h^{2j+1} \, dy \right),$$

with $\partial_{\mathbf{n}}^j v(y) = \sum_{|\alpha|=j} D^\alpha v(y)\mathbf{n}^\alpha$. *Using that the norms* $\|v_2\|_{T_1}^2$ *and* $\|v_2\|_{T_2}^2$ *are equivalent by shape regularity this leads to the key result of the ghost penalty mechanism*

$$\|v\|_{T_1}^2 \leq C \left(\|v\|_{T_2}^2 + \sum_{j \leq k_s} h^{2j+1} \big([\![\partial_{\mathbf{n}}^j v(y)]\!], [\![\partial_{\mathbf{n}}^j v(y)]\!] \big)_F \right). \tag{3.4}$$

If we perform a minor modification of this argument by bringing $v_2(x)$ *in (3.3) to the other side we arrive at*

$$\|v_1 - v_2\|_{T_1}^2 \leq C \sum_{j \leq k_s} h^{2j+1} \big([\![\partial_{\mathbf{n}}^j v(y)]\!], [\![\partial_{\mathbf{n}}^j v(y)]\!] \big)_F.$$

Then

$$\begin{aligned} \int_{\omega_F} [\![v]\!]_{\omega_F}^2 \, dx &= \|v_1 - v_2\|_{T_1}^2 + \|v_2 - v_1\|_{T_2}^2 \\ &\leq 2C \sum_{j \leq k_s} h^{2j+1} \big([\![\partial_{\mathbf{n}}^j v(y)]\!], [\![\partial_{\mathbf{n}}^j v(y)]\!] \big)_F. \end{aligned}$$

Thus, the stabilization used in this thesis is bounded from above by the 'derivative-jump'-based ghost penalty stabilization which is prevalent in the literature, see e.g. [BH12], [MLLR14], [BHL15], [BHLZ16].

Compared to the 'derivative-jump'-based stabilization it has certain computational advantages especially for higher order methods. To regain control over cut elements, the 'derivative-jump'-based stabilization needs to take into account the normal derivatives over the facets up to order k_s *as seen in equation (3.4). Thus, the computational effort increases with the polynomial degree of the ansatz functions. Moreover, the 'derivative-jump'-based stabilization usually associates a different stabilization parameter to each* $j = 0, \ldots, k_s$. *Then one faces the task to determine an optimal choice of all these parameters. The stabilization employed in this thesis is not affected by these problems: It is the same for all polynomial degrees. Hence, there are less terms to assemble than for the 'derivative-jump'-based stabilization if the polynomial degree exceeds one. Also there is just a single stabilization parameter to choose. This makes it particularly suited for higher order methods.*

A further discussion of implementational and practical aspects of 'derivative-jump'-based and 'projection'-based ghost penalty can be found in section 3.4.3.3 of [Sch17].

Lemma 3.1 allows to bound the norm of a discrete function on the extended time slab $\mathcal{E}(Q^n)$ by its norm on $\mathcal{I}(Q^n)$ and the corresponding stabilization terms.

Lemma 3.2. *There exists a constant* $C > 0$ *such that for every* $u \in W_h \oplus \nabla W_h$ *there holds*

$$\|u\|_{\mathcal{E}(Q^n)}^2 \leq C \left(\frac{h^2}{\gamma_J} j_h^n(u,u) + \|u\|_{\mathcal{I}(Q^n)}^2 \right). \tag{3.5}$$

Proof. Decompose the norm $\|u\|^2_{\mathcal{E}(Q^n)}$ into a sum over elements $Q^n_T = T \times I_n$:

$$\begin{aligned}\|u\|^2_{\mathcal{E}(Q^n)} &= \sum_{T\in\mathcal{E}(\Omega^n)} \int_{t_{n-1}}^{t_n} \|u(\cdot,t)\|^2_T \, dt \\ &= \sum_{T\in\mathcal{I}(\Omega^n)} \int_{t_{n-1}}^{t_n} \|u(\cdot,t)\|^2_T \, dt + \sum_{T\in\mathcal{E}(\Omega^n)\setminus\mathcal{I}(\Omega^n)} \int_{t_{n-1}}^{t_n} \|u(\cdot,t)\|^2_T \, dt.\end{aligned}$$

If $T \in \mathcal{I}(\Omega^n)$ we are done. For $T \in \mathcal{E}(\Omega^n) \setminus \mathcal{I}(\Omega^n)$ we use assumption A.1: There exists a $\mathcal{B}(T) = T_0 \in \mathcal{I}(\Omega^n)$ and elements $\{T_i\}_{i=0}^M$ with correponding facet patches contained in $\{\omega_F \mid F \in \mathcal{F}_R^{*,n}\}$ that can be crossed in order to traverse from $T_M = T$ to T_0. We then apply Lemma 3.1 iteratively to each neighboring pair $\{T_i, T_{i-1}\}$ to bound the norm on T_M against the norm on T_0 at the expense of stabilization terms:

$$\int_{t_{n-1}}^{t_n} \|u(\cdot,t)\|^2_T \, dt \le C \left(\int_{t_{n-1}}^{t_n} \|u(\cdot,t)\|^2_{\mathcal{B}(T)} \, dt + \sum_{F\in\mathcal{F}_R^{*,n}} \int_{t_{n-1}}^{t_n} \|[\![u]\!]_{\omega_F}(\cdot,t)\|^2_{\omega_F} \, dt \right).$$

Repeating this for every element $T \in \mathcal{E}(\Omega^n) \setminus \mathcal{I}(\Omega^n)$ one ends up with

$$\begin{aligned}\|u\|^2_{\mathcal{E}(Q^n)} &\le C \Bigg(\sum_{T\in\mathcal{I}(\Omega^n)} \big(1 + \#(\mathcal{B}^{-1}(T))\big) \int_{t_{n-1}}^{t_n} \|u(\cdot,t)\|^2_T \, dt \\ &\qquad + \#\{T \in \mathcal{E}(\Omega^n) \setminus \mathcal{I}(\Omega^n)\} \sum_{F\in\mathcal{F}_R^{*,n}} \int_{t_{n-1}}^{t_n} \|[\![u]\!]_{\omega_F}(\cdot,t)\|^2_{\omega_F} \, dt \Bigg) \\ &\le C \left(\sum_{T\in\mathcal{I}(\Omega^n)} \int_{t_{n-1}}^{t_n} \|u(\cdot,t)\|^2_T \, dt + \sum_{F\in\mathcal{F}_R^{*,n}} \left(1 + \frac{\Delta t}{h}\right) \int_{t_{n-1}}^{t_n} \|[\![u]\!]_{\omega_F}(\cdot,t)\|^2_{\omega_F} \, dt \right) \\ &= C \left(\|u\|^2_{\mathcal{I}(Q^n)} + C_{\mathrm{B}} \frac{h^2}{\gamma_J} j_h^n(u,u) \right),\end{aligned}$$

in view of $\#(\mathcal{B}^{-1}(T_0)) \le C$ for $T_0 \in \mathcal{I}(\Omega^n)$ and $\#\{T \in \mathcal{E}(\Omega^n)\setminus\mathcal{I}(\Omega^n)\} \le C_{\mathrm{B}} \left(1 + \frac{\Delta t}{h}\right)$. □

The previous Lemma allows to extend estimates for finite elements with tensor product structure to the unfitted case at the expense of additional stabilization terms.

Lemma 3.3 (Stabilized inverse inequality in time)**.** *For $u \in W_h$ it holds that*

$$\left(u_+^{n-1}, u_+^{n-1}\right)_{\Omega^{n-1}} \le \frac{C_{3.3}}{\Delta t} \left(\frac{h^2}{\gamma_J} j_h^n(u,u) + \|u\|^2_{\mathcal{I}(Q^n)} \right),$$

$$\left(u_-^{n}, u_-^{n}\right)_{\Omega^{n}} \le \frac{C_{3.3}}{\Delta t} \left(\frac{h^2}{\gamma_J} j_h^n(u,u) + \|u\|^2_{\mathcal{I}(Q^n)} \right).$$

Proof. We employ the extension operator $\mathcal{E}$ to extend the domain Q^n to a domain $\mathcal{E}(Q^n) = \mathcal{E}(\Omega^n) \times I_n$ that has tensor product structure. At a fixed point $x \in \mathcal{E}(\Omega^n)$,

the function $u(x,\cdot)$ is a polynomial of degree k_t in time. Thus, the trace inverse inequality on the time interval I_n from Theorem 2 of [WH03] can be applied:

$$|u(x,t_n)|^2 \leq \frac{C(k_t)}{\Delta t} \int\limits_{I_n} |u(x,t)|^2 \ dt,$$

where the constant $C(k_t)$ only depends on k_t. Then

$$\begin{aligned}
\left\|u_-^n\right\|_{\Omega^n}^2 \leq \left\|u_-^n\right\|_{\mathcal{E}(\Omega^n)}^2 &= \int\limits_{\mathcal{E}(\Omega^n)} |u(x,t_n)|^2 \ dx \\
&\leq \int\limits_{\mathcal{E}(\Omega^n)} \frac{C(k_t)}{\Delta t} \int\limits_{I_n} |u(x,t)|^2 \ dt \ dx = \frac{C(k_t)}{\Delta t} \|u\|_{\mathcal{E}(Q^n)}^2 \\
&\leq \frac{C_{3.3}}{\Delta t} \left(\frac{h^2}{\gamma_J} j_h^n(u,u) + \|u\|_{\mathcal{I}(Q^n)}^2 \right),
\end{aligned}$$

where the last inequality follows by applying Lemma 3.2. Analogously for u_+^{n-1}. □

Lemma 3.4 (Stabilized inverse inequality for time derivative)**.** *For $u \in W_h \oplus \nabla W_h$ it holds that*

$$\Delta t (\partial_t u, \partial_t u)_{Q^n} \leq \frac{C_{3.4}}{\Delta t} \left(\frac{h^2}{\gamma_J} j_h^n(u,u) + \|u\|_{\mathcal{I}(Q^n)}^2 \right). \tag{3.6}$$

Proof. For a fixed point $x \in \mathcal{E}(\Omega^n)$, Theorem 4.5.11 in [BS08] implies

$$\Delta t \int\limits_{I_n} |\partial_t u(x,t)|^2 \ dt \leq \frac{C_{\text{inv}}}{\Delta t} \int\limits_{I_n} |u(x,t)|^2 \ dt,$$

where C_{inv} does not depend on x, but only on k_t. Integrating over $\mathcal{E}(\Omega^n)$ and using that $\mathcal{E}(\Omega^n) \times I_n = \mathcal{E}(Q^n)$ leads to

$$\Delta t (\partial_t u, \partial_t u)_{\mathcal{E}(Q^n)} \leq \frac{C_{\text{inv}}}{\Delta t} \|u\|_{\mathcal{E}(Q^n)}^2 .$$

Hence, the desired estimate again follows by extending Q^n to a domain with tensor product structure:

$$\begin{aligned}
\Delta t (\partial_t u, \partial_t u)_{Q^n} &\leq \Delta t (\partial_t u, \partial_t u)_{\mathcal{E}(Q^n)} \\
&\leq \frac{C_{\text{inv}}}{\Delta t} \|u\|_{\mathcal{E}(Q^n)}^2 \\
&\leq \frac{C_{3.4}}{\Delta t} \left(\frac{h^2}{\gamma_J} j_h^n(u,u) + \|u\|_{\mathcal{I}(Q^n)}^2 \right),
\end{aligned}$$

where the last inequality uses Lemma 3.2. □

Note that on W_h we have

$$[\![u]\!]_*^2 \leq \frac{C_{3.3}}{\Delta t} \sum_{n=1}^{N} \left(\frac{h^2}{\gamma_J} j_h^n(u,u) + \|u\|_{\mathcal{I}(Q^n)}^2 \right).$$

Lemma 3.5 (Derivatives in ghost penalty)**.** *There exist constants $C_{3.5}^t \geq 1, C_{3.5}^s \geq 1$ only depending on the polynomial degree and the shape regularity of the background mesh $\tilde{\mathcal{T}}_h$ such that:*

$$J(\partial_t u, \partial_t u) \leq \frac{C_{3.5}^t}{\Delta t^2} J(u,u), \tag{3.7}$$

$$J(\nabla u, \nabla u) \leq \frac{C_{3.5}^s}{h^2} J(u,u) \tag{3.8}$$

holds for all $u \in W_h$.

Proof. The set of space-time facet patches has a tensor product structure within each time slab: $\cup_{F \in \mathcal{F}_R^{*,n}} \omega_F \times I_n$. This allows to proceed similarly to the previous proofs.

For $u \in W_h$ one obtains by applying Theorem 4.5.11 from [BS08] for the time integral on I_n that

$$\begin{aligned}
J(\partial_t u, \partial_t u) &= \sum_{n=1}^{N} \left(1 + \frac{\Delta t}{h}\right) \gamma_J \sum_{F \in \mathcal{F}_R^{*,n}} \frac{1}{h^2} \int_{\omega_F} \int_{I_n} \left(\partial_t [\![u]\!]_{\omega_F}(x,t)\right)^2 \, dt \, dx \\
&\leq \frac{C_{3.5}^t}{\Delta t^2} \sum_{n=1}^{N} \left(1 + \frac{\Delta t}{h}\right) \gamma_J \sum_{F \in \mathcal{F}_R^{*,n}} \frac{1}{h^2} \int_{\omega_F} \int_{I_n} \left([\![u]\!]_{\omega_F}(x,t)\right)^2 \, dt \, dx \\
&= \frac{C_{3.5}^t}{\Delta t^2} J(u,u).
\end{aligned}$$

The result for the gradient follows by applying Theorem 4.5.11 from [BS08] for the integral over the facet patch ω_F:

$$\begin{aligned}
J(\nabla u, \nabla u) &= \sum_{n=1}^{N} \left(1 + \frac{\Delta t}{h}\right) \gamma_J \sum_{F \in \mathcal{F}_R^{*,n}} \frac{1}{h^2} \int_{I_n} \int_{\omega_F} \left(\nabla [\![u]\!]_{\omega_F}(x,t)\right)^2 \, dt \, dx \\
&\leq \frac{C_{3.5}^s}{h^2} \sum_{n=1}^{N} \left(1 + \frac{\Delta t}{h}\right) \gamma_J \sum_{F \in \mathcal{F}_R^{*,n}} \frac{1}{h^2} \int_{I_n} \int_{\omega_F} \left([\![u]\!]_{\omega_F}(x,t)\right)^2 \, dt \, dx \\
&= \frac{C_{3.5}^s}{h^2} J(u,u).
\end{aligned}$$

□

3.2.2 Stability

The inverse estimates from the last section will be needed to derive a discrete inf-sup stability result. We begin by proving some auxiliary Lemmas.

Lemma 3.6 (positiveness)**.** *For $u \in W_h$ there holds*

(a) $d(u,u) = \frac{1}{2} \sum_{n=1}^{N-1} \left(\left\| u_-^n \right\|_{\Omega^n}^2 - \left\| u_+^n \right\|_{\Omega^n}^2 \right) + \frac{1}{2} \left\| u_-^N \right\|_{\Omega^N}^2 - \frac{1}{2} \left\| u_+^0 \right\|_{\Omega_+^0}^2,$

(b) $b(u,u) = \frac{1}{2} \sum_{n=1}^{N-1} \| [\![u]\!]^n \|_{\Omega^n}^2 + \frac{1}{2} \sum_{n=1}^{N-1} \left(\left\| u_+^n \right\|_{\Omega^n}^2 - \left\| u_-^n \right\|_{\Omega^n}^2 \right) + \left\| u_+^0 \right\|_{\Omega^0}^2,$

(c) $B(u,u) + J(u,u) = \frac{1}{2} [\![u]\!]^2 + \sum_{n=1}^{N} (\nabla u, \nabla u)_{Q^n} + J(u,u).$

Proof. *(a)* In the proof of Lemma 2.1 it was derived that

$$d(u,v) = \sum_{n=1}^{N} \{ \left(u_-^n, v_-^n\right)_{\Omega^n} - \left(u_+^{n-1}, v_+^{n-1}\right)_{\Omega^{n-1}} \} + d'(u,v).$$

Setting $v = u$ and noting that $d(u,u) = -d'(u,u)$ yields

$$\begin{aligned} d(u,u) &= \frac{1}{2} \sum_{n=1}^{N} \left(\left\| u_-^n \right\|_{\Omega^n}^2 - \left\| u_+^{n-1} \right\|_{\Omega^{n-1}}^2 \right) \\ &= \frac{1}{2} \sum_{n=1}^{N-1} \left(\left\| u_-^n \right\|_{\Omega^n}^2 - \left\| u_+^n \right\|_{\Omega^n}^2 \right) + \frac{1}{2} \left\| u_-^N \right\|_{\Omega^N}^2 - \frac{1}{2} \left\| u_+^0 \right\|_{\Omega^0}^2 . \end{aligned}$$

(b) Some rewriting gives

$$\begin{aligned} b(u,u) &= \frac{1}{2} \sum_{n=1}^{N-1} \left([\![u]\!]^n, u_+^n \right)_{\Omega^n} + \frac{1}{2} \sum_{n=1}^{N-1} \left([\![u]\!]^n, u_+^n \right)_{\Omega^n} + \left\| u_+^0 \right\|_{\Omega^0}^2 \\ &= \frac{1}{2} \sum_{n=1}^{N-1} \| [\![u]\!]^n \|_{\Omega^n}^2 + \frac{1}{2} \sum_{n=1}^{N-1} \left(u_+^n - u_-^n, u_+^n + u_-^n \right)_{\Omega^n} + \left\| u_+^0 \right\|_{\Omega^0}^2 \\ &= \frac{1}{2} \sum_{n=1}^{N-1} \| [\![u]\!]^n \|_{\Omega^n}^2 + \frac{1}{2} \sum_{n=1}^{N-1} \left(\left\| u_+^n \right\|_{\Omega^n}^2 - \left\| u_-^n \right\|_{\Omega^n}^2 \right) + \left\| u_+^0 \right\|_{\Omega^0}^2 . \end{aligned}$$

(c) Adding the expression obtained in (a) and (b) gives

$$\begin{aligned} b(u,u) + d(u,u) &= \frac{1}{2} \sum_{n=1}^{N-1} \| [\![u]\!]^n \|_{\Omega^n}^2 + \frac{1}{2} \left\| u_+^0 \right\|_{\Omega^0}^2 + \frac{1}{2} \left\| u_-^N \right\|_{\Omega^N}^2 \\ &= \frac{1}{2} [\![u]\!]^2. \end{aligned}$$

Since

$$B(u,u) = b(u,u) + d(u,u) + \sum_{n=1}^{N} \left(\nabla u, \nabla u \right)_{Q^n}$$

this gives the result. □

Lemma 3.7 (control on time derivative)**.** *For $u \in W_h$ there holds*

$$\begin{aligned} B(u, \Delta t \partial_t u) + J(u, \Delta t \partial_t u) \geq \frac{1}{2} \sum_{n=1}^{N} \Delta t (\partial_t u, \partial_t u)_{Q^n} - C_{3.7} [\![u]\!]^2 \\ - C_{3.7} \sum_{n=1}^{N} \left(\nabla u, \nabla u \right)_{Q^n} - C_{3.7} J(u,u), \end{aligned}$$

with

$$C_{3.7} = \max\{ \tilde{C_{3.3}}, \frac{h^2}{4\gamma_J \Delta t} + \frac{\sqrt{\tilde{C_{3.4}}}}{2\gamma_J} + \sqrt{C_{3.5}^t}, \sqrt{\tilde{C_{3.4}}} + C_o \left\| \mathbf{w} \right\|_\infty^2 \}$$

where $\tilde{C_{3.4}} = C_{3.4} C_{3.5}^s$ and $\tilde{C_{3.3}} = C_{3.3} C_{3.5}^t$.

Remark 7. *Under assumption A.3, i.e.* $h^2 \leq C_G \Delta t$*, the constant* $C_{3.7}$ *can be bounded independently of* Δt *and* h*.*

Proof. Consider

$$
\begin{aligned}
B(u, \Delta t \partial_t u) - \sum_{n=1}^{N} \Delta t (\partial_t u, \partial_t u)_{Q^n} = & \sum_{n=1}^{N} (\mathbf{w} \cdot \nabla u, \Delta t \partial_t u)_{Q^n} && \text{I} \\
& + \sum_{n=1}^{N-1} \left([\![u]\!]^n, \Delta t (\partial_t u)_+^n \right)_{\Omega^n} + \left(u_+^0, \Delta t (\partial_t u)_+^0 \right)_{\Omega^0} && \text{II} \\
& + \sum_{n=1}^{N} (\nabla u, \nabla (\Delta t \partial_t u))_{Q^n}. && \text{III}
\end{aligned}
$$

Each of the terms on the right hand side will be treated separately. First we always apply the Cauchy-Schwarz inequality. Then Young's inequality for some $\varepsilon_j > 0$ will be used. We start with

$$
\begin{aligned}
\text{II} = & \sum_{n=1}^{N-1} \left([\![u]\!]^n, \Delta t (\partial_t u)_+^n \right)_{\Omega^n} + \left(u_+^0, \Delta t (\partial_t u)_+^0 \right)_{\Omega^0} \\
\leq & \frac{\varepsilon_1}{2} [\![u]\!]^2 + \frac{1}{2\varepsilon_1} \sum_{n=1}^{N} \Delta t^2 \left((\partial_t u)_+^{n-1}, (\partial_t u)_+^{n-1} \right)_{\Omega^{n-1}} \\
\leq & \frac{\varepsilon_1}{2} [\![u]\!]^2 + \frac{C_{3.3}}{2\varepsilon_1} \left(\Delta t \frac{h^2}{\gamma_J} J(\partial_t u, \partial_t u) + \Delta t \sum_{n=1}^{N} (\partial_t u, \partial_t u)_{Q^n} \right) \\
\leq & \frac{\varepsilon_1}{2} [\![u]\!]^2 + \frac{C_{3.3}}{2\varepsilon_1} \left(\frac{h^2}{\gamma_J \Delta t} C_{3.5}^t J(u, u) + \Delta t \sum_{n=1}^{N} (\partial_t u, \partial_t u)_{Q^n} \right) \\
\leq & \frac{\varepsilon_1}{2} [\![u]\!]^2 + \frac{\tilde{C_{3.3}}}{2\varepsilon_1} \left(\frac{h^2}{\gamma_J \Delta t} J(u, u) + \Delta t \sum_{n=1}^{N} (\partial_t u, \partial_t u)_{Q^n} \right),
\end{aligned}
$$

where Lemma 3.3 was used in line three and Lemma 3.5 in line four. Here $\tilde{C_{3.3}} = C_{3.3} C_{3.5}^t$.

For the diffusion term one can use Lemma 3.4 and Lemma 3.5 to estimate

$$
\begin{aligned}
\text{III} = \sum_{n=1}^{N} (\nabla u, \nabla (\Delta t \partial_t u))_{Q^n} & \leq \frac{\varepsilon_2}{2} (\nabla u, \nabla u)_Q + \frac{1}{2\varepsilon_2} \Delta t^2 \sum_{n=1}^{N} (\partial_t \nabla u, \partial_t \nabla u)_{Q^n} \\
& \leq \frac{\varepsilon_2}{2} (\nabla u, \nabla u)_Q + \frac{C_{3.4}}{2\varepsilon_2} \left(\frac{h^2}{\gamma_J} J(\nabla u, \nabla u) + (\nabla u, \nabla u)_Q \right) \\
& \leq \frac{\varepsilon_2}{2} (\nabla u, \nabla u)_Q + \frac{\tilde{C_{3.4}}}{2\varepsilon_2} \left(\frac{1}{\gamma_J} J(u, u) + (\nabla u, \nabla u)_Q \right)
\end{aligned}
$$

with $\tilde{C_{3.4}} = C_{3.4} C_{3.5}^s$. Choosing $\varepsilon_2 = \sqrt{\tilde{C_{3.4}}}$ leads to:

$$
\sum_{n=1}^{N} (\nabla u, \nabla (\Delta t \partial_t u))_{Q^n} \leq \sqrt{\tilde{C_{3.4}}} (\nabla u, \nabla u)_Q + \frac{\sqrt{\tilde{C_{3.4}}}}{2\gamma_J} J(u, u).
$$

It remains to treat the convection term:

$$\begin{aligned}\mathrm{I} = \sum_{n=1}^{N} (\mathbf{w}\cdot\nabla u, \Delta t\partial_t u)_{Q^n} &\leq \frac{\varepsilon_3}{2}\Delta t \sum_{n=1}^{N} (\mathbf{w}\cdot\nabla u, \mathbf{w}\cdot\nabla u)_{Q^n} + \frac{\Delta t}{2\varepsilon_3}\sum_{n=1}^{N}(\partial_t u, \partial_t u)_{Q^n} \\ &\leq \frac{\varepsilon_3}{2}\Delta t \left\|\mathbf{w}\right\|_\infty^2 (\nabla u, \nabla u)_Q + \frac{\Delta t}{2\varepsilon_3}\sum_{n=1}^{N}(\partial_t u, \partial_t u)_{Q^n}.\end{aligned}$$

Finally, the ghost penalty term is estimated by invoking Lemma 3.5:

$$\begin{aligned}J(u, \Delta t\partial_t u) &\leq \frac{\varepsilon_4}{2}J(u,u) + \frac{\Delta t^2}{2\varepsilon_4}J(\partial_t u, \partial_t u) \\ &\leq \frac{\varepsilon_4}{2}J(u,u) + \frac{C_{3.5}^t}{2\varepsilon_4}J(u,u) \\ &= \sqrt{C_{3.5}^t}J(u,u),\end{aligned}$$

where $\varepsilon_4 = \sqrt{C_{3.5}^t}$ was chosen.

Assembling all the estimates gives:

$$\begin{aligned}B(u, \Delta t\partial_t u) + J(u, \Delta t\partial_t u) \geq (\Delta t\partial_t u, \partial_t u)_Q &\left[1 - \frac{1}{2\varepsilon_3} - \frac{\tilde{C_{3.3}}}{2\varepsilon_1}\right] \\ - J(u,u) &\left[\frac{\tilde{C_{3.3}}}{2\varepsilon_1}\frac{h^2}{\gamma_J \Delta t} + \frac{\sqrt{\tilde{C_{3.4}}}}{2\gamma_J} + \sqrt{C_{3.5}^t}\right] \\ - (\nabla u, \nabla u)_{Q^n} &\left[\sqrt{\tilde{C_{3.4}}} + \frac{\varepsilon_3}{2}\Delta t \left\|\mathbf{w}\right\|_\infty^2\right] - \frac{\varepsilon_1}{2}[\![u]\!]^2.\end{aligned}$$

Choosing $\varepsilon_1 = 2\tilde{C_{3.3}}$ and $\varepsilon_3 = 2$ yields:

$$\begin{aligned}B(u, \Delta t\partial_t u) + J(u, \Delta t\partial_t u) \geq \frac{1}{2}(\Delta t\partial_t u, \partial_t u)_Q - \tilde{C_{3.3}}[\![u]\!]^2 - J(u,u)&\left[\frac{h^2}{4\gamma_J\Delta t} + \frac{\sqrt{\tilde{C_{3.4}}}}{2\gamma_J} + \sqrt{C_{3.5}^t}\right] \\ - (\nabla u, \nabla u)_Q &\left[\sqrt{\tilde{C_{3.4}}} + \Delta t \left\|\mathbf{w}\right\|_\infty^2\right].\end{aligned}$$

Using assumption A.4, the claim follows with

$$C_{3.7} = \max\{\tilde{C_{3.3}}, \frac{h^2}{4\gamma_J\Delta t} + \frac{\sqrt{\tilde{C_{3.4}}}}{2\gamma_J} + \sqrt{C_{3.5}^t}, \sqrt{\tilde{C_{3.4}}} + C_{\mathrm{o}}\left\|\mathbf{w}\right\|_\infty^2\}.$$

□

Lemma 3.8 (special function)**.** *For u in W_h there holds*

$$|||\Delta t\partial_t u|||_j \leq C_{3.8}|||u|||_j,$$

with $(C_{3.8})^2 = \max\{C_{3.4} + 4C_{3.3}, \frac{h^2}{\gamma_J\Delta t}C_{3.5}^t[C_{3.4} + 4C_{3.3}] + \frac{C_{3.4}}{\gamma_J}C_{3.5}^s + C_{3.5}^t\}$.

Remark 8. *The constant $C_{3.8}$ can be bounded independently of Δt and h if assumption A.3 is used.*

Proof. Most of the estimates have already been used in the previous proof.

- From Lemma 3.4 and Lemma 3.5 it follows that

$$\begin{aligned}\Delta t^3\left(\partial_t^2 u, \partial_t^2 u\right)_Q &\leq C_{3.4}\Delta t\left(\frac{h^2}{\gamma_J}J(\partial_t u, \partial_t u) + (\partial_t u, \partial_t u)_Q\right)\\ &\leq C_{3.4}C_{3.5}^t\frac{h^2}{\gamma_J\Delta t}J(u,u) + C_{3.4}\Delta t(\partial_t u, \partial_t u)_Q.\end{aligned}$$

- With Lemma 3.3 and Lemma 3.5 we have:

$$\begin{aligned}\Delta t^2[\![\partial_t u]\!]^2 &\leq 2\Delta t^2\sum_{n=1}^{N}\left[\left((\partial_t u)_+^{n-1}, (\partial_t u)_+^{n-1}\right)_{\Omega^{n-1}} + \left((\partial_t u)_-^{n}, (\partial_t u)_-^{n}\right)_{\Omega^{n}}\right]\\ &\leq 4C_{3.3}\Delta t\left(\frac{h^2}{\gamma_J}J(\partial_t u, \partial_t u) + (\partial_t u, \partial_t u)_Q\right)\\ &\leq 4C_{3.3}C_{3.5}^t\frac{h^2}{\gamma_J\Delta t}J(u,u) + 4C_{3.3}\Delta t(\partial_t u, \partial_t u)_Q.\end{aligned}$$

- Another application of Lemma 3.4 and Lemma 3.5 yields

$$\begin{aligned}\Delta t^2(\nabla\partial_t u, \nabla\partial_t u)_Q &\leq C_{3.4}\left(\frac{h^2}{\gamma_J}J(\nabla u, \nabla u) + (\nabla u, \nabla u)_Q\right)\\ &\leq C_{3.5}^s\frac{C_{3.4}}{\gamma_J}J(u,u) + C_{3.4}(\nabla u, \nabla u)_Q.\end{aligned}$$

- Finally, the Ghost-Penalty term is bounded by Lemma 3.5: $\Delta t^2 J(\partial_t u, \partial_t u) \leq C_{3.5}^t J(u,u)$.

Collecting all the terms gives:

$$\begin{aligned}|||\Delta t\partial_t u|||_j^2 &\leq (C_{3.4} + 4C_{3.3})\sum_{n=1}^{N}\Delta t(\partial_t u, \partial_t u)_{Q^n} + C_{3.4}\sum_{n=1}^{N}(\nabla u, \nabla u)_{Q^n}\\ &\quad + \left(\frac{h^2}{\gamma_J\Delta t}C_{3.5}^t[C_{3.4} + 4C_{3.3}] + \frac{C_{3.4}}{\gamma_J}C_{3.5}^s + C_{3.5}^t\right)J(u,u)\\ &\leq (C_{3.8})^2|||u|||_j^2,\end{aligned}$$

with $(C_{3.8})^2 = \max\{C_{3.4} + 4C_{3.3}, \frac{h^2}{\gamma_J\Delta t}C_{3.5}^t[C_{3.4} + 4C_{3.3}] + \frac{C_{3.4}}{\gamma_J}C_{3.5}^s + C_{3.5}^t\}$. □

The previous Lemmas can now be combined to show discrete stability.

Proposition 3.9 (Stability)**.** *For all $u \in W_h$ there exists a $\tilde{v}(u) \in W_h$ such that there holds*

$$B(u, \tilde{v}(u)) + J(u, \tilde{v}(u)) \geq C_{3.9}|||u|||_j|||\tilde{v}(u)|||_j,$$

with $C_{3.9} = \frac{1}{2(2C_{3.7}+C_{3.8}+1)}$.

Remark 9. *Consider the constants $C_{3.7}(\gamma_J), C_{3.8}(\gamma_J)$ as a function of the ghost-penalty stabilization parameter. Then*

$$\lim_{\gamma_J\to+0}C_{3.7}(\gamma_J) = \infty, \quad \lim_{\gamma_J\to+0}C_{3.8}(\gamma_J) = \infty, \text{ which implies } \lim_{\gamma_J\to+0}C_{3.9}(\gamma_J) = 0.$$

That is, the stability estimate deteriorates as γ_J decreases since we loose control over the norms on the elements of the extended domain.

Remark 10. *If one chooses not to include the stabilization factor* $\left(1+\frac{\Delta t}{h}\right)$ *in the ghost penalty term then it appears as* $1/\left(1+\frac{\Delta t}{h}\right)$ *in front of the constant* $C_{3.9}$ *in the stability estimate.*

Proof. Consider $\tilde{v}(u) = (2C_{3.7}+1)u + v^*(u) \in W_h$ with $v^*(u) = \Delta t \partial_t u \in W_h$. Using the triangle inequality and Lemma 3.8 there holds

$$\begin{aligned}\left|\!\left|\!\left|\tilde{v}(u)\right|\!\right|\!\right|_j &\leq (2C_{3.7}+1)\left|\!\left|\!\left|u\right|\!\right|\!\right|_j + \left|\!\left|\!\left|v^*(u)\right|\!\right|\!\right|_j \\ &\leq (2C_{3.7}+C_{3.8}+1)\left|\!\left|\!\left|u\right|\!\right|\!\right|_j.\end{aligned}$$

Hence with Lemma 3.6 and Lemma 3.7:

$$\begin{aligned}&B(u,\tilde{v}(u)) + J(u,\tilde{v}(u)) \\ &= (2C_{3.7}+1)\left[B(u,u)+J(u,u)\right] + B(u,\Delta_t\partial_t u) + J(u,\Delta_t\partial_t u) \\ &\geq (2C_{3.7}+1)\left(\frac{1}{2}\left[\!\left[u\right]\!\right]^2 + \sum_{n=1}^{N}(\nabla u,\nabla u)_{Q^n} + J(u,u)\right) + \frac{1}{2}\sum_{n=1}^{N}\Delta t(\partial_t u,\partial_t u)_{Q^n} \\ &\quad - C_{3.7}\left(\left[\!\left[u\right]\!\right]^2 + \sum_{n=1}^{N}(\nabla u,\nabla u)_{Q^n} + J(u,u)\right) \\ &= \frac{1}{2}\left[\!\left[u\right]\!\right]^2 + (1+C_{3.7})\left(\sum_{n=1}^{N}(\nabla u,\nabla u)_{Q^n} + J(u,u)\right) + \frac{1}{2}\sum_{n=1}^{N}\Delta t(\partial_t u,\partial_t u)_{Q^n} \\ &\geq \frac{1}{2}\left|\!\left|\!\left|u\right|\!\right|\!\right|_j^2 \geq \frac{1}{2(2C_{3.7}+C_{3.8}+1)}\left|\!\left|\!\left|u\right|\!\right|\!\right|_j\left|\!\left|\!\left|\tilde{v}(u)\right|\!\right|\!\right|_j.\end{aligned}$$

□

3.2.3 Continuity

The continuity of the bilinear form $B(\cdot,\cdot)$ with respect to the first argument is needed in a non-discrete space, since it has to be evaluated later at the solution of the continuous problem.

Proposition 3.10 (Continuity)**.** *For all* $u \in W_h + H^1(Q)$ *and* $v \in W_h$ *there holds*

$$\begin{aligned}B(u,v) &\leq C_{3.10}\left|\!\left|\!\left|u\right|\!\right|\!\right|_*\left|\!\left|\!\left|v\right|\!\right|\!\right|, \\ J(u,v) &\leq \left\|u\right\|_J\left\|v\right\|_J,\end{aligned}$$

for $C_{3.10} = 4 + \left\|\mathbf{w}\right\|_\infty \sqrt{C_o}$.

Proof. Here one can use the representation $B(u,v) = d'(u,v) + b'(u,v) + a(u,v)$ obtained in Lemma 2.1. We bound the terms one after another:

- By the Cauchy-Schwarz inequality and the boundedness assumption on $\|\mathbf{w}\|_\infty$:

$$\begin{aligned}
d'(u,v) &= \sum_{n=1}^{N} \left(u, -\partial_t v - \mathbf{w}\cdot\nabla v\right)_{Q^n} \\
&\leq \sum_{n=1}^{N} \sqrt{\left(\frac{1}{\Delta t}u, u\right)_{Q^n} (\Delta t \partial_t v, \partial_t v)_{Q^n}} + \sum_{n=1}^{N} \sqrt{\left(\frac{1}{\Delta t}u, u\right)_{Q^n} (\Delta t \mathbf{w}\cdot\nabla v, \mathbf{w}\cdot\nabla v)_{Q^n}} \\
&\leq \sqrt{\sum_{n=1}^{N} \left(\frac{1}{\Delta t}u, u\right)_{Q^n}} \left(\sqrt{\sum_{n=1}^{N} (\Delta t \partial_t v, \partial_t v)_{Q^n}} + \|\mathbf{w}\|_\infty \sqrt{\Delta t} \sqrt{\sum_{n=1}^{N} (\nabla v, \nabla v)_{Q^n}}\right) \\
&\leq \left(1 + \|\mathbf{w}\|_\infty \sqrt{C_{\mathrm{o}}}\right) |||u|||_* |||v|||.
\end{aligned}$$

- For $u \in H^1(Q)$ the inverse inequality from Lemma 3.3 is not available. Thus, the term $[\![u]\!]_*$ has been included into the $|||\cdot|||_*$-norm.

$$\begin{aligned}
b'(u,v) &\leq \sum_{n=1}^{N-1} \sqrt{(u_-^n, u_-^n)_{\Omega^n}} \sqrt{([\![v]\!]^n, [\![v]\!]^n)_{\Omega^n}} + \sqrt{(u_-^N, u_-^N)_{\Omega^N}} \sqrt{(v_-^N, v_-^N)_{\Omega^N}} \\
&\leq \sqrt{\sum_{n=1}^{N-1} (u_-^n, u_-^n)_{\Omega^n}} \sqrt{\sum_{n=1}^{N-1} ([\![v]\!]^n, [\![v]\!]^n)_{\Omega^n}} + \sqrt{(u_-^N, u_-^N)_{\Omega^N}} \sqrt{(v_-^N, v_-^N)_{\Omega^N}} \\
&\leq |||u|||_* \left(\sqrt{\sum_{n=1}^{N-1} ([\![v]\!]^n, [\![v]\!]^n)_{\Omega^n}} + \sqrt{(v_-^N, v_-^N)_{\Omega^N}}\right) \\
&\leq 2|||u|||_* |||v|||.
\end{aligned}$$

- The diffusion term is easily bounded:

$$a(u,v) \leq \sqrt{\sum_{n=1}^{N} (\nabla u, \nabla u)_{Q^n}} \sqrt{\sum_{n=1}^{N} (\nabla v, \nabla v)_{Q^n}} \leq |||u|||_* |||v|||.$$

- The stabilization term can be bounded by repeated application of the Cauchy-Schwarz inequality:

$$\begin{aligned}
J(u,v) &= \sum_{n=1}^{N} \left(1 + \frac{\Delta t}{h}\right) \gamma_J \sum_{F \in \mathcal{F}_R^{*,n}} \int_{\omega_F \times I_n} \frac{1}{h} [\![u]\!]_{\omega_F} \frac{1}{h} [\![v]\!]_{\omega_F} \\
&\leq \sum_{n=1}^{N} \left(1 + \frac{\Delta t}{h}\right) \gamma_J \sum_{F \in \mathcal{F}_R^{*,n}} \sqrt{\int_{\omega_F \times I_n} \frac{1}{h^2} [\![u]\!]^2_{\omega_F}} \sqrt{\int_{\omega_F \times I_n} \frac{1}{h^2} [\![v]\!]^2_{\omega_F}} \\
&\leq \sum_{n=1}^{N} \sqrt{\left(1 + \frac{\Delta t}{h}\right) \gamma_J \sum_{F \in \mathcal{F}_R^{*,n}} \int_{\omega_F \times I_n} \frac{1}{h^2} [\![u]\!]^2_{\omega_F}} \sqrt{\left(1 + \frac{\Delta t}{h}\right) \gamma_J \sum_{F \in \mathcal{F}_R^{*,n}} \int_{\omega_F \times I_n} \frac{1}{h^2} [\![v]\!]^2_{\omega_F}} \\
&\leq \sqrt{\sum_{n=1}^{N} \left(1 + \frac{\Delta t}{h}\right) \gamma_J \sum_{F \in \mathcal{F}_R^{*,n}} \int_{\omega_F \times I_n} \frac{1}{h^2} [\![u]\!]^2_{\omega_F}} \sqrt{\sum_{n=1}^{N} \left(1 + \frac{\Delta t}{h}\right) \gamma_J \sum_{F \in \mathcal{F}_R^{*,n}} \int_{\omega_F \times I_n} \frac{1}{h^2} [\![v]\!]^2_{\omega_F}} \\
&= \sqrt{J(u,u)} \sqrt{J(v,v)} = \|u\|_J \|v\|_J .
\end{aligned}$$

□

3.2.4 Consistency

Proposition 3.11 (consistency error)**.** *Let $u \in H^2(Q)$ be the solution of (2.1) and u_h be the solution of (2.7). Then there holds:*

$$B(u - u_h, v_h) - J(u_h, v_h) = 0 \text{ for all } v_h \in W_h.$$

Proof. Let $v \in W_h$. From $u \in H^2(Q)$ it folllows that $-\Delta u \in L^2(Q)$ and $[\![u]\!]^n = 0$ for $n = 1, \dots, N-1$ in the $L^2(\Omega^n)$ sense. Thus, $b(u, v) = \left(u_0, v_+^0\right)_{\Omega^0}$.

Moreover, integration by parts of the diffusion term leads to $a(u, v) = -\sum_{n=1}^{N} (\Delta u, v)_{Q^n}$ due to homogeneous Neumann boundary conditions. Hence,

$$\begin{aligned} B(u, v) &= d(u, v) + b(u, v) + a(u, v) \\ &= \sum_{n=1}^{N} (\partial_t u + \mathbf{w} \cdot \nabla u - \Delta u, v)_{Q^n} + \left(u_0, v_+^0\right)_{\Omega^0} \\ &= \sum_{n=1}^{N} (f, v)_{Q^n} + \left(u_0, v_+^0\right)_{\Omega^0} = f(v). \end{aligned}$$

Subtracting from this the equation

$$B(u_h, v) + J(u_h, v) = f(v)$$

for the discrete solution yields the claim. □

3.2.5 Céa-like result

Theorem 3.12 (Céa-like result)**.** *Let $u \in H^2(Q)$ be the solution of (2.1) and u_h be the solution of (2.7). Then there holds:*

$$|||u - u_h||| \leq \inf_{w_h \in W_h} \left(|||u - w_h||| + C_{3.12} |||u - w_h|||_* + (C_{3.9})^{-1} \|w_h\|_J \right), \tag{3.9}$$

with $C_{3.12} = C_{3.10}(C_{3.9})^{-1}$.

Remark 11. *The first two terms in the estimate (3.9) above describe the approximation error of the solution u in the space W_h with respect to the norms $|||\cdot|||$ and $|||\cdot|||_*$. Denote by w_h the best approximation to u in W_h. Then the last term in (3.9) measures the semi-norm $\|w_h\|_J$ of the best approximation rather than the approximation error $u - w_h$ itself. This is reasonable, since we have defined $J(\cdot, \cdot)$ only for discrete functions. An estimate for $\|w_h\|_J$ will be shown in Proposition 3.26. The key observation for obtaining this estimate is the possibility to bound the jump on the facet patches ω_F from above by the approximation error of an L^2-projection P_{ω_F} on the facet patch:*

$$\|[\![w_h]\!](\cdot, t)\|_{\omega_F} \leq C \|(w_h - P_{\omega_F} w_h)(\cdot, t)\|_{\omega_F}.$$

Proof. Choose an arbitrary $w_h \in W_h$ and split the error into two parts:

$$|||u - u_h||| \leq |||e_u||| + |||e_w|||,$$

with $e_u = u - w_h$ and $e_w = w_h - u_h$. Combining Propositions 3.9, 3.10 and 3.11 from above (and introducing $q = \tilde{v}(e_w)$ with $\tilde{v}(\cdot)$ as in Proposition 3.9) yields

$$\begin{aligned}
|||e_w|||\,|||q|||_j \leq |||e_w|||_j |||q|||_j &\leq (C_{3.9})^{-1} \left(B(e_w, q) + J(e_w, q)\right) \\
&= (C_{3.9})^{-1} \left(B(w_h, q) + J(w_h, q) - B(u_h, q) - J(u_h, q)\right) \\
&= (C_{3.9})^{-1} \left(B(w_h, q) + J(w_h, q) - B(u, q)\right) \\
&= (C_{3.9})^{-1} \left(B(-e_u, q) + J(w_h, q)\right) \\
&\leq C_{3.10}(C_{3.9})^{-1} |||e_u|||_* |||q|||_j + (C_{3.9})^{-1} \|w_h\|_J \, |||q|||_j.
\end{aligned}$$

It follows that:

$$|||e_w||| \leq C_{3.10}(C_{3.9})^{-1} |||e_u|||_* + (C_{3.9})^{-1} \|w_h\|_J .$$

As w_h may be chosen arbitrarily the result follows.

□

3.3 Interpolation in space-time

In order to derive an a priori estimate from Theorem 3.12 an interpolation operator I_Γ mapping $H^k(Q)$ into the space-time finite element space W_h is needed. The global interpolation operator will be defined by its restriction to the time slabs $I_\Gamma^n : H^k(Q^n) \to W_n$. So the task is to construct I_Γ^n. This operator will be build step by step.

In subsection 3.3.1 we first construct an interpolation operator $\Pi_W^n : L^2(\mathcal{E}(Q^n)) \to W_n$. Here the space-time domain $\mathcal{E}(Q^n) = \mathcal{E}(\Omega^n) \times I_n$ has a tensor product structure. In order to keep the notation short we denote $Q^n = \Omega \times I_n$ in this subsection with a generic polyhedral domain Ω. We may think of Ω as the extended spatial domain which combined with I_n forms the extended space-time slab. The operator Π_W^n is obtained by concatenation of purely temporal and purely spatial interpolation operators. Consequently, the first task will be the construction of these operators.

If the operator Π_W^n for tensor product domains with the desired approximation properties is available, then I_Γ^n can be defined by means of assumption A.5.

3.3.1 Interpolation in tensor-product space-time spaces

In this section we consider space-time slabs with tensor product structure $Q^n = \Omega \times I_n$. In [Leh15] suitable space-time interpolation operators for the piecewise linear case have been constructed. The aim of this section is to generalize these results.

Anisotropic Sobolev spaces

We introduce anisotropic Sobolev spaces (see eg. [BIN78],[WYW06]) on the space-time domain Q in which temporal and spatial derivatives are treated differently. Due to the special role of the time, these spaces are also called t-anisotropic Sobolev spaces. Define:

$$H^{k,l}(Q) := \{u \mid \partial_t^p D_x^\alpha u \in L^2(Q), p, q \in \mathbb{N}, q = |\alpha|, \frac{q}{k} + \frac{p}{l} \leq 1\}. \tag{3.10}$$

For $k = l$ the isotropic Sobolev spaces are retained: $H^{k,k}(Q) = H^k(Q)$. Moreover, there exists a (time) trace operator $H^{0,1}(Q^n) \to L^2(\Omega)$, which is bounded:

$$\|u(\cdot, t)\|_\Omega \leq C \|u\|_{H^{0,1}(Q^n)} .$$

Semi-discrete spaces

For the tensor product case $Q^n = \Omega \times I_n$, with a polygonal domain Ω, we define the following spaces on the time slab. Let $\mathcal{P}^{k_t}$ denote the space of polynomials up to degree k_t on I_n.

For $X \subset L^2(\Omega)$ define

$$X \otimes \mathcal{P}^{k_t} := \{v \in L^2(Q^n) \mid v(x,t) = \sum_{m=0}^{k_t} t^m v_m(x),\ v_m \in X\}. \tag{3.11}$$

For $Y \subset L^2(I_n)$ and $V_h^{k_s}$ a standard finite element space on Ω define

$$V_h^{k_s} \otimes Y := \{v \in L^2(Q^n) \mid v(x,t) = \sum_{i=0}^{N} v_i(t)\phi_i(x),\ v_i \in Y, \phi_i \in V_h^{k_s}, N = \dim(V_h^{k_s})\}. \tag{3.12}$$

For $Q^n = \Omega \times I_n$ we seek to construct an interpolation operator into the space:

$$W_n = \{v : Q^n \to \mathbb{R} \mid v(x,t) = \sum_{m=0}^{k_t} t^m \phi_m(x),\ \phi_m \in V_h^{k_s}, m = 0, \ldots, k_t\}. \tag{3.13}$$

Using the notation introduced above one has $W_n = V_h^{k_s} \otimes \mathcal{P}^{k_t}$. Later this operator will be extended to the unfitted case.

Interpolation in time

For $u \in L^2(I_n; X)$ define the temporal interpolation $\Pi^{k_t}(u)$ as the $L^2(I_n; X)$ projection of u into $X \otimes \mathcal{P}^{k_t}$, so that $\Pi^{k_t}(u)$ solves

$$(\Pi^{k_t}(u) - u, v)_{Q^n} = 0 \quad \forall v \in X \otimes \mathcal{P}^{k_t}. \tag{3.14}$$

In the following the general case $X = L^2(\Omega)$ is considered.

On sufficiently smooth functions, Π^{k_t} coincides with a standard temporal $L^2(I_n)$ (quasi-) interpolation I^{k_t} defined by

$$\left(I^{k_t} u, \chi\right)_{I_n} = (u, \chi)_{I_n} \quad \forall\ \chi \in \mathcal{P}^{k_t}.$$

That is, for $u \in C^0(\Omega; L^2(I_n))$ it will be shown in the next Lemma that $\Pi^{k_t} u = I^{k_t} u$ holds in the $L^2(Q^n)$ sense. Another important property of Π^{k_t} is that it commutes with spatial derivatives ∂_{x_j}. For the standard temporal interpolation on $L^2(I_n)$ this property readily follows by an explicit description of this operator: Let $\phi_i(t)$ for $i = 0, \ldots, k_t$ be a basis of $\mathcal{P}^{k_t}$ and $\psi_j, j = 0, \ldots, k_t$ be its dual basis with respect to $(\cdot,\cdot)_{I_n}$, i.e. $(\phi_i, \psi_j)_{I_n} = \delta_{i,j}$ for $i, j = 0, \ldots, k_t$. Then

$$I^{k_t} u(x,\cdot) = \sum_{i=0}^{k_t} (u(x,\cdot), \psi_i)_{I_n} \phi_i$$

holds for $u \in C^1(\Omega; I_n)$. Hence,

$$\begin{aligned} \partial_{x_j} I^{k_t} u(x,\cdot) &= \sum_{i=0}^{k_t} \left((\partial_{x_j} u)(x,\cdot), \psi_i\right)_{I_n} \phi_i \\ &= I^{k_t} \partial_{x_j} u(x,\cdot) \end{aligned}$$

follows. In order to extend this property to Π^{k_t}, which is defined for functions with weaker regularity, the following Lemma is needed.

Lemma 3.13 (equivalent characterization of weak derivatives)**.** *Consider $\hat{Q} = \Omega \times \hat{I}$, with $\hat{I} = (0, 1]$ and let $u \in L^2(\hat{Q})$. Denote by $C_c^\infty(\hat{Q})$ the smooth functions with compact support in $\hat{Q}$ and by $C^\infty(\hat{I}; C_c^\infty(\Omega))$ the smooth functions ϕ such that $\phi(\cdot, t) \in C_c^\infty(\Omega)$ for every $t \in \hat{I}$. Then $w \in L^2(\hat{Q})$ fulfills*

$$\big(w, \bar{\phi}\big)_{\hat{Q}} = -\big(u, \partial_{x_j}\bar{\phi}\big)_{\hat{Q}} \quad \forall \bar{\phi} \in C_c^\infty(\hat{Q}), \tag{3.15}$$

if and only if w fulfills

$$(w, \phi)_{\hat{Q}} = -\big(u, \partial_{x_j}\phi\big)_{\hat{Q}} \quad \forall \phi \in C^\infty(\hat{I}; C_c^\infty(\Omega)). \tag{3.16}$$

Proof. Since $C_c^\infty(\hat{Q})$ is a subset of $C^\infty(\hat{I}; C_c^\infty(\Omega))$ the direction (3.16) $\implies$ (3.15) immediately follows. We need to show (3.15) $\implies$ (3.16). Let $\phi \in C^\infty(\hat{I}; C_c^\infty(\Omega))$ be given. We will construct a sequence $\phi_\varepsilon \in C_c^\infty(\hat{Q})$ which converges to ϕ in an $L^2(\hat{Q})$ sense. To this end, pick $\psi \in C^\infty(\mathbb{R})$ such that

$$0 \le \psi \le 1 \quad \text{and} \quad \psi(t) = \begin{cases} 1 & t \ge 1, \\ 0 & t \le 1/2. \end{cases}$$

For $\varepsilon \le 1/2$ set

$$\psi_\varepsilon(t) = \psi\left(\frac{t}{\varepsilon}\right)\psi\left(\frac{1-t}{\varepsilon}\right) = \begin{cases} 0 & t \le \varepsilon/2, \\ 1 & \varepsilon \le t \le 1-\varepsilon, \\ 0 & t \ge 1-\varepsilon/2. \end{cases}$$

Then ψ_ε is smooth, compactly supported in $[\varepsilon/2, 1-\varepsilon/2]$ and fulfills $0 \le \psi_\varepsilon \le 1$. Figure 3.3 shows a sketch of this function. Setting $\phi_\varepsilon(x,t) = \psi_\varepsilon(t)\phi(x,t)$ yields $\phi_\varepsilon \in C_c^\infty(\hat{Q})$, which fulfills:

$$|\phi_\varepsilon(x,t) - \phi(x,t)|^2 = |\psi_\varepsilon(t) - 1|^2 \, |\phi(x,t)|^2 \le 4 \, |\phi(x,t)|^2 .$$

Hence, an application of Lebesgue's dominated convergence theorem yields

$$\lim_{\varepsilon \to +0} \|\phi_\varepsilon - \phi\|_{\hat{Q}}^2 = \int_\Omega \int_{\hat{I}} \lim_{\varepsilon \to +0} |\psi_\varepsilon(t) - 1|^2 \, |\phi(x,t)|^2 \; dt \, dx = 0,$$

since ψ_ε converges to the identity on $\hat{I}$ as $\varepsilon \to +0$.

From $\partial_{x_j}\phi_\varepsilon(x,t) = \psi_\varepsilon(t)\partial_{x_j}\phi(x,t)$ we also obtain that

$$\big\|\partial_{x_j}\phi_\varepsilon - \partial_{x_j}\phi\big\|_{\hat{Q}} \to 0, \text{ as } \varepsilon \to +0.$$

This allows to show the claim. As $\phi_\varepsilon \in C_c^\infty(\hat{Q})$ it holds that $(w, \phi_\varepsilon)_{\hat{Q}} = -\big(u, \partial_{x_j}\phi_\varepsilon\big)_{\hat{Q}}$. Hence,

$$(w, \phi)_{\hat{Q}} = \lim_{\varepsilon \to +0} (w, \phi_\varepsilon)_{\hat{Q}} = -\lim_{\varepsilon \to +0} \big(u, \partial_{x_j}\phi_\varepsilon\big)_{\hat{Q}} = -\big(u, \partial_{x_j}\phi\big)_{\hat{Q}}.$$

□

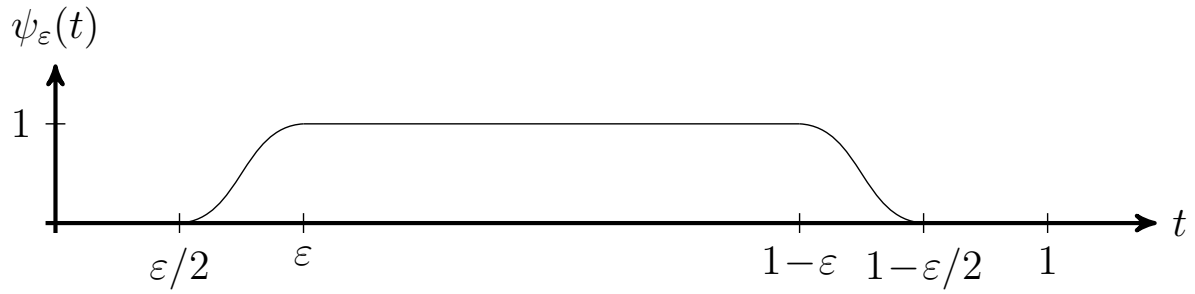

Figure 3.3: Sketch of the function ψ_ε for $\varepsilon = 1/4$.

This allows to prove the following Lemma which serves as a basis for the approximation properties of Π^{k_t}.

Lemma 3.14. *For $u \in C^0(\Omega; L^2(I_n))$ there holds*

$$\Pi^{k_t} u = I^{k_t} u \text{ in the } L^2(Q^n) \text{ sense.}$$

Moreover, for $u \in H^{1,0}(Q^n)$ the temporal interpolation commutes with spatial derivatives

$$\partial_{x_j} \Pi^{k_t} u = \Pi^{k_t} \partial_{x_j} u$$

for $j = 1, \dots, d$.

Proof. Let $u \in C^0(\Omega; L^2(I_n))$. Then for every $x \in \Omega$ it follows that $I^{k_t} u(x, \cdot)$ is well defined. We will show that $I^{k_t} u$ fulfills (3.14). Let $v_h \in L^2(\Omega) \otimes \mathcal{P}^{k_t}$ be given. There are $v_m \in L^2(\Omega)$ and $\chi_m \in \mathcal{P}^{k_t}$ such that $v_h(x,t) = \sum_{m=0}^{k_t} v_m(x)\chi_m(t)$. By definition of I^{k_t} one has that

$$\big(I^{k_t} u(x,\cdot), \chi_m\big)_{I_n} = (u(x,\cdot), \chi_m)_{I_n}$$

holds for all $m = 0, \dots, k_t$. Multiplying this equality by $v_m(x)$, summing up over $m = 0, \dots, k_t$ and integrating over Ω leads to

$$\int_\Omega \int_{I_n} I^{k_t} u(x,t) \sum_{m=0}^{k_t} v_m(x)\chi_m(t)\, dt\, dx = \int_\Omega \int_{I_n} u(x,t) \sum_{m=0}^{k_t} v_m(x)\chi_m(t)\, dt\, dx.$$

That is, $\big(I^{k_t} u, v_h\big)_{Q^n} = (u, v_h)_{Q^n}$ holds. Comparing with (3.14) it follows that: $\Pi^{k_t} u = I^{k_t} u$ in the $L^2(Q^n)$ sense.

It remains to show that Π^{k_t} commutes with spatial derivatives. Let $u \in H^{1,0}(Q^n)$ be given. We will show that $\partial_{x_j} \Pi^{k_t} u = \Pi^{k_t} \partial_{x_j} u$ holds in the sense of weak derivatives. To this end, it suffices to test against functions $\phi \in C^\infty(\hat{I}; C_c^\infty(\Omega))$ due to Lemma 3.13. Then

$$\begin{aligned}\big(\partial_{x_j} \Pi^{k_t} u, \phi\big)_{Q^n} &= -\big(\Pi^{k_t} u, \partial_{x_j}\phi\big)_{Q^n} = -\big(u, \Pi^{k_t} \partial_{x_j}\phi\big)_{Q^n} \\ &= -\big(u, I^{k_t} \partial_{x_j}\phi\big)_{Q^n} = -\big(u, \partial_{x_j} I^{k_t}\phi\big)_{Q^n},\end{aligned}$$

where it was used that ϕ is smooth such that Π^{k_t} coincides with the standard temporal $L^2(I_n)$ interpolation which is known to commute with spatial derivatives. Since $\phi \in$

$C^\infty(\hat{I}; C_c^\infty(\Omega))$, we have $I^{k_t}\phi \in C^\infty(\hat{I}; C_c^\infty(\Omega))$. From the definition of weak derivatives we conclude that

$$-\big(u, \partial_{x_j} I^{k_t}\phi\big)_{Q^n} = \big(\partial_{x_j} u, I^{k_t}\phi\big)_{Q^n} = \big(\partial_{x_j} u, \Pi^{k_t}\phi\big)_{Q^n} = \big(\Pi^{k_t}\partial_{x_j} u, \phi\big)_{Q^n}.$$

This implies: $\partial_{x_j}\Pi^{k_t} u = \Pi^{k_t}\partial_{x_j} u$ for $j = 1, \dots, d$. □

Remark 12. *Note that $\phi \in C_c^\infty(Q^n)$ does not imply $I^{k_t}\phi \in C_c^\infty(Q^n)$. Therefore, we use the equivalent definition of weak derivatives from Lemma 3.13 in this proof.*

Let $\mathcal{L}^{k_t} = id - \Pi^{k_t}$ denote the temporal interpolation error. The stability and approximation properties of Π^{k_t} can now be derived from the corresponding properties for I^{k_t}.

Lemma 3.15. *For the projector $\Pi^{k_t} : L^2(Q^n) \to L^2(\Omega) \otimes \mathcal{P}^{k_t}$ there hold the following stability and approximation properties:*

(a) $\big\|\Pi^{k_t} u\big\|_{Q^n} \leq \|u\|_{Q^n} \quad \forall u \in L^2(Q^n)$,

(b) $\big\|\partial_t \Pi^{k_t} u\big\|_{Q^n} \leq C \|u\|_{H^{0,1}(Q^n)} \quad \forall u \in H^{0,1}(Q^n)$,

(c) $\big\|\mathcal{L}^{k_t} u\big\|_{Q^n} \leq C\Delta t^l \|u\|_{H^{0,l}(Q^n)} \quad \forall u \in H^{0,l}(Q^n), \quad l \in \{1, \dots, k_t + 1\}$,

(d) $\big\|\partial_t \mathcal{L}^{k_t} u\big\|_{Q^n} \leq C\Delta t^{l-1} \|u\|_{H^{0,l}(Q^n)} \quad \forall u \in H^{0,l}(Q^n), \quad l \in \{2, \dots, k_t + 1\}$.

Proof. *(a)* To prove this, one does not need to resort to results about I^{k_t}. We have

$$\begin{aligned}
0 &\leq \big(\Pi^{k_t} u - u, \Pi^{k_t} u - u\big)_{Q^n} \\
&= \big(\Pi^{k_t} u, \Pi^{k_t} u\big)_{Q^n} + (u, u)_{Q^n} - 2\big(\Pi^{k_t} u, u\big)_{Q^n} \\
&= \big(\Pi^{k_t} u, \Pi^{k_t} u\big)_{Q^n} + (u, u)_{Q^n} - 2\big(\Pi^{k_t} u, \Pi^{k_t} u\big)_{Q^n} \\
&= -\big(\Pi^{k_t} u, \Pi^{k_t} u\big)_{Q^n} + (u, u)_{Q^n},
\end{aligned}$$

which implies (a).

(b) Let $u \in H^{0,1}(Q^n)$ be given. Since smooth functions are dense in the anisotropic Sobolev spaces there exists a sequence $u^\varepsilon \in C^1(Q^n)$ such that $\|u^\varepsilon - u\|_{H^{0,1}(Q^n)} \to 0$ as $\varepsilon \to +0$. Then

$$\begin{aligned}
\big\|\partial_t \Pi^{k_t} u\big\|_{Q^n} &\leq \big\|\partial_t \Pi^{k_t}(u - u^\varepsilon)\big\|_{Q^n} + \big\|\partial_t \Pi^{k_t} u^\varepsilon\big\|_{Q^n} \\
&\leq \frac{C}{\Delta t} \big\|\Pi^{k_t}(u - u^\varepsilon)\big\|_{Q^n} + \big\|\partial_t \Pi^{k_t} u^\varepsilon\big\|_{Q^n} \\
&\leq \frac{C}{\Delta t} \|u - u^\varepsilon\|_{Q^n} + \big\|\partial_t \Pi^{k_t} u^\varepsilon\big\|_{Q^n},
\end{aligned}$$

where the inverse inequality for polynomials and the stability estimate from (a) was used. Since $\|u - u^\varepsilon\|_{Q^n} \to 0$ as $\varepsilon \to +0$, it remains to treat $\big\|\partial_t \Pi^{k_t} u^\varepsilon\big\|_{Q^n}$. As u^ε is sufficiently smooth we have $\Pi^{k_t} u^\varepsilon = I^{k_t} u^\varepsilon$. For I^{k_t} there is the stability estimate (see Corollary 7.8 in [Bra07]):

$$\big\|\partial_t I^{k_t} u^\varepsilon(x, \cdot)\big\|_{I_n} \leq C \|u^\varepsilon(x, \cdot)\|_{H^1(I_n)}.$$

Integrating over Ω yields:

$$\left\|\partial_t I^{k_t} u^\varepsilon\right\|_{Q^n} \leq C \left\|u^\varepsilon\right\|_{H^{0,1}(Q^n)}.$$

Letting $\varepsilon \to +0$ then gives

$$\left\|\partial_t \Pi^{k_t} u\right\|_{Q^n} \leq C \left\|u\right\|_{H^{0,1}(Q^n)}.$$

(c) Here one proceeds similar to (b). For $u \in H^{0,l}(Q^n)$ pick a sequence $u^\varepsilon \in C^l(Q^n)$ such that $\|u^\varepsilon - u\|_{H^{0,l}(Q^n)} \to 0$ as $\varepsilon \to +0$. By the triangle inequality and (a):

$$\begin{aligned}\left\|\mathcal{L}^{k_t} u\right\|_{Q^n} &\leq \left\|\mathcal{L}^{k_t}(u - u^\varepsilon)\right\|_{Q^n} + \left\|\mathcal{L}^{k_t} u^\varepsilon\right\|_{Q^n} \\ &\leq 2\left\|u - u^\varepsilon\right\|_{Q^n} + \left\|\mathcal{L}^{k_t} u^\varepsilon\right\|_{Q^n}.\end{aligned}$$

The first term goes to zero as $\varepsilon \to +0$. As u^ε is sufficiently smooth: $\mathcal{L}^{k_t} u^\varepsilon = (id - I^{k_t}) u^\varepsilon$ holds. This allows to use the interpolation results for I^{k_t} (cf. Lemma 1.58 of [DPE12]):

$$\begin{aligned}\left\|\mathcal{L}^{k_t} u^\varepsilon\right\|_{Q^n}^2 &= \int_\Omega \left\|(id - I^{k_t}) u^\varepsilon(x, \cdot)\right\|_{I_n}^2 \, dx \\ &\leq C\Delta t^{2l} \int_\Omega \left\|u^\varepsilon(x, \cdot)\right\|_{H^l(I_n)}^2 \, dx.\end{aligned}$$

Letting $\varepsilon \to +0$ gives

$$\left\|\mathcal{L}^{k_t} u\right\|_{Q^n} \leq C\Delta t^l \left\|u\right\|_{H^{0,l}(Q^n)} \quad \text{for } l \in \{1, \ldots, k_t + 1\}.$$

(d) The proof is done as in (c) with the difference that there is an additional time derivative in the norms. One then estimates

$$\begin{aligned}\left\|\partial_t \mathcal{L}^{k_t} u\right\|_{Q^n} &\leq \left\|\partial_t \mathcal{L}^{k_t}(u - u^\varepsilon)\right\|_{Q^n} + \left\|\partial_t \mathcal{L}^{k_t} u^\varepsilon\right\|_{Q^n} \\ &\leq 2C\left\|u - u^\varepsilon\right\|_{H^{0,1}(Q^n)} + \left\|\partial_t \mathcal{L}^{k_t} u^\varepsilon\right\|_{Q^n}\end{aligned}$$

by using (b) instead of (a) and proceeds as above.

□

Interpolation in space

Define the projector $\Pi^{k_s} : L^2(Q^n) \to V_h^{k_s} \otimes Y$, so that for $u \in L^2(Q^n)$

$$(\Pi^{k_s}(u) - u, v_h)_{Q^n} = 0, \quad \text{for all } v_h \in V_h^{k_s} \otimes Y. \tag{3.17}$$

In the following the general case $Y = L^2(\Omega)$ is considered. This interpolation operator is a generalization of the standard $L^2(\Omega)$ (quasi) interpolation. The argument for establishing stability and approximation properties of this operator then runs similar as for the temporal interpolation Π^{k_t}. On sufficiently smooth functions Π^{k_s} coincides with a spatial $L^2(\Omega)$ projector $I^{k_s} : L^2(\Omega) \to V_h^{k_s}$. This is proven in [Leh15] with an argument which is independent of the polynomial degree k_s. Thus, we only cite the result and move on.

Lemma 3.16. *Let $I^{k_s} : L^2(\Omega) \to V_h^{k_s}$ be the spatial $L^2(\Omega)$ (quasi-) interpolation operator. Then there holds for $u \in L^2(\Omega) \otimes C^0(I_n) = C^0(I_n, L^2(\Omega))$*

$$\Pi^{k_s} u = I^{k_s} u \quad \text{in the } L^2(Q^n) \text{ sense.} \tag{3.18}$$

Further, for $u \in H^{0,1}(Q^n)$ there holds:

$$\Pi^{k_s} \partial_t u = \partial_t \Pi^{k_s} u. \tag{3.19}$$

Proof. See Lemma 3.3.5 of [Leh15]. □

Let $\mathcal{L}^{k_s} = id - \Pi^{k_s}$ denote the spatial interpolation error. The next Lemma shows that the projection into the semi-discrete space is stable and has the expected approximation properties.

Lemma 3.17. *For the projector $\Pi^{k_s} : L^2(Q^n) \to V_h^{k_s} \otimes L^2(\Omega)$ there hold the following stability and approximation results:*

(a) $\left\|\Pi^{k_s} u\right\|_{Q^n} \leq \|u\|_{Q^n} \quad \forall u \in L^2(Q^n),$

(b) $\left\|\nabla \Pi^{k_s} u\right\|_{Q^n} \leq C \|u\|_{H^{1,0}(Q^n)} \quad \forall u \in H^{1,0}(Q^n),$

(c) $\left\|\mathcal{L}^{k_s} u\right\|_{Q^n} \leq C h^s \|u\|_{H^{s,0}(Q^n)} \quad \forall u \in H^{s,0}(Q^n), \quad s \in \{1, \ldots, k_s + 1\},$

(d) $\left\|\nabla \mathcal{L}^{k_s} u\right\|_{Q^n} \leq C h^{s-1} \|u\|_{H^{s,0}(Q^n)} \quad \forall u \in H^{s,0}(Q^n), \quad s \in \{2, \ldots, k_s + 1\}.$

Proof. *(a)* The proof is similar to the corresponding property for the temporal interpolation (cf. Lemma 3.15 (a)).

The arguments for (b)-(d) use the same approximation argument to reduce the claims to statements about the spatial $L^2(\Omega)$ (quasi-) interpolation operator I^{k_s}.

(b) The proof of (b) with suitable references for the higher order case has been given in Lemma 3.3.6 of [Leh15].

Hence, we will only show statement (c):

(c) Let $u \in H^{s,0}(Q^n)$. Pick a sequence $u^\varepsilon \in C^s(Q^n)$ such that $\|u^\varepsilon - u\|_{H^{s,0}(Q^n)} \to 0$ as $\varepsilon \to +0$. Using the triangle inequality and the stability estimate (a) yields:

$$\begin{aligned} \left\|\mathcal{L}^{k_s} u\right\|_{Q^n} &\leq \left\|\mathcal{L}^{k_s}(u - u^\varepsilon)\right\|_{Q^n} + \left\|\mathcal{L}^{k_s} u^\varepsilon\right\|_{Q^n} \\ &\leq 2 \|u - u^\epsilon\|_{Q^n} + \left\|\mathcal{L}^{k_s} u^\varepsilon\right\|_{Q^n}, \end{aligned}$$

where $\|u - u^\epsilon\|_{Q^n} \to 0$ as $\varepsilon \to +0$. It remains to estimate the other term. Since u^ϵ is sufficiently smooth we have that $\Pi^{k_s} u(\cdot, t) = I^{k_s} u(\cdot, t)$ where I^{k_s} is the (quasi-) $L^2(\Omega)$ interpolation operator. This allows to use the interpolation results for I^{k_s}. One obtains:

$$\begin{aligned} \left\|\mathcal{L}^{k_s} u^\varepsilon\right\|_{Q^n}^2 &= \int_{I^n} \left\|(id - I^{k_s}) u^\varepsilon(\cdot, t)\right\|_\Omega^2 \, dt \\ &\leq C h^{2s} \int_{I^n} \|u^\varepsilon(\cdot, t)\|_{H^s(\Omega)}^2 \, dt. \end{aligned}$$

Letting $\varepsilon \to +0$ yields

$$\left\|\mathcal{L}^{k_s} u\right\|_{Q^n} \leq C h^s \|u\|_{H^{s,0}(Q^n)}, \quad s \in \{1, \ldots, k_s + 1\}.$$

(d) The proof is done as in (c) with the difference that there is an additional gradient operator ∇ in the norms. One then estimates $\left\|\nabla\mathcal{L}^{k_s}(u-u^\varepsilon)\right\|_{Q^n} \leq C\left\|u-u^\varepsilon\right\|_{H^{1,0}(Q^n)}$ by using (b) instead of (a).

□

Interpolation in space-time

One can now define a space-time interpolation operator Π_W^n for the tensor product case $Q^n = \Omega \times I_n$ into the space W_n defined in (3.13). This is achieved by concatenating the spatial and temporal interpolation operation:

$$\Pi_W^n : L^2(Q^n) \to W_n, \quad \Pi_W^n(v) = \Pi^{k_t}(\Pi^{k_s}(v)),\ \forall v \in L^2(Q^n). \tag{3.20}$$

Since Π^{k_s} and Π^{k_t} are L^2-projections, the overall interpolation operator Π_W^n is an L^2-projection on $L^2(Q^n)$. For ease of notation we drop the index n of Π_W^n in this section and simply write Π_W.

Remark 13. *As an alternative, one may consider to replace the temporal L^2-projection Π^{k_t} in (3.20) by temporal nodal interpolation. For space-time functions $u(x,t)$ which are sufficiently regular in time it follows that the jump between the time slabs $[\![\Pi_W u]\!]^n = 0$ vanishes in an $L^2(\Omega^n)$ sense. But since this property is not needed in the subsequent analysis, we will keep working with Π^{k_t} as a temporal L^2-projection.*

Denote the interpolation error of Π_W by $\mathcal{L}_W = (id - \Pi_W)$. An important ingredient for establishing the approximation results of Π_W is that spatial derivatives commute with the temporal interpolation and vice versa (cf. Lemma 3.14 and Lemma 3.16).

Theorem 3.18. *For the interpolation operator Π_W as in (3.20) there hold the following approximation error bounds:*

(a) $\|u - \Pi_W u\|_{Q^n} \leq C\left(\Delta t^{l_t}\|u\|_{H^{0,l_t}(Q^n)} + h^{l_s}\|u\|_{H^{l_s,0}(Q^n)}\right)$ *for* $l_s \in \{1,\dots,k_s+1\}$ *and* $l_t \in \{1,\dots,k_t+1\}$.

(b) $\|\partial_t(u - \Pi_W u)\|_{Q^n} \leq C\left(\Delta t^{l_t-1}\|u\|_{H^{0,l_t}(Q^n)} + h^{l_s}\left(\|u\|_{H^{l_s,0}(Q^n)} + \|\partial_t u\|_{H^{l_s,0}(Q^n)}\right)\right)$, *for* $l_s \in \{1,\dots,k_s+1\}$ *and* $l_t \in \{2,\dots,k_t+1\}$.

(c) $\|\nabla(u - \Pi_W u)\|_{Q^n} \leq C\left(\Delta t^{l_t}\|\nabla u\|_{H^{0,l_t}(Q^n)} + h^{l_s-1}\|u\|_{H^{l_s,0}(Q^n)}\right)$, *for* $l_s \in \{2,\dots,k_s+1\}$ *and* $l_t \in \{1,\dots,k_t+1\}$.

Proof. For a differential operator $D \in \{id, \nabla, \partial_t\}$ one has:

$$\begin{aligned}
\|D\mathcal{L}_W u\|_{Q^n} &= \left\|D(u - \Pi^{k_t}\Pi^{k_s}u)\right\|_{Q^n} \\
&\leq \left\|D(u - \Pi^{k_t}u)\right\|_{Q^n} + \left\|D(\Pi^{k_t}u - \Pi^{k_t}\Pi^{k_s}u)\right\|_{Q^n} \\
&= \left\|D\mathcal{L}^{k_t}u\right\|_{Q^n} + \left\|D\Pi^{k_t}\mathcal{L}^{k_s}u\right\|_{Q^n}
\end{aligned}$$

We now consider the different cases for D:

- $D = id$:

  Here we apply the stability estimate for Π^{k_t} (Lemma 3.15 (a)) and then the approximation results for $\mathcal{L}^{k_t}$ (Lemma 3.15 (c)) and $\mathcal{L}^{k_s}$ (Lemma 3.17 (c)):

$$\begin{aligned}\|\mathcal{L}_W u\|_{Q^n} &\leq \left\|\mathcal{L}^{k_t} u\right\|_{Q^n} + \left\|\Pi^{k_t}\mathcal{L}^{k_s} u\right\|_{Q^n} \\ &\leq \left\|\mathcal{L}^{k_t} u\right\|_{Q^n} + \left\|\mathcal{L}^{k_s} u\right\|_{Q^n} \\ &\leq C\left(\Delta t^{l_t} \|u\|_{H^{0,l_t}(Q^n)} + h^{l_s} \|u\|_{H^{l_s,0}(Q^n)}\right),\end{aligned}$$

  for $l_s \in \{1, \dots, k_s + 1\}$ and $l_t \in \{1, \dots, k_t + 1\}$.

- $D = \nabla$:

  First we use that temporal interpolation commutes with the spatial derivatives. Then the stability estimate for the temporal interpolation is employed. Finally, one can apply the approximation results: Lemma 3.15 (c)) and Lemma 3.17 (d).

$$\begin{aligned}\|\nabla\mathcal{L}_W u\|_{Q^n} &\leq \left\|\nabla\mathcal{L}^{k_t} u\right\|_{Q^n} + \left\|\nabla\Pi^{k_t}\mathcal{L}^{k_s} u\right\|_{Q^n} \\ &= \left\|\mathcal{L}^{k_t}\nabla u\right\|_{Q^n} + \left\|\Pi^{k_t}\nabla\mathcal{L}^{k_s} u\right\|_{Q^n} \\ &\leq \left\|\mathcal{L}^{k_t}\nabla u\right\|_{Q^n} + \left\|\nabla\mathcal{L}^{k_s} u\right\|_{Q^n} \\ &\leq C\left(\Delta t^{l_t} \|\nabla u\|_{H^{0,l_t}(Q^n)} + h^{l_s-1} \|u\|_{H^{l_s,0}(Q^n)}\right),\end{aligned}$$

  for $l_s \in \{2, \dots, k_s + 1\}$ and $l_t \in \{1, \dots, k_t + 1\}$.

- $D = \partial_t$:

  Using the stability estimate Lemma 3.15 (b)) gives:

$$\begin{aligned}\|\partial_t\mathcal{L}_W u\|_{Q^n} &\leq \left\|\partial_t\mathcal{L}^{k_t} u\right\|_{Q^n} + \left\|\partial_t\Pi^{k_t}\mathcal{L}^{k_s} u\right\|_{Q^n} \\ &\leq \left\|\partial_t\mathcal{L}^{k_t} u\right\|_{Q^n} + C\left\|\mathcal{L}^{k_s} u\right\|_{H^{0,1}(Q^n)}.\end{aligned}$$

  Since spatial interpolation commutes with the time derivative we obtain by using Lemma 3.17 (c):

$$\begin{aligned}\left\|\mathcal{L}^{k_s} u\right\|^2_{H^{0,1}(Q^n)} &= \left\|\mathcal{L}^{k_s} u\right\|^2_{Q^n} + \left\|\mathcal{L}^{k_s}\partial_t u\right\|^2_{Q^n} \\ &\leq Ch^{2l_s}\left(\|u\|^2_{H^{l_s,0}(Q^n)} + \|\partial_t u\|^2_{H^{l_s,0}(Q^n)}\right).\end{aligned}$$

  Combinig this with the estimate $\left\|\partial_t\mathcal{L}^{k_t} u\right\|_{Q^n} \leq C\Delta t^{l_t-1} \|u\|_{H^{0,l_t}(Q^n)}$ from Lemma 3.15 (d) gives:

$$\|\partial_t\mathcal{L}_W u\|_{Q^n} \leq C\left(\Delta t^{l_t-1} \|u\|_{H^{0,l_t}(Q^n)} + h^{l_s}\left(\|u\|_{H^{l_s,0}(Q^n)} + \|\partial_t u\|_{H^{l_s,0}(Q^n)}\right)\right)$$

  for $l_s \in \{1, \dots, k_s + 1\}$ and $l_t \in \{2, \dots, k_t + 1\}$.

Together these inequalities give the claim. □

This yields the following bounds in terms of the norm in the isotropic Sobolev spaces on the time slab.

Corollary 3.19. *For $l_t, l_s \in \mathbb{N}$ define $l_{\max} = \max\{l_s, l_t\}$. For the interpolation operator Π_W as in (3.20) there hold the following approximation error bounds:*

(a) $\|u - \Pi_W u\|_{Q^n} \leq C\left(\Delta t^{l_t} + h^{l_s}\right)\|u\|_{H^{l_{\max}}(Q^n)}$, *for* $l_s \in \{1, \dots, k_s + 1\}$ *and* $l_t \in \{1, \dots, k_t + 1\}$.

(b) $\|\partial_t(u - \Pi_W u)\|_{Q^n} \leq C\left(\Delta t^{l_t - 1} + h^{l_s}\right)\|u\|_{H^{l_{\max}+1}(Q^n)}$, *for* $l_s \in \{1, \dots, k_s + 1\}$ *and* $l_t \in \{2, \dots, k_t + 1\}$.

(c) $\|\nabla(u - \Pi_W u)\|_{Q^n} \leq C\left(\Delta t^{l_t} + h^{l_s - 1}\right)\|u\|_{H^{l_{\max}+1}(Q^n)}$, *for* $l_s \in \{2, \dots, k_s + 1\}$ *and* $l_t \in \{1, \dots, k_t + 1\}$.

The previous estimates allow also to derive a bound on the approximation error of the interpolation operator Π_W at discrete time levels. For this we need a discrete inverse inequality in time:

Lemma 3.20 (Discrete inverse inequality in time)**.** *There exist a constant $C > 0$ such that*

$$\|u(\cdot, t_n)\|_\Omega \leq C\Delta t^{-1/2}\|u\|_{Q^n} \tag{3.21}$$

for all $u \in L^2(\Omega) \otimes \mathcal{P}^{k_t}$.

Proof. Denote by $C_c^\infty(\Omega)$ the C^∞ functions with compact support in Ω. By density of $C_c^\infty(\Omega)$ in $L^2(\Omega)$ it suffices to prove the claim for $u \in C_c^\infty(\Omega) \otimes \mathcal{P}^{k_t}$. Then we can proceed similarly as in the proof of Lemma 3.3: For fixed $x \in \Omega$, $u(x, \cdot)$ is a polynomial of degree k_t in time. By Theorem 2 of [WH03] there exists a constant $C(k_t)$ such that:

$$|u(x, t_n)|^2 \leq \frac{C(k_t)}{\Delta t}\int_{I_n} |u(x, t)|^2 \, dt.$$

Integration over Ω yields

$$\int_\Omega |u(x, t_n)|^2 \, dx \leq \frac{C(k_t)}{\Delta t}\int_\Omega\int_{I_n} |u(x, t)|^2 \, dt \, dx.$$

That is, $\|u(\cdot, t_n)\|_\Omega \leq C\Delta t^{-1/2}\|u\|_{Q^n}$. □

Lemma 3.21 (Approximation error bounds at fixed time levels)**.** *For $u \in H^{0,l_t}(Q^n) \cap H^{l_s,0}(Q^n)$ there holds the estimate*

$$\|(u - \Pi_W u)(\cdot, t_n)\|_\Omega \leq C\left(\Delta t^{l_t - 1/2}\|u\|_{H^{0,l_t}(Q^n)} + \Delta t^{-1/2} h^{l_s}\|u\|_{H^{l_s,0}(Q^n)}\right), \tag{3.22}$$

for $l_s \in \{1, \dots, k_s + 1\}$ and $l_t \in \{2, \dots, k_t + 1\}$.

Proof. Similar to the proof of Theorem 3.18 consider the splitting $\mathcal{L}_W = \mathcal{L}^{k_t} + \Pi^{k_t}\mathcal{L}^{k_s}$. An application of the triangle inequality yields:

$$\|\mathcal{L}_W u(\cdot, t_n)\|_\Omega \leq \left\|\mathcal{L}^{k_t} u(\cdot, t_n)\right\|_\Omega + \left\|\Pi^{k_t}\mathcal{L}^{k_s} u(\cdot, t_n)\right\|_\Omega.$$

For the second term we can apply the discrete inverse inequality in time (3.21) which yields:

$$\left\|\Pi^{k_t}\mathcal{L}^{k_s} u(\cdot, t_n)\right\|_\Omega \leq C\Delta t^{-1/2}\left\|\Pi^{k_t}\mathcal{L}^{k_s} u\right\|_{Q^n} \leq C\Delta t^{-1/2}\left\|\mathcal{L}^{k_s} u\right\|_{Q^n}.$$

Combining this with the bound from Lemma 3.17 (c) for the spatial interpolation leads to:

$$\left\|\Pi^{k_t}\mathcal{L}^{k_s}u(\cdot,t_n)\right\|_\Omega \leq C\Delta t^{-1/2}h^{l_s}\left\|u\right\|_{H^{l_s,0}(Q^n)},$$

for $u \in H^{l_s,0}(Q^n)$ and $l_s \in \{1,\dots,k_s+1\}$.

To treat the term $\left\|\mathcal{L}^{k_t}u(\cdot,t_n)\right\|_\Omega$ we transform the interval $I_n = (t_{n-1},t_n]$ to the reference interval $\hat{I} = (0,1]$ and consider the problem there. Denote the corresponding transformation by $\Phi : \hat{Q} \to Q^n$ with $\hat{Q} = \Omega \times \hat{I}$. The transformed function and operator are given by $\hat{u} = u \circ \Phi$ and $\hat{\mathcal{L}}^{k_t} = \Phi^{-1} \circ \mathcal{L}^{k_t} \circ \Phi$. Using that the time trace operator is continuous in $H^{0,1}(\hat{Q})$ and the interpolation estimates for Π^{k_t} (Lemma 3.15) yields:

$$\begin{aligned}
\left\|\mathcal{L}^{k_t}u(\cdot,t_n)\right\|_\Omega^2 &= \left\|\hat{\mathcal{L}}^{k_t}\hat{u}(\cdot,1)\right\|_\Omega^2 \leq C\left\|\hat{\mathcal{L}}^{k_t}\hat{u}\right\|_{H^{0,1}(\hat{Q})}^2 \\
&= C\left(\left\|\hat{\mathcal{L}}^{k_t}\hat{u}\right\|_{\hat{Q}}^2 + \left\|\partial_t\hat{\mathcal{L}}^{k_t}\hat{u}\right\|_{\hat{Q}}^2\right) \\
&\leq C\left(\frac{1}{\Delta t}\left\|\mathcal{L}^{k_t}u\right\|_{Q^n}^2 + \Delta t\left\|\partial_t\mathcal{L}^{k_t}u\right\|_{Q^n}^2\right) \\
&\leq C\left(\frac{\Delta t^{2l_t}}{\Delta t}\left\|u\right\|_{H^{0,l_t}(Q^n)}^2 + \Delta t\Delta t^{2(l_t-1)}\left\|u\right\|_{H^{0,l_t}(Q^n)}^2\right) \\
&= C\Delta t^{2(l_t-1/2)}\left\|u\right\|_{H^{0,l_t}(Q^n)}^2
\end{aligned}$$

for $u \in H^{0,l_t}(Q^n)$ and $l_t \in \{2,\dots,k_t+1\}$.

Combining both inequalities gives the claim. □

3.3.2 Interpolation in unfitted space-time finite element spaces

Now an interpolation operator $I_\Gamma^n : H^k(Q^n) \to W_n$ into the space-time FE-space on the time slab $Q^n = \cup_{t\in I_n}\Omega(t)\times\{t\}$ defined in (2.3) is required. From the previous section we have the space-time interpolation operator

$$\Pi_W^n : L^2(\mathcal{E}(Q^n)) \to W_n$$

for the tensor product case at our disposal. This operator can be used by recalling that assumption A.5 guarantees the existence of a linear extension operator

$$E^n : H^k(Q^n) \to H^k(\mathcal{E}(Q^n)),\ k \in \mathbb{N}, \tag{3.23}$$

which is bounded: $\left\|E^n u\right\|_{H^k(\mathcal{E}(Q^n))} \leq C\left\|u\right\|_{H^k(Q^n)}$. This allows to define the interpolation operator by

$$I_\Gamma^n := \Pi_W^n E^n.$$

The global interpolation $I_\Gamma : H^k(Q) \to W_h$ is defined by $(I_\Gamma u)_{|\mathcal{E}(Q^n)} = I_\Gamma^n u$. There hold the following interpolation results:

Theorem 3.22 (space-time unfitted interpolation)**.** *For $l_t, l_s \in \mathbb{N}$ define $l_{\max} = \max\{l_s, l_t\}$. Then*

(a) $\left\|u - I_\Gamma^n u\right\|_{Q^n} \leq C\left(\Delta t^{l_t} + h^{l_s}\right)\left\|u\right\|_{H^{l_{\max}}(Q^n)}$, *for $l_s \in \{1,\dots,k_s+1\}$ and $l_t \in \{1,\dots,k_t+1\}$.*

(b) $\|\partial_t(u - I_\Gamma^n u)\|_{Q^n} \leq C\left(\Delta t^{l_t-1} + h^{l_s}\right)\|u\|_{H^{l\max+1}(Q^n)}$, *for* $l_s \in \{1,\ldots,k_s+1\}$ *and* $l_t \in \{2,\ldots,k_t+1\}$.

(c) $\|\nabla(u - I_\Gamma^n u)\|_{Q^n} \leq C\left(\Delta t^{l_t} + h^{l_s-1}\right)\|u\|_{H^{l\max+1}(Q^n)}$, *for* $l_s \in \{2,\ldots,k_s+1\}$ *and* $l_t \in \{1,\ldots,k_t+1\}$.

(d) $\|(u - I_\Gamma^n u)(\cdot,t_n)\|_{\Omega^n} \leq C\left(\Delta t^{l_t-1/2} + \Delta t^{-1/2}h^{l_s}\right)\|u\|_{H^{l\max}(Q^n)}$, *for* $l_s \in \{1,\ldots,k_s+1\}$ *and* $l_t \in \{2,\ldots,k_t+1\}$.

Proof. For $D \in \{Id, \partial_t, \nabla\}$ it holds that

$$\begin{aligned}\|D(u - I_\Gamma^n u)\|_{Q^n} &= \|D(Id - \Pi_W^n)E^n u\|_{Q^n}\\ &\leq \|D(Id - \Pi_W^n)E^n u\|_{\mathcal{E}(Q^n)}.\end{aligned}$$

Now we can make use of the interpolation results on $\mathcal{E}(Q^n)$ established in Corollary 3.19. Consider the different cases:

- $D = Id$:

$$\begin{aligned}\|(Id - \Pi_W^n)E^n u\|_{\mathcal{E}(Q^n)} &\leq C\left(\Delta t^{l_t} + h^{l_s}\right)\|E^n u\|_{H^{l\max}(\mathcal{E}(Q^n))}\\ &\leq C\left(\Delta t^{l_t} + h^{l_s}\right)\|u\|_{H^{l\max}(Q^n)}\end{aligned} \tag{3.24}$$

  for $l_s \in \{1,\ldots,k_s+1\}$ and $l_t \in \{1,\ldots,k_t+1\}$, where the continuity of the extension operator was employed to obtain the second inequality.

  The cases $D \in \{\partial_t, \nabla\}$ are analogous.

- $D = \partial_t$:

$$\|\partial_t(Id - \Pi_W^n)E^n u\|_{\mathcal{E}(Q^n)} \leq C\left(\Delta t^{l_t-1} + h^{l_s}\right)\|u\|_{H^{l\max+1}(Q^n)},$$

  for $l_s \in \{1,\ldots,k_s+1\}$ and $l_t \in \{2,\ldots,k_t+1\}$.

- $D = \nabla$:

$$\|\nabla(Id - \Pi_W^n)E^n u\|_{\mathcal{E}(Q^n)} \leq C\left(\Delta t^{l_t} + h^{l_s-1}\right)\|u\|_{H^{l\max+1}(Q^n)},$$

  for $l_s \in \{2,\ldots,k_s+1\}$ and $l_t \in \{1,\ldots,k_t+1\}$.

The result at the fixed time levels is obtained by estimating

$$\begin{aligned}\|(u - I_\Gamma^n u)(\cdot,t_n)\|_{\Omega^n} &= \|((Id - \Pi_W^n)E^n u)(\cdot,t_n)\|_{\Omega^n}\\ &\leq \|((Id - \Pi_W^n)E^n u)(\cdot,t_n)\|_{\mathcal{E}(\Omega^n)}\end{aligned}$$

and then inserting the result for the tensor product case from Lemma 3.21.

□

3.4 A priori error estimate in discrete norm

To bound the right hand side in Theorem 3.12, the interpolation error in the norms $|||\cdot|||, |||\cdot|||_*$ and $\|\cdot\|_J$ needs to be estimated. The desired bounds in $|||\cdot|||$ and $|||\cdot|||_*$ follow directly from Theorem 3.22.

Proposition 3.23 (Approximation in $|||\cdot|||$)**.** *Let $k_{\max} = \max\{k_s, k_t\}$ and $u \in H^{k_{\max}+2}(Q)$. Then there holds (for a fixed constant $C > 0$)*

$$|||u - I_\Gamma u||| \leq C \left(h^{k_s+1}\Delta t^{-1/2} + \Delta t^{k_t+1/2} + h^{k_s}\right) \|u\|_{H^{k_{\max}+2}(Q)}.$$

Under assumption A.3 this simplifies to

$$|||u - I_\Gamma u||| \leq C \left(\Delta t^{k_t+1/2} + h^{k_s}\right) \|u\|_{H^{k_{\max}+2}(Q)}.$$

Proof. Consider the interpolation errors, denoted by $e_u = u - I_\Gamma u$ for the different parts in the norm $|||\cdot|||$ one after another:

1. The last part in the norm is the anisotropic semi-norm which was bounded in Theorem 3.22 (c):

$$\sum_{n=1}^{N} (\nabla e_u, \nabla e_u)_{Q^n} \leq C \left(\Delta t^{2(k_t+1)} + h^{2k_s}\right) \|u\|^2_{H^{k_{\max}+2}(Q)}.$$

2. For the scaled space-time $H^{0,1}$-semi-norm (first part) an application of Theorem 3.22 (b) yields:

$$\sum_{n=1}^{N} (\Delta t \partial_t e_u, \partial_t e_u)_{Q^n} \leq C\Delta t \left(\Delta t^{2k_t} + h^{2(k_s+1)}\right) \|u\|^2_{H^{k_{\max}+2}(Q)}.$$

3. For the DG-jump norm $[\![\cdot]\!]$ we can make use of Theorem 3.22 (d):

$$\begin{aligned}[\![e_u]\!]^2 &\leq 2\sum_{n=1}^{N} \left[\left\|(e_u)_+^{n-1}(\cdot, t_{n-1})\right\|^2_{\Omega^{n-1}} + \left\|(e_u)_-^{n}(\cdot, t_n)\right\|^2_{\Omega^n}\right] \\ &\leq C \left(\Delta t^{2(k_t+1/2)} + h^{2(k_s+1)}\Delta t^{-1}\right) \|u\|^2_{H^{k_{\max}+1}(Q)}.\end{aligned}$$

Combining these estimates yields the first result. Under assumption A.3. one has $h^{k_s+1}\Delta t^{-1/2} = h^{k_s}(h^2\Delta t^{-1})^{1/2} \leq Ch^{k_s}$, which implies the second statement. □

Proposition 3.24 (Approximation in $|||\cdot|||_*$)**.** *Let $k_{\max} = \max\{k_s, k_t\}$ and $u \in H^{k_{\max}+2}(Q)$. Then there holds (for a fixed constant $C > 0$)*

$$|||u - I_\Gamma u|||_* \leq C \left(h^{k_s+1}\Delta t^{-1/2} + \Delta t^{k_t+1/2} + h^{k_s}\right) \|u\|_{H^{k_{\max}+2}(Q)}.$$

Under assumption A.3 this simplifies to

$$|||u - I_\Gamma u|||_* \leq C \left(\Delta t^{k_t+1/2} + h^{k_s}\right) \|u\|_{H^{k_{\max}+2}(Q)}.$$

Proof. Consider the interpolation errors, denoted by $e_u = u - I_\Gamma u$ for the different parts in the norm $|||\cdot|||_*$ one after another:

1. The last part in the norm is the anisotropic semi-norm which is bounded as above:

$$\sum_{n=1}^{N} (\nabla e_u, \nabla e_u)_{Q^n} \leq C \left(\Delta t^{2(k_t+1)} + h^{2k_s}\right) \|u\|^2_{H^{k_{\max}+2}(Q)}.$$

2. For the scaled space-time L^2-error we get by means of Theorem 3.22 (a) that:

$$\sum_{n=1}^{N} \left(\Delta t^{-1} e_u, e_u\right)_{Q^n} \leq C\Delta t^{-1} \left(\Delta t^{2(k_t+1)} + h^{2(k_s+1)}\right) \|u\|^2_{H^{k_{\max}+1}(Q)} .$$

3. The contribution stemming from the time levels is bounded by Theorem 3.22 (d):

$$[\![e_u]\!]^2_* = \sum_{n=1}^{N} \left\|(e_u)^n_-(\cdot, t_n)\right\|^2_{\Omega^n} \leq C \left(\Delta t^{2(k_t+1/2)} + h^{2(k_s+1)}\Delta t^{-1}\right) \|u\|^2_{H^{k_{\max}+1}(Q)} .$$

The claim follows by combining these estimates. □

To treat the term in (3.9) that involves the $\|\cdot\|_J$-seminorm some preliminaries are required:

For a facet patch ω_F, let $\mathcal{P}^{k_s}(\omega_F)$ denote the space of polynomials of degree at most k_s on ω_F. Let the L^2-projection $P_{\omega_F} : L^2(\omega_F) \to \mathcal{P}^{k_s}(\omega_F)$ be defined by

$$\int_{\omega_F} (v - P_{\omega_F} v)\phi = 0 \quad \forall \phi \in \mathcal{P}^{k_s}(\omega_F). \tag{3.25}$$

It has the following properties, that are known e.g. from the theory of local projection stabilization (cf. Remark 3.69 in [RST08]):

Lemma 3.25. (a) *Stability:*

For $v \in L^2(\omega_F)$ it holds that: $\|P_{\omega_F} v\|_{L^2(\omega_F)} \leq \|v\|_{L^2(\omega_F)}$,

(b) *Approximation:*

For $v \in H^{k_s+1}(\omega_F)$ it holds that

$$\|v - P_{\omega_F} v\|_{L^2(\omega_F)} \leq C h^{k_s+1} |v|_{H^{k_s+1}(\omega_F)} .$$

Proof. *(a)* This is a fundamental property of the L^2-projection:

$$\begin{aligned} 0 &\leq \int_{\omega_F} (P_{\omega_F} v - v)(P_{\omega_F} v - v)\, dx \\ &= \|P_{\omega_F} v\|^2_{\omega_F} + \|v\|^2_{\omega_F} - 2\int_{\omega_F} (P_{\omega_F} v) v\, dx \\ &= \|P_{\omega_F} v\|^2_{\omega_F} + \|v\|^2_{\omega_F} - 2\int_{\omega_F} P_{\omega_F} v P_{\omega_F} v\, dx \\ &= -\|P_{\omega_F} v\|^2_{\omega_F} + \|v\|^2_{\omega_F} . \end{aligned}$$

(b) The definition (3.25) implies that P_{ω_F} coincides with the identity mapping on $\mathcal{P}^{k_s}(\omega_F)$. Hence, the approximation property follows from Theorem 4.28 of [GR07], which is a consequence of the Bramble-Hilbert Lemma.

□

Proposition 3.26 (Approximation in $\|\cdot\|_J$)**.** *Let u be the solution of the continuous problem.*

(a) *For any $F \in \mathcal{F}_R^{*,n}$ it holds that*

$$\|[\![I_\Gamma^n u]\!]_{\omega_F}(\cdot,t)\|_{\omega_F} \leq C\left(\left\|(I_\Gamma^n u - \Pi^{k_t} E^n u)(\cdot,t)\right\|_{\omega_F} + \left\|(\Pi^{k_t} E^n u - P_{\omega_F}\Pi^{k_t} E^n u)(\cdot,t)\right\|_{\omega_F}\right),$$

where

- *P_{ω_F} is the L^2-projection onto the facet-patch from above,*
- *E^n the extension operator from (3.23),*
- *and Π^{k_t} the temporal L^2-projection on $\mathcal{E}(Q^n) = \mathcal{E}(\Omega^n) \times I_n$ from (3.14).*

(b) *It holds that*

$$\|I_\Gamma u\|_J \leq C\sqrt{\gamma_J}\sqrt{\left(1 + \frac{\Delta t}{h}\right)} h^{k_s} \|u\|_{H^{k_s+1}(Q)}.$$

Remark 14. *The proof below assumes that the solution is sufficiently regular in time so that evaluations at a fixed time level are well defined. This leads to a requirement of the form $E^n u \in C(I_n, H^{k_s+1}(\mathcal{E}(\Omega^n)))$. To treat solutions with lower regularity, this assumption may be relaxed by means of a density argument.*

Proof. *(a)* Consider a facet patch $\omega_F = \bar{T}_1 \cup \bar{T}_2$ and set $w_h = (I_\Gamma^n u)(\cdot,t)$. Denote by w_i the extension of the polynomial $(w_h)_{|T_i}$ to ω_F. Let $v = P_{\omega_F} w_h \in \mathcal{P}^{k_s}(\omega_F)$ be the L^2 projection onto the facet patch. We have

$$\begin{aligned}
\|[\![w_h]\!]_{\omega_F}\|_{\omega_F}^2 &= \|w_1 - w_2\|_{\omega_F}^2 \\
&\leq 2\left(\|w_1 - v\|_{\omega_F}^2 + \|v - w_2\|_{\omega_F}^2\right) \\
&= 2\left(\|w_1 - v\|_{T_1}^2 + \|w_1 - v\|_{T_2}^2 + \|v - w_2\|_{T_1}^2 + \|v - w_2\|_{T_2}^2\right).
\end{aligned}$$

Shape regularity ensures the existence of a constant $C > 0$, only depending on the polynomial degree k_s, such that

$$\|w_1 - v\|_{T_2}^2 \leq C\|w_1 - v\|_{T_1}^2 \text{ and } \|v - w_2\|_{T_1}^2 \leq C\|v - w_2\|_{T_2}^2.$$

It follows that:

$$\begin{aligned}
\|[\![w_h]\!]\|_{\omega_F}^2 &\leq C\left(\|w_1 - v\|_{T_1}^2 + \|v - w_2\|_{T_2}^2\right) \\
&= C\|w_h - P_{\omega_F} w_h\|_{\omega_F}^2.
\end{aligned}$$

By using the triangle inequality we can further estimate:

$$\begin{aligned}
&\|w_h - P_{\omega_F} w_h\|_{\omega_F}^2 \\
&= \left\|(w_h - \Pi^{k_t} E^n u) + (\Pi^{k_t} E^n u - P_{\omega_F}\Pi^{k_t} E^n u) + (P_{\omega_F}\Pi^{k_t} E^n u - P_{\omega_F} w_h)\right\|_{\omega_F}^2 \\
&\leq 4\left(\left\|w_h - \Pi^{k_t} E^n u\right\|_{\omega_F}^2 + \left\|\Pi^{k_t} E^n u - P_{\omega_F}\Pi^{k_t} E^n u\right\|_{\omega_F}^2 + \left\|P_{\omega_F}(\Pi^{k_t} E^n u - w_h)\right\|_{\omega_F}^2\right) \\
&\leq 4\left(2\left\|w_h - \Pi^{k_t} E^n u\right\|_{\omega_F}^2 + \left\|\Pi^{k_t} E^n u - P_{\omega_F}\Pi^{k_t} E^n u\right\|_{\omega_F}^2\right),
\end{aligned}$$

where the last step used the stability of the L^2-projection.

(b) The sum

$$\|I_\Gamma u\|_J^2 = \sum_{n=1}^{N} \int_{t_{n-1}}^{t_n} \left(1 + \frac{\Delta t}{h}\right) \frac{\gamma_J}{h^2} \sum_{F \in \mathcal{F}_R^{*,n}} \|[\![I_\Gamma^n u]\!]_{\omega_F}\|_{\omega_F}^2 \, dt \tag{3.26}$$

can now be split into two parts by using the result from (a).

$$\begin{aligned}\|I_\Gamma u\|_J^2 \leq C \left(1 + \frac{\Delta t}{h}\right) \frac{\gamma_J}{h^2} \Big(& \sum_{n=1}^{N} \left\| I_\Gamma^n u - \Pi^{k_t} E^n u \right\|_{\mathcal{E}(Q^n)}^2 \\ & + \sum_{n=1}^{N} \int_{t_{n-1}}^{t_n} \sum_{F \in \mathcal{F}_R^{*,n}} \left\| (\Pi^{k_t} E^n u - P_{\omega_F} \Pi^{k_t} E^n u)(\cdot, t) \right\|_{\omega_F}^2 \, dt \Big).\end{aligned}$$

To estimate the first term we recall that $I_\Gamma^n = \Pi_W^n E^n = \Pi^{k_t} \Pi^{k_s} E^n$, where Π^{k_s} is the spatial L^2-projection. Then

$$I_\Gamma^n u - \Pi^{k_t} E^n u = \Pi^{k_t} \left(\Pi^{k_s} E^n u - E^n u \right).$$

Combining the stability of the temporal L^2-projection (Lemma 3.15 (a)) and the approximation results for the spatial-projection (Lemma 3.17 (c)) yields:

$$\begin{aligned}\left\| I_\Gamma u - \Pi^{k_t} E^n u \right\|_{\mathcal{E}(Q^n)}^2 \leq & \left\| \Pi^{k_s} E^n u - E^n u \right\|_{\mathcal{E}(Q^n)}^2 \\ \leq & C h^{2(k_s+1)} \left\| E^n u \right\|_{H^{k_s+1}(\mathcal{E}(Q^n))}^2 \leq C h^{2(k_s+1)} \left\| u \right\|_{H^{k_s+1}(Q^n)}^2.\end{aligned}$$

For the other part we first use the previous Lemma 3.25 (b):

$$\begin{aligned}& \int_{t_{n-1}}^{t_n} \sum_{F \in \mathcal{F}_R^{*,n}} \left\| (\Pi^{k_t} E^n u - P_{\omega_F} \Pi^{k_t} E^n u)(\cdot, t) \right\|_{\omega_F}^2 \, dt \\ \leq & C h^{2(k_s+1)} \int_{t_{n-1}}^{t_n} \sum_{F \in \mathcal{F}_R^{*,n}} \left| \Pi^{k_t} E^n u(\cdot, t) \right|_{H^{k_s+1}(\omega_F)}^2 \, dt \\ \leq & C h^{2(k_s+1)} \int_{t_{n-1}}^{t_n} \left| \Pi^{k_t} E^n u(\cdot, t) \right|_{H^{k_s+1}(\mathcal{E}(\Omega^n))}^2 \, dt \\ = & C h^{2(k_s+1)} \left| \Pi^{k_t} E^n u \right|_{H^{k_s+1,0}(\mathcal{E}(Q^n))}^2.\end{aligned}$$

From the fact that Π^{k_t} commutes with the spatial derivatives and is L^2-stable it follows that

$$\left| \Pi^{k_t} E^n u \right|_{H^{k_s+1,0}(\mathcal{E}(Q^n))}^2 \leq \left| E^n u \right|_{H^{k_s+1,0}(\mathcal{E}(Q^n))}^2 \leq \left\| E^n u \right\|_{H^{k_s+1}(\mathcal{E}(Q^n))}^2.$$

Hence,

$$\begin{aligned}& \int_{t_{n-1}}^{t_n} \sum_{F \in \mathcal{F}_R^{*,n}} \left\| (\Pi^{k_t} E^n u - P_{\omega_F} \Pi^{k_t} E^n u)(\cdot, t) \right\|_{\omega_F}^2 \, dt \\ \leq & C h^{2(k_s+1)} \left\| E^n u \right\|_{H^{k_s+1}(\mathcal{E}(Q^n))}^2 \leq C h^{2(k_s+1)} \left\| u \right\|_{H^{k_s+1}(Q^n)}^2.\end{aligned}$$

Combining both estimates we arrive at

$$\|I_\Gamma u\|_J^2 \leq C \left(1 + \frac{\Delta t}{h}\right) \frac{\gamma_J}{h^2} h^{2(k_s+1)} \|u\|_{H^{k_s+1}(Q)}^2$$

by summing up over $n = 1, \ldots, N$.

□

In view of Theorem 3.12, we arrive at the following a priori error estimate in the discrete norm $|||\cdot|||$.

Theorem 3.27 (A priori error estimate)**.** *Let u be the solution of (2.1) and u_h be the solution of (2.7). Let $k_{\max} = \max\{k_s, k_t\}$ and assume $u \in H^{k_{\max}+2}(Q)$. Then there holds:*

$$\begin{aligned} |||u - u_h||| \leq C \left(1 + C_{3.12}(\gamma_J)\right) \left(h^{k_s+1} \Delta t^{-1/2} + \Delta t^{k_t+1/2} + h^{k_s}\right) \|u\|_{H^{k_{\max}+2}(Q)} \\ + \frac{C\sqrt{\gamma_J}}{C_{3.9}(\gamma_J)} \sqrt{\left(1 + \frac{\Delta t}{h}\right)} h^{k_s} \|u\|_{H^{k_s+1}(Q)}. \end{aligned}$$

Under assumption A.3 this simplifies to

$$|||u - u_h||| \leq C \left(\Delta t^{k_t+1/2} + \sqrt{\left(1 + \frac{\Delta t}{h}\right)} h^{k_s}\right) \|u\|_{H^{k_{\max}+2}(Q)},$$

where C depends on γ_J.

Proof. Combine Theorem 3.12 and Propositions 3.23, 3.24 and 3.26. □

Remark 15. *Since stability is lost for $\gamma_J \to +0$ also the energy norm estimate blows up in this case. This can be seen from $\lim_{\gamma_J \to +0} C_{3.12}(\gamma_J) = \infty$.*

Remark 16. *The Céa-like result involves the inverse of the stabilization constant in front of the $|||\cdot|||_*$-norm. Consider now the case where the ghost penalty terms are not scaled with the factor $\left(1 + \frac{\Delta t}{h}\right)$. According to Remark 10 this will result in a scaling of the approximation error in the $|||\cdot|||_*$-norm by $\left(1 + \frac{\Delta t}{h}\right)$. Since this approximation error involves the factor $\Delta t^{k_t+1/2}$, this approach would result in a worse a priori error estimate.*

Remark 17. *The error estimate is suboptimal with respect to the Sobolev smoothness required from the exact solution. This defect stems from the interpolation estimates established in Theorem 3.18. By considering Sobolev interpolation in non-integer spaces one may lower the required smoothness of the solution by half an order. We do not follow this approach here in order to avoid technicalities.*

Corollary 3.28 (L^2 estimate at final time)**.** *Let u be the solution of (2.1) and u_h be the solution of (2.7). Then there holds:*

$$\left\|(u - u_h)_-^N\right\|_{\Omega^N} \leq C \left(h^{k_s+1} \Delta t^{-1/2} + \Delta t^{k_t+1/2} + \sqrt{\left(1 + \frac{\Delta t}{h}\right)} h^{k_s}\right) \|u\|_{H^{k_{\max}+2}(Q)}.$$

Under assumption A.3 this simplifies to

$$\left\|(u - u_h)_-^N\right\|_{\Omega^N} \leq C \left(\Delta t^{k_t+1/2} + \sqrt{\left(1 + \frac{\Delta t}{h}\right)} h^{k_s}\right) \|u\|_{H^{k_{\max}+2}(Q)}.$$

Remark 18 (Relation of analysis to literature)**.** *The analysis presented in this chapter was motivated by [LR13], [Leh15] and to a lesser extent by [Sch10]. Let us discuss some of the similarities and differences.*

- *The contributions [LR13] and [Leh15] present an error analysis for a Space-Time-DG Nitsche-XFEM method for a two-phase mass transport problem with piecewise linear elements in time and space. The moving domain problem considered in this contribution is simpler, because it does not involve interface terms. But compared to [LR13] and [Leh15], we prove a higher order bound (order greater-than two) which is anisotropic with respect to the polynomial degrees in space and time. One of the main differences already lies in the construction of the method. While this thesis utilizes a ghost penalty stabilization, [LR13] and [Leh15] do not. In the end, we prove a similar Céa-like Theorem as in [Leh15] (cf. Lemma 3.3.14 in [Leh15]) , but the ghost penalty stabilization opened up a different way to arrive at this result. In particular, the norms that are used in this thesis differ significantly from the ones in [LR13] and [Leh15], because we also control the time derivative. Furthermore, our proof of inf-sup stability relies on inverse inequalities which are ensured by the ghost penalty stabilization. Since [LR13] and [Leh15] do not use ghost penalty, the proof of stability in these contributions is naturally quite different from the one presented here.*

- *The proof of inf-sup stability in this thesis is closer to the one given in [Sch10]. This paper analyzes a general evolution equation in a Hilbert space. The problem is considered in a semi-discrete setting with discretization in time only. To this end, a discontinuous Galerkin-Petrov time discretization is applied. This is very different from our setting already by the fact that we consider a fully discretized problem and also a different time discretization. However, there is a similarity, namely that the time derivative of the discrete solution is contained in the discrete test space. Both in [Sch10] (cf. Lemma 3 in [Sch10]) and in this thesis, this property is utilized for deriving inf-sup stability.*

Note also that we use a different variant of the ghost penalty stabilization than prevalent in the literature. Thus, some fundamental properties of this stabilization first had to be derived (cf. subsection 3.2.1). This includes in particular the properties for time-dependent problems.

Chapter 4

Isoparametric space-time discretization for a moving domain problem

In this chapter we drop the assumption of an exact handling of the geometry. First, a stationary problem is considered. It is discussed how to obtain a higher order explicit description of implicitly defined geometries by a parametric mapping of the underlying mesh. We briefly sketch the construction of this mapping and outline how it is applied in the setting of finite element methods. This gives rise to an isoparametric (unfitted) finite element method [Leh16],[LR17].

Whereas the stationary situation has been fully analyzed in the literature [LR17], the extension to moving domain problems is an open field. In section 4.2 we generalize the parametric mapping to a space-time mesh transformation. In this regard, some new difficulties occur that are not present in the stationary case and need to be adressed (see section 4.2.2 and 4.3). Finally, we discuss how to apply the space-time mesh transformation for the solution of the moving domain problem from chapter 2. To this end, the space-time discretization from this chapter needs to be adapted. The changes entailed by the isoparametric method are discussed in section 4.3.

4.1 Isoparametric (unfitted) FEM

The problem to compute integrals on implictedly defined domains

Consider a stationary version of our model problem

$$\begin{aligned} -\Delta u + u &= f && \text{in } \Omega, \\ \nabla u \cdot \mathbf{n}_{\partial\Omega} &= 0 && \text{on } \partial\Omega. \end{aligned} \tag{4.1}$$

Here the domain Ω is contained in a larger background domain $\tilde{\Omega}$. The triangulation is not fitted to the boundary of Ω. We assume that the domain Ω is described by a smooth level set function ϕ, that is $\Omega = \{x \in \tilde{\Omega} \mid \phi(x) < 0\}$ and $\partial\Omega = \{x \in \tilde{\Omega} \mid \phi(x) = 0\}$. Consider the weak formulation of (4.1): Find u in an appropriate space such that for all test functions v:

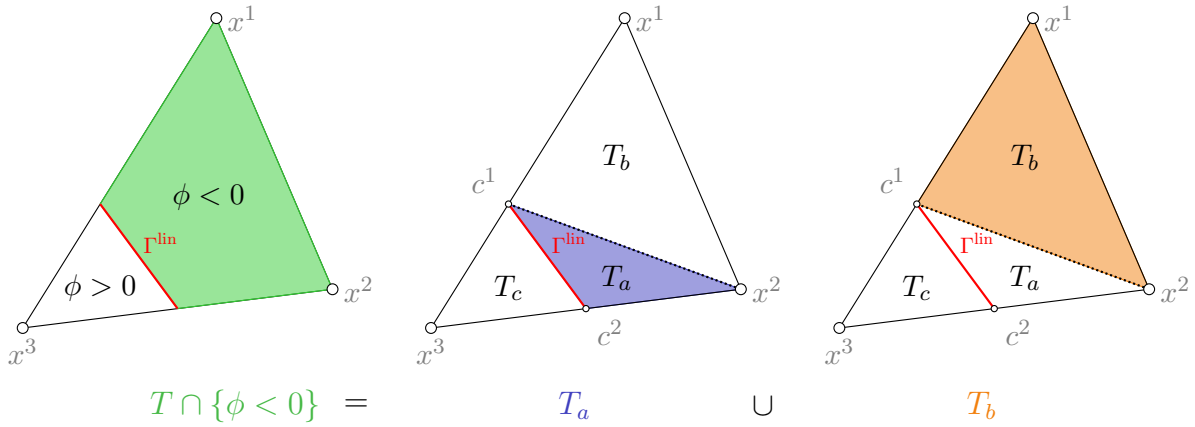

Figure 4.1: The shown element T is cut by the piecewise linear interface $\Gamma^{\text{lin}} = \{x \in \tilde{\Omega} \mid \hat{\phi}_h(x) = 0\}$. The integral over $T \cap \{\phi < 0\}$ has to be computed. To this end, new vertices c^1 and c^2 are introduced. This allows to split $T \cap \{\phi < 0\}$ into the two triangles T_a and T_b on which standard quadrature rules can be applied.

$$\int_\Omega \nabla u \nabla v + uv \, dx = \int_\Omega fv \, dx$$

holds. This gives rise to the problem of having to compute integrals $\int_\Omega f \, dx$ over the implicitly described domain $\Omega = \{x \in \tilde{\Omega} \mid \phi(x) < 0\}$. For other non-homogeneous boundary conditions or interface problems also integrals over $\{x \in \tilde{\Omega} \mid \phi(x) = 0\}$ have to be evaluated. A highly accurate and robust computation of these integrals is crucial for the numerical realization of higher order methods.

A low-order approach for numerical integration

A popular approach to compute the integrals $\int_\Omega f \, dx$ on simplicial meshes is based on tesselation, see e.g. [Nær14] and [MGW09]. The level set function ϕ is approximated by a piecewise linear level set function $\hat{\phi}_h = I_1 \phi$, where I_1 is the nodal interpolation operator. Accordingly, the integral over $\Omega = \{x \in \tilde{\Omega} \mid \phi(x) < 0\}$ is approximated by an integral over $\Omega^{\text{lin}} = \{x \in \tilde{\Omega} \mid \hat{\phi}_h(x) < 0\}$:

$$\int_\Omega f \, dx \approx \int_{\Omega^{\text{lin}}} f \, dx.$$

The boundary $\Gamma^{\text{lin}} = \partial\Omega^{\text{lin}} = \{x \in \tilde{\Omega} \mid \hat{\phi}_h(x) = 0\}$ is then piecewise planar. To elements which are cut by a piecewise linear approximation of the level set function, a tesselation algorithm, as illustrated in Figure 4.1, can be applied. This algorithm subdivides the cut elements into simpler geometries on which standard quadrature rules with positive weights ω_i can be applied:

$$\int_\Omega f \, dx \approx \int_{\Omega^{\text{lin}}} f \, dx = \sum_{T \in \mathbb{T}_h} \sum_i \omega_i f(x_i). \tag{4.2}$$

Unfortunately, this approach is limited to second order accuracy because the geometry is approximated by the piecewise linear level set function $\hat{\phi}_h$. In particular,

$$\operatorname{dist}\left(\partial\Omega, \partial\Omega^{\text{lin}}\right) \leq \mathcal{O}(h^2).$$

Basic concept of isoparametric unfitted FEM

In [Leh16],[LR17] a method to compute integrals on implicitly described domains with high order accuracy is presented. It is based on a parametric mapping of the underlying mesh which gives rise to an explicit, high order representation of the level set domain. In the following we describe only the basic idea of this approach. For a thorough discussion and the actual construction of the mapping we refer to the literature cited above.

- One starts from a higher order interpolation $\phi_h = I_{k_s}\phi \in V_h^{k_s}$ of the level set function ϕ and a piecewise linear nodal interpolation $\hat{\phi}_h = I_1\phi_h$ of ϕ_h.
- Using $\hat{\phi}_h$ and the high-order information given by ϕ_h as input one constructs a mapping Θ_h of the underlying mesh such that

  $$\hat{\phi}_h \approx \phi_h \circ \Theta_h.$$

  That is, Θ_h maps the piecewise planar interface $\{x \in \tilde{\Omega} \mid \hat{\phi}_h(x) = 0\}$ approximately onto the zerolevel set of a high order accurate level set function. The image of the piecewise planar domain under this mapping $\Theta_h(\Omega^{\text{lin}})$ is then a high-order accurate approximation to Ω:

  $$\operatorname{dist}\left(\partial\Omega, \partial\left(\Theta_h(\Omega^{\text{lin}})\right)\right) \leq \mathcal{O}(h^{k_s+1}).$$

- The integrals are approximated by

  $$\int_{\Omega} f \, dx \approx \int_{\Theta_h(\Omega^{\text{lin}})} f \, dx.$$

  By means of the transformation formula for integrals this integral can be reduced to an integral over the piecewise linear approximation Ω^{lin}. That is, this approach leads to a high-order approximation of the geometry which admits by construction an explicit representation. The cut topology is unchanged since the integrals are formulated with respect to the piecewise planar reference configuration on which e.g. the tesselation approach mentioned above can be applied:

  $$\begin{aligned}\int_{\Theta_h(\Omega^{\text{lin}})} f \, dx &= \int_{\Omega^{\text{lin}}} f \circ \Theta_h \left|\det\left(D\Theta_h\right)\right| \, dy \\ &= \sum_{T\in\mathbb{T}_h} \sum_i \omega_i \left|\det\left(D\Theta_h(y_i)\right)\right| f(\Theta_h(y_i)).\end{aligned}$$

  The quadrature weights are the same as in (4.2), in particular, they are positive. The accuracy of the quadrature now depends on Θ_h.

- This approach requires adapted finite element spaces which depend on $\hat{\phi}_h$ and the parametric mapping. Let V_h be the finite element space corresponding to the piecewise planar approximation with $\hat{\phi}_h$. Applying the transformation Θ_h leads to the isoparametric FE-space

  $$\mathcal{V}_h = \{\phi_h \circ \Theta_h^{-1} \mid \phi_h \in V_h\}.$$

Construction of the stationary mesh-transformation

We sketch the main steps that are required to construct the parametric mapping Θ_h. For a detailed and rigorous construction we refer to section 3 of [LR17]. First, some new notation will be introduced.

Let $\Gamma^{\text{lin}} \coloneqq \{\hat{\phi} = 0\}$ denote the low order geometry approximation of the boundary. The elements of the triangulation $\tilde{\mathcal{T}}_h$ of the background domain $\tilde{\Omega}$ which are cut by Γ^{lin} are collected in the set $\mathcal{T}^\Gamma \coloneqq \{T \in \tilde{\mathcal{T}}_h,\ T \cap \Gamma^{\text{lin}} \neq \emptyset\}$. The corresponding domain is denoted by $\Omega^\Gamma \coloneqq \{x \in T,\ T \in \mathcal{T}^\Gamma\}$. The set $\mathcal{T}_+^\Gamma \coloneqq \{T \in \tilde{\mathcal{T}}_h,\ T \cap \Omega^\Gamma \neq \emptyset\}$ contains additionally all elements that share at least one vertex with elements in $\mathcal{T}^\Gamma$. The corresponding domain is $\Omega_+^\Gamma \coloneqq \{x \in T,\ T \in \mathcal{T}_+^\Gamma\}$. Furthermore, we distinguish the set of continuous functions $C(\Omega^\Gamma)$ on Ω^Γ from the set of piecewise continuous functions by denoting the latter as $C(\mathcal{T}^\Gamma) \coloneqq \oplus_{T\in\mathcal{T}^\Gamma} C(T)$. The functions in $C(\mathcal{T}^\Gamma)$ may have jumps over the element interfaces.

The mesh-deformation is constructed in the following steps:

1. Element-local construction for $T \in \mathcal{T}^\Gamma$:

   Let $\mathcal{E}_T\phi_h$ be the polynomial extension of $(\phi_h)_{|T}$. For sufficiently small $\delta > 0$ we define the function $d_h : T \to [-\delta, \delta]$ by requiring that $d_h(x)$ is the (in absolute value) smallest number such that

   $$\mathcal{E}_T\phi_h(x + d_h(x)G_h(x)) = \hat{\phi}(x) \quad \text{for } x \in T \in \mathcal{T}^\Gamma \tag{4.3}$$

   holds. Here, $G_h(x)$ is a search direction. Possible choices are $G_h(x) = \nabla\phi_h(x)$ which may be discontinuous across element interfaces or a smoothed version $G_h(x) = \left(P_h^\Gamma \nabla\phi_h\right)(x)$, where $P_h^\Gamma : C(\mathcal{T}^\Gamma)^d \to V_h^{k_s}(\Omega^\Gamma)^d$ is a projection operator. This operator can be chosen as an Oswald-type projection which proceeds by averaging (see section 2.2 of [LR17]).

   The problem (4.3) can be solved by means of a Newton search. The obtained function $d_hG_h \in C(\mathcal{T}^\Gamma)^d$ is used to define

   $$\Psi_h^\Gamma(x) \coloneqq x + d_h(x)G_h(x) \quad \text{for } x \in T \in \mathcal{T}^\Gamma. \tag{4.4}$$

   The function Ψ_h^Γ is projected to a finite element function by solving local $L^2(T)$ problems.

2. Smoothing by averaging with a projection operator:

   The function Ψ_h^Γ is possibly discontinuous across element interfaces. These discontinuities can be removed by applying the projection operator P_h^Γ from above. This leads to the definition of $\Theta_h^\Gamma \in C(\Omega^\Gamma)$ by setting

   $$\Theta_h^\Gamma \coloneqq P_h^\Gamma\Psi_h^\Gamma = \text{id} + P_h^\Gamma\left(d_hG_h\right). \tag{4.5}$$

   The transformation Θ_h^Γ maps the piecewise linear interface Γ^{lin} to $\Gamma_h = \Theta_h^\Gamma(\Gamma^{\text{lin}})$, which turns out to approximate the exact interface $\Gamma = \{\phi = 0\}$ with optimal order (Lemma 3.7 in [LR17]):

   $$\text{dist}\left(\Gamma, \Gamma_h\right) \lesssim h^{k_s+1}. \tag{4.6}$$

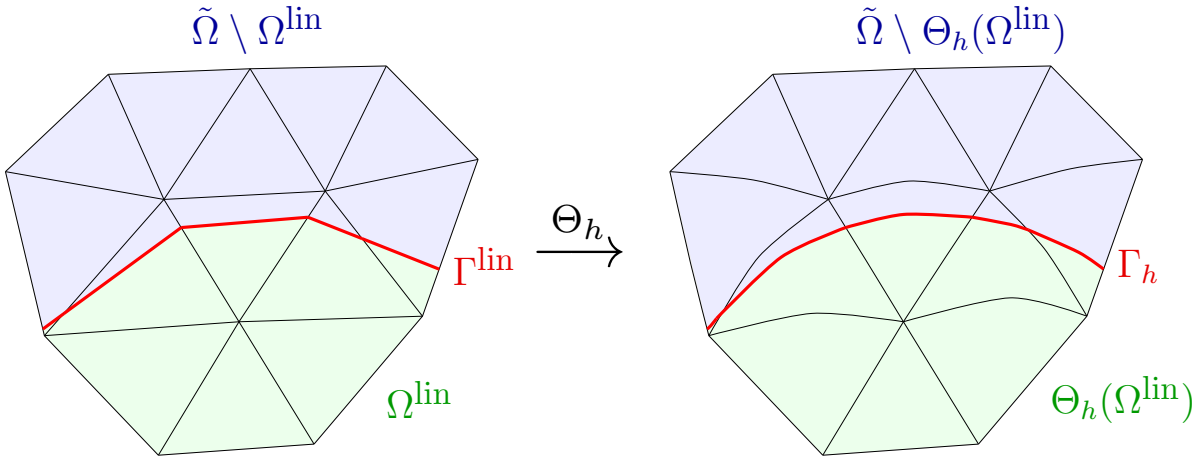

Figure 4.2: Illustration of the mesh deformation: A piecewise linear approximation of the zero level set Γ^{lin} is mapped to a high order accurate approximation Γ_h.

3. Extension from Ω^Γ to $\tilde{\Omega}$:

   There exists an extension operator $\mathcal{E}^{\partial\Omega^\Gamma} : C(\partial\Omega^\Gamma) \to C(\tilde{\Omega} \setminus \Omega^\Gamma)$ which extends piecewise smooth functions given on $\partial\Omega^\Gamma$ to the domain $\tilde{\Omega} \setminus \Omega^\Gamma$ in such a way that the extension is zero on $\tilde{\Omega} \setminus \Omega^\Gamma_+$ and piecewise smooth on $\Omega^\Gamma_+ \setminus \Omega^\Gamma$. This operator is derived by means of standard tools from isoparametric finite element methods (see [Len86] and [Ber89]). Given $\mathcal{E}^{\partial\Omega^\Gamma}$ and the local transformation Θ^Γ_h we define the globally continuous mapping $\Theta_h \in V_h^{k_s}(\tilde{\Omega})^d$ by

$$\Theta_h = \begin{cases} \Theta^\Gamma_h & \text{on } \Omega^\Gamma, \\ \text{id} \ + \mathcal{E}^{\partial\Omega^\Gamma}\left(\Theta^\Gamma_h - \ \text{id}\right) & \text{on } \Omega^\Gamma_+ \setminus \Omega^\Gamma, \\ \text{id} & \text{on } \tilde{\Omega} \setminus \Omega^\Gamma_+. \end{cases} \tag{4.7}$$

   It follows from this definition that the transformation acts only in the vicinity of the interface. The situation is sketched in Figure 4.2. Moreover, it can be shown that

$$\|D\Theta_h - \ \text{id}\|_{\infty,\tilde{\Omega}} \lesssim h. \tag{4.8}$$

   Hence, $D\Theta_h$ is invertible for h sufficiently small and $\Theta_h : T \to \Theta_h(T)$ is a bijection. Moreover, the property (4.8) ensures shape-regularity of the transformed simplices $\{\Theta_h(T),\ T \in \tilde{\mathcal{T}}_h\}$ for h sufficiently small. In the underresolved case, where h is too large, the deformation needs to be limited in order to guarantee shape-regularity (see section 2.6 of [Leh16]).

4.2 Space-Time mesh deformation

4.2.1 Construction

The aim of this section is to construct a space-time version of the mesh deformation. We assume that there is a smooth level set function $\phi : \tilde{Q} \to \mathbb{R}$ available which describes the

exact geometry:

$$\phi(x,t)\begin{cases} <0 & x\in\Omega(t),\\ =0 & x\in\partial\Omega(t),\\ >0 & x\in\tilde{\Omega}\setminus\Omega(t).\end{cases}$$

Then the following two tasks are carried out on the time slabs $\tilde{Q}^n$:

1. Reference geometry representation:

   Based on ϕ we compute a high order accurate approximation

   $$\phi_h(x,t)=\sum_{l=0}^{k_t} t^l\phi_l(x)\in V_h^{k_t,k_s}=V_h^{k_s}\otimes\mathcal{P}^{k_t},\ \text{where } \phi_l\in V_h^{k_s},$$

   of the exact geometry. Here $V_h^{k_s}$ is a standard finite element space of degree k_s on the background domain $\tilde{\Omega}$, so that $V_h^{k_t,k_s}$ coincides with the space W_n from (3.13) on $\tilde{Q}^n$. Applying the spatial, nodal $P1$ interpolation operator I_1 to each ϕ_l leads to:

   $$\hat{\phi}_h(x,t)=\sum_{l=0}^{k_t} t^l\hat{\phi}_l(x)\in V_h^{k_t,1},\ \text{where } \hat{\phi}_l=I_1\phi_l\in V_h^1.$$

   This function describes the reference geometry. Note that it is high order in time but linear in space. Similar to the method for the stationary case all integrals that need to be computed in the implementation of the space-time version will be reduced to integrals on the reference geometry. The integrals over $\{\hat{\phi}_h\lesseqgtr 0\}$ and $\{\hat{\phi}_h=0\}$ on the space-time prisms can be simplified by iterated integrals. Since $\hat{\phi}_h(\cdot,\bar{t})$ is piecewise linear for a fixed $\bar{t}$ the spatial integration only needs to treat elements whose cut topology is described by a piecewise linear approximation of the level set function.

2. Higher order accurate geometry representation with space-time mapping:

   The space-time version of the mesh deformation is constructed by employing the machinery available from the stationary case. Feeding ϕ_l and $\hat{\phi}_l$ into this mechanism produces a spatial mesh deformation $\Theta_l(x)\in[V_h^{k_s}]^d$ such that

   $$\hat{\phi}_l(x)\approx\phi_l(\Theta_l(x))$$

   for every $l=0,\dots,k_t$. This allows to define the space-time mapping:

   $$\Theta_h(x,t)\coloneqq\sum_{l=0}^{k_t} t^l\Theta_l(x)\in[V_h^{k_t,k_s}]^d. \tag{4.9}$$

   To ensure continuity of Θ_h within the time slab $\tilde{Q}^n$ it is necessary to enlarge the set of elements $\mathcal{T}^\Gamma$ on which the local transformation $\Psi_{h,l}^\Gamma$ in steps 1-2 of the stationary case is computed. For every $l\in 0,\dots,k_t$ the local construction needs to be performed on each element from the set

   $$\mathcal{T}^{\Gamma_n}\coloneqq\{T\in\tilde{\mathcal{T}}_h^n,\ T\cap\Gamma^{\text{lin}}(t)\neq\emptyset\text{ for some } t\in I_n\},$$

   where $\Gamma^{\text{lin}}(t)=\{\hat{\phi}(\cdot,t)=0\}$. This set contains all the elements which are cut by the interface at some point in time within the time slab. The corresponding sets Ω^{Γ_n}, $\mathcal{T}_+^{\Gamma_n}$ and $\Omega_+^{\Gamma_n}$ are defined analogously as for the stationary case.

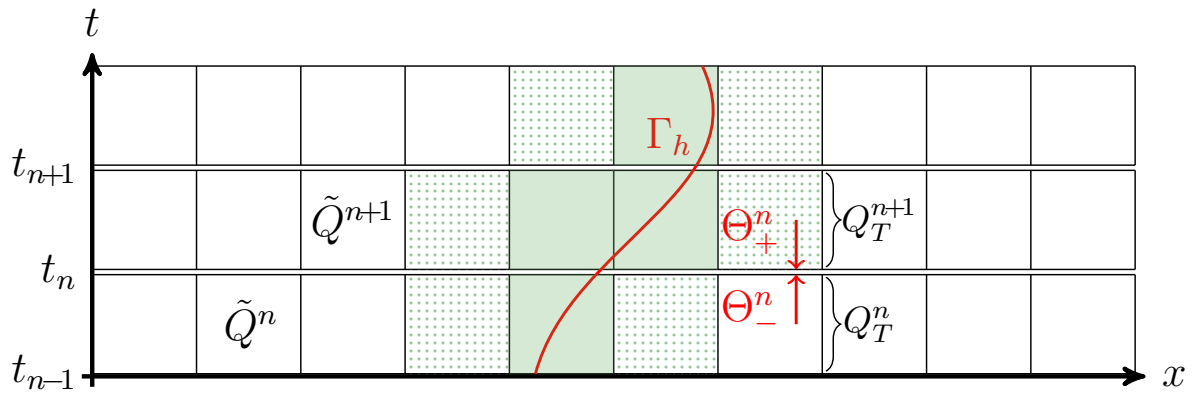

Figure 4.3: Discontinuity of space-time mapping between time slabs: The marking of the elements (filled/dotted/none) corresponds to the value of the mesh-deformation on these elements.

4.2.2 Discontinuity of mesh deformation between time slabs

The space-time mesh deformation is defined on each time slab $\tilde{Q}^n$ by means of (4.9). Unfortunately, the construction from the previous subsection leads to a space-time mapping which is in general discontinuous between different time slabs. This is illustrated in Figure 4.3. Consider the space-time prisms $Q_T^n = T \times I_n$ and $Q_T^{n+1} = T \times I_{n+1}$. On the time slab $\tilde{Q}^n$ the corresponding simplex T belongs to the set $\tilde{\mathcal{T}}_h \setminus \mathcal{T}_+^{\Gamma_n}$. According to the definition (4.7) we have $(\Theta_-^n)_{|T} = \mathrm{id}$, where $\Theta_\pm^n = \lim_{s\to 0} \Theta_h(t_n \pm s, \cdot)$. However, in the next time slab $\tilde{Q}^{n+1}$ the same simplex T is now a neighbor of a cut element. Hence, $T \in \mathcal{T}_+^{\Gamma_{n+1}}$. Again according to (4.7) we have $(\Theta_+^n)_{|T} \neq \mathrm{id}$. Therefore, $(\Theta_-^n)_{|T} \neq (\Theta_+^n)_{|T}$. That is, the transformation is in general discontinuous between the time slabs. This is in contrast to the discrete space-time domains which are matching by construction.

Since the derived method involves passing on the solution on the time slab Q^n as an initial condition for the variational formulation on the time slab Q^{n+1} these discontinuities will cause difficulties in the implementation. We will address this problem when discussing the isoparametric space-time discretization and sketch a possible solution.

4.2.3 Test problem: Circle moving through mesh

We expect that the space-time mesh transformation provides a higher order accurate description of the geometry. That is, a space-time version of equation (4.6) should hold true. More precisely, the distance of the space-time interface $\Gamma_* = \cup_{t\in(0,T]}\Gamma(t) \times \{t\}$, where $\Gamma(t) = \{\phi(\cdot, t) = 0\}$, to its approximation $\Gamma_{*,h} = \cup_{t\in(0,T]}\Gamma_h(t) \times \{t\}$, where $\Gamma_h(t) = \Theta_h(t)(\Gamma^{\mathrm{lin}}(t))$ should be controlled as

$$\mathrm{dist}\,(\Gamma_*, \Gamma_{*,h}) \lesssim \Delta t^{k_t+1} + h^{k_s+1}. \tag{4.10}$$

To test this we consider a circle moving through the mesh. The level set function is given by

$$\phi(x, y, t) = \sqrt{(x - 1 - \frac{1}{4}\sin(\pi t))^2 + (y - 1)^2} - \frac{1}{2}.$$

At $t = 0$ the center of the disk described by $\{\phi(t) < 0\}$ is at position $(x, y) = (1, 1)$. From $t = 0$ to $t = 1/2$ the disk shifts to the right so that the center at $t = 1/2$ is at

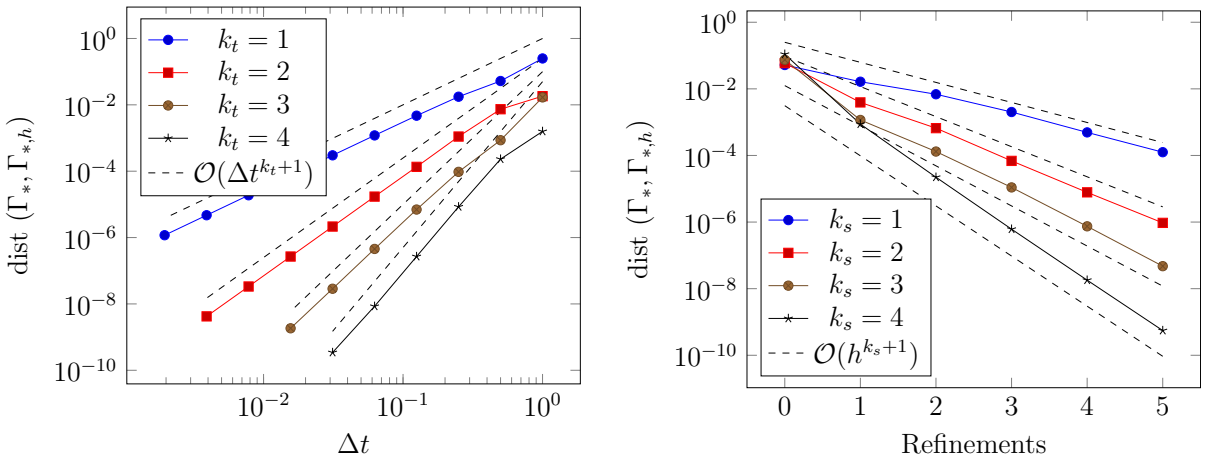

Figure 4.4: Circle moving through the mesh: geometry error.

$(x, y) = (5/4, 1)$. Then it switches direction and has returned to its original position at $t = 1$.

We consider a discrete set S_n of ten equally spaced sample points in I_n to approximate the geometry error:

$$\begin{aligned}\operatorname{dist}(\Gamma_*, \Gamma_{*,h}) &= \max_{n=1,\dots,N} \max_{t\in I_n} \operatorname{dist}(\Gamma(t), \Gamma_h(t)) \\ &\approx \max_{n=1,\dots,N} \max_{t\in S_n} \operatorname{dist}(\Gamma(t), \Gamma_h(t)).\end{aligned}$$

The refinement in time has been performed on a mesh of 57344 triangles with $k_s = 4$. The refinement in space was carried out with a time step of $\Delta t = 1/64$ and $k_t = 4$. The results are shown in Figure 4.4.The numerical test confirms the prediction (4.10).

4.3 Isoparametric space-time discretization

In this section we describe the adaptations that are necessary when switching from a space-time discretization that assumes exact geometry handling to the isoparametric case. As a start, consider the variational formulation from chapter 2.

Find u in W_h such that for all v in W_h

$$B(u, v) + J(u, v) = f(v)$$

holds true. In practice, the alternative representation $B(u, v) = d'(u, v) + b'(u, v) + a(u, v)$ is preferred in order to stay as close to the mass conservation property as possible (cf. Remark 3). For v which is supported in Q^n it holds that $v_+^n = v_-^{n-1} = 0$. By testing with such a function one obtains the problem for the time slab Q^n:

$$(u, -\partial_t v - \mathbf{w}\cdot\nabla v)_{Q^n} + (\nabla u, \nabla v)_{Q^n} + \left(u_-^n, v_-^n\right)_{\Omega^n} + j_h^n(u, v) = (f, v)_{Q^n} + \left(u_-^{n-1}, v_+^{n-1}\right)_{\Omega^{n-1}}. \tag{4.11}$$

The transition to isoparametric (unfitted) FEM works similar as described for the stationary case. The integrals $\int_{Q^n} f$ are approximated by

$$\int_{Q^n} f \approx \int_{\Theta_h(Q^{n,\mathrm{lin}})} f, \quad \text{with} \quad \Theta_h(Q^{n,\mathrm{lin}}) = \bigcup_{t\in I_n} \Theta_h(t)\left(\Omega^{\mathrm{lin}}(t)\right) \times \{t\}.$$

This requires to replace u and v in (4.11) by functions from the isoparametric space-time finite element space

$$W_{n,\Theta_h} \coloneqq \{v \mid v(t,\Theta_h(t,\hat{x})) = \hat{v}(t,\hat{x}) \text{ for } \hat{x} \in \Omega^{\text{lin}}(t), \text{ with } \hat{v} \in W_n\}.$$

Here we follow the convention to denote a function defined on the undeformed mesh by $\hat{v} : Q^{n,\text{lin}} \mapsto \mathbb{R}$, while $v : \Theta_h(Q^{n,\text{lin}}) \mapsto \mathbb{R}$ is defined on the deformed mesh. Using u and v from this space entails two adjustments for the variational formulation (4.11).

Contribution of the mesh velocity

The functions from the isoparametric FE-space are of the form

$$v(t,\Theta_h(t,\hat{x})) = \hat{v}(t,\hat{x}),$$

which means that the space-time mapping introduces an implicit time dependence. Therefore, the time derivative in (4.11) will also act on the space-time mapping. This leads to:

$$\begin{aligned}\frac{d}{dt}v(t,\Theta_h(t,\hat{x})) &= \frac{\partial \hat{v}}{\partial t} + \left(\frac{\partial \Theta_h}{\partial t}\right) \cdot \nabla v \\ &= \frac{\partial \hat{v}}{\partial t} + \left(\frac{\partial \Theta_h}{\partial t}\right) \cdot (D\Theta_h)^{-T} \nabla \hat{v}.\end{aligned}$$

The contribution $\partial_t \Theta_h$ corresponds to a "mesh velocity".

Treating the discontinuity of the space-time mapping between time slabs

The right hand side of (4.11) contains the term $(u_-^{n-1}, v_+^{n-1})_{\Omega^{n-1}}$. Here, the value of the solution at the top of the previous time slab Q^{n-1} is passed on as an initial condition to the variational formulation on the next time slab Q^n. If $n = 1$ so that we were to start fresh with our calculation, then we would project the initial condition into the isoparametric FE-Space: $u_-^{n-1} = u_0 \circ (\Theta_+^{n-1})^{-1}$. But for $n > 1$ all that we have at our disposal is $u_-^{n-1} = \hat{u}_-^{n-1} \circ (\Theta_-^{n-1})^{-1}$. As the space-time mapping is in general not continuous between time slabs one has

$$u_-^{n-1} = \hat{u}_-^{n-1} \circ (\Theta_-^{n-1})^{-1} \neq \hat{u}_-^{n-1} \circ (\Theta_+^{n-1})^{-1}.$$

In numerical experiments it is observed that this problem needs to be taken seriously. Using directly $u_-^{n-1} = \hat{u}_-^{n-1} \circ (\Theta_-^{n-1})^{-1}$ available from the previous time slab leads to a drop in the convergence rate.

We sketch an idea how to adress this issue: One replaces u_-^{n-1} by a projection Pu_-^{n-1} which fulfills:

$$Pu_-^{n-1} \approx \hat{u}_-^{n-1} \circ (\Theta_+^{n-1})^{-1} = u_-^{n-1} \circ \Theta_-^{n-1} \circ (\Theta_+^{n-1})^{-1}.$$

This problem can be restated as: Given the function $x \mapsto u_-^{n-1}(x)$ evaluate it at the shifted position $x \mapsto u_-^{n-1}(z)$, where $z = s(x)$ is obtained from

$$z = \Theta_-^{n-1} \circ (\Theta_+^{n-1})^{-1}(x).$$

In the implementation z is computed by a fixed point iteration. A detailed description of this projection operator will be provided in a forthcoming publication.

Remark 19 (Violation of mass conservation)**.** *In Remark 3 it was mentioned that the space-time DG method that assumes exact geometry handling is mass conserving. Unfortunately, for the isoparametric method as derived here, mass conservation cannot be guaranteed anymore. The necessity to replace u_-^{n-1} in (4.11) by the projection Pu_-^{n-1} leads to a violation of this property. Indeed, testing in (4.11) with a constant function we obtain:*

$$\int_{\Omega^n} u_-(x,t_n)\,dx = \int_{\Omega^{n-1}} (Pu_-^{n-1})(x)\,dx + \int_{Q^n} f\,dx. \tag{4.12}$$

Thus, the projection can interfere with mass conservation on the time slabs by modifying the initial condition at t_{n-1}.

Chapter 5

Implementational aspects

Most finite element packages are geared towards fitted discretizations. Thus, the realization of unfitted methods requires some additional efforts. Among these are the numerical integration on cut elements, a suitable handling of the degrees of freedom on subdomains of the mesh (often described implicitly via a level set function) and the implementation of stabilization terms. Most functionality required for the implementation of our method is provided by the following tools:

- `Netgen`: An automatic mesh generator [Sch97].
- `NGSolve`: A finite element library [Sch14] which comes as an Add-On to `Netgen`. `Netgen` and `NGSolve` are written in `C++`. Together they provide a complete package for finite element simulation. `NGSolve` features a Python frontend that allows to control the flow of the program by Python-scripting. `Netgen/NGSolve` is open source and available at `www.ngsolve.org`.
- `ngsxfem`: An Add-On to `NGSolve` which enables the use of unfitted discretizations. It provides the functionality for the numerical integration on unfitted geometries which are implicitedly described by a level set function. Moreover, the degrees of freedom belonging to the partition of the mesh induced by the level set function can be handled flexibly. A special feature of `ngsxfem` is the mesh transformation technique as described in Chapter 4. This allows for an explicit higher order representation of implicit level set geometries and provides the basis for our approach towards higher order unfitted discretizations. The Add-On is available at `https://github.com/ngsxfem/ngsxfem`.

The implementation of our method for moving domain problems required some extensions of `ngsxfem`. First, the finite element spaces on the time slab need to be implemented. These were then also used for extending the mesh transformation technique to the instationary case. Furthermore, the numerical quadrature on space-time level set domains has to be carried out. These two aspects of the implementation will be described further in this chapter.

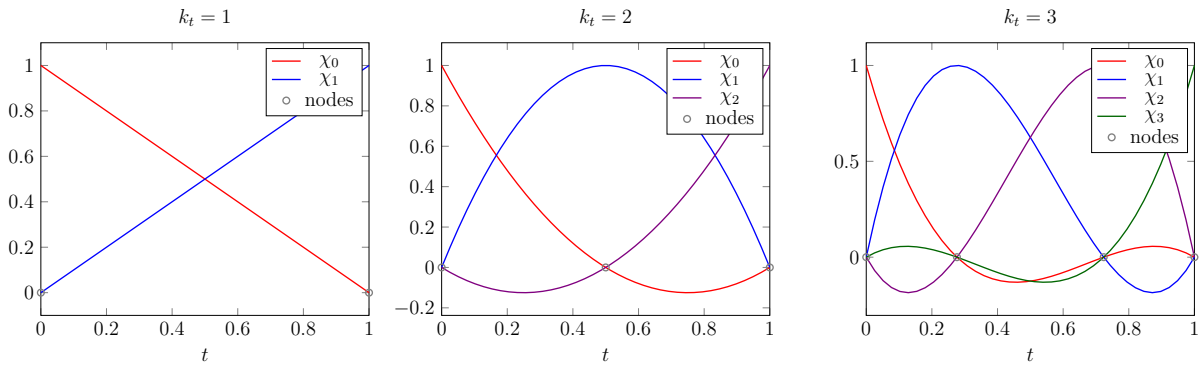

Figure 5.1: Shape functions of nodal finite element for $k_t \in \{1, 2, 3\}$.

5.1 Space-time finite element spaces

Implementing the space-time method requires a tensor product finite element space on the time slabs of the form

$$\{\hat{v} : \tilde{\Omega} \times I_n \to \mathbb{R} \mid \hat{v}(x,t) = \sum_{m=0}^{k_t} \chi_m(t)\hat{v}_m(x), \text{ with } \hat{v}_m \in V_h^{k_s}, \chi_m \in V^{k_t}\},$$

where

- $V_h^{k_s}$ is a spatial finite element space on the background mesh $\tilde{\mathcal{T}}_h$,
- V^{k_t} is a one-dimensional finite element space for the time dependence.

Nodal finite element in time

For V^{k_t} we choose a nodal finite element.This has advantages for the implementation of the reference geometry representation and the space-time mapping.

As the reference element we take the unit interval $\hat{I} = [0, 1]$. The nodes are chosen as Gauss-Lobatto points $\tau_0, \tau_1, \ldots, \tau_{k_t}$. The shape-functions are given by Lagrange polynomials

$$\chi_{k_t,m}(t) = \frac{\prod_{0 \le j \le k_t;\ j \ne m} (t - \tau_j)}{\prod_{0 \le j \le k_t;\ j \ne m} (\tau_m - \tau_j)}.$$

Figure 5.1 visualizes the shape-functions for $k_t \in \{1, 2, 3\}$.

Finite element in space

We use a triangulation of the background domain $\tilde{\Omega}$ into simplices $T \in \tilde{\mathcal{T}}_h$. The elements T are related to the reference simplex $\hat{T}$ by an affine linear transformation. The shape functions on $\hat{T}$ will be denoted by

$$\varphi_1(x), \varphi_2(x), \ldots, \varphi_{N_s}(x),$$

where N_s denotes the degrees of freedom.

Space-time finite element

Here the reference element is given by the space-time prism $\hat{Q}_T = \hat{T} \times \hat{I}$. The shape functions on $\hat{Q}_T$ are obtained by simply taking tensor products of the shape functions on $\hat{T}$ and $\hat{I}$:

$$\chi_m(t)\varphi_j(x), \quad m = 0, \dots, k_t;\ j = 1, \dots, N_s.$$

The space-time FE space then provides the connnection between the local reference prism and the global mesh.

Implementation of space-time mesh deformation

The constructed space-time finite element space is based on a nodal basis in time. This allows for a convenient implementation of the reference geometry approximation and the space-time mapping from chapter 4.2. For the high order accurate geometry approximation of the exact level set function $\phi(x,t)$ we make the ansatz

$$\phi_h(x,t) = \sum_{m=0}^{k_t} \chi_m(t)\phi_m(x), \text{ with } \phi_m \in V_h^{k_s}.$$

On the nodes τ_m we have that

$$\phi_h(x, \tau_m) = \phi_m(x),$$

for which we can choose $\phi_m = P_{k_s}\phi(\cdot, \tilde{\tau}_m)$ where $\tilde{\tau}_m = t_{n-1} + \Delta t \cdot \tau_m$ and P_{k_s} is a suitable projector into $V_h^{k_s}$. This ensures that the approximation error at the nodes τ_m for $m = 0, \dots, k_t$ is of order $\mathcal{O}(h^{k_s+1})$.

The reference geometry approximation

$$\hat{\phi}_h(x,t) = \sum_{m=0}^{k_t} \chi_m(t)\hat{\phi}_m(x), \text{ with } \hat{\phi}_m = I_1\phi_m \in V_h^1$$

and the space-time mapping

$$\Theta_h(x,t) = \sum_{m=0}^{k_t} \chi_m(t)\Theta_m(x), \text{ with } \Theta_m \in [V_h^{k_s}]^d$$

with $\hat{\phi}_m(x) \approx \phi_m(\Theta_m(x))$ follow accordingly. At the nodes τ_m we then have

$$\begin{aligned} \phi_h(\tau_m, \Theta_h(x, \tau_m)) &= \phi_m(\Theta_m(x)) \\ &\approx \hat{\phi}_m(x) \\ &= \hat{\phi}_h(x, \tau_m), \end{aligned}$$

for every $m = 0, \dots, k_t$.

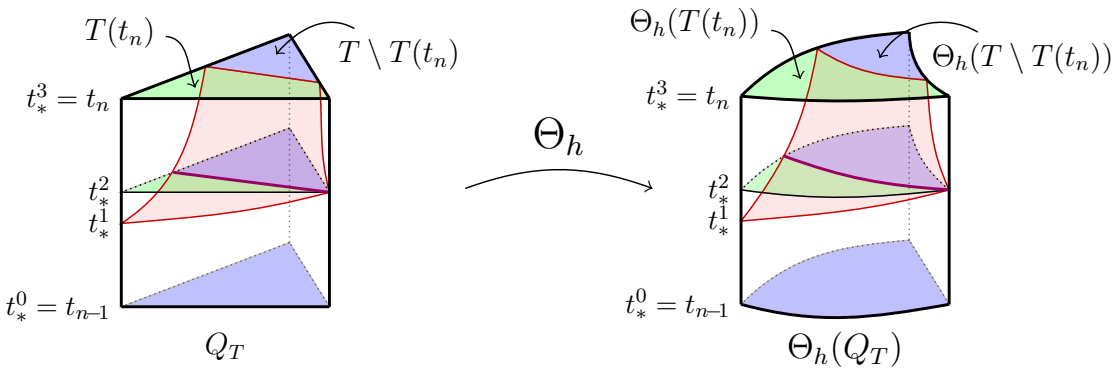

Figure 5.2: Numerical integration on a space-time prism in isoparametric unfitted finite elements.

5.2 Quadrature on space-time level set domains

The main idea for computing the integrals for the space-time method is similar to the stationary case. In the isoparametric method the integrals over Q^n are approximated by integrals over the high order accurate geometry description provided by the space-time mapping. So one has to compute integrals of the form

$$\int_{\Theta_h(Q^{n,\mathrm{lin}})} f = \sum_{Q_T^n \cap Q^{n,\mathrm{lin}} \neq \emptyset} \int_{t_{n-1}}^{t_n} \int_{\Theta_h(T(t))} f \, dx \, dt,$$

where $T(t) = T \cap \{\hat{\phi}_h(\cdot, t) < 0\}$ is the part of the element which belongs to $\Omega^{\mathrm{lin}}(t)$. The corresponding decomposition of the space time prism Q_T is shown in Figure 5.2. By means of the transformation formula the integrals over the deformed space-time prisms can be reduced to the undeformed case

$$\int_{t_{n-1}}^{t_n} \int_{\Theta_h(T(t))} f(x,t) \, dx \, dt = \int_{t_{n-1}}^{t_n} \int_{T(t)} f(\Theta_h(y,t),t) \, |\det D\Theta_h(y,t)| \, dy \, dt.$$

It remains to treat integrals of the form

$$\int_{t_{n-1}}^{t_n} \int_{T(t)} g(x,t) \, dx \, dt$$

for which we can use the fact that $T(t)$ is described by $\hat{\phi}_h \in V_h^{k_t,1}$. This means that at a fixed time $\bar{t}$ the function $\hat{\phi}_h(\cdot, \bar{t})$ is piecewise linear. Thus, the cut topology of the element $T(t)$ at $t = \bar{t}$ is determined by the values of $\hat{\phi}_h(x, \bar{t})$ at the spatial vertices $x = x_V$ of T. For the cut topology to change it is necessary that $\hat{\phi}_h(x_V, \cdot)$ switches its sign on one of the vertices x_V. This leads to the following procedure:

- For each space-time edge $x_V \times [t_{n-1}, t_n]$ compute the zeros t_*^j of the one-dimensional function $\hat{\phi}_h(x_V, \cdot)$. An illustration is given in Figure 5.2. Collect these in the set $\{t_*^j\}$ and add the initial t_{n-1} and final time t_n.

- Between consecutive times $[t_*^j, t_*^{j+1}]$ the cut topology remains the same. Hence, we can write

$$\int_{t_{n-1}}^{t_n} \int_{T(t)} g(x,t)\, dx\, dt = \sum_j \int_{t_*^j}^{t_*^{j+1}} \int_{T(t)} g(x,t)\, dx\, dt$$

  and treat the integrals over $[t_*^j, t_*^{j+1}]$ separately. We notice that $t \mapsto \int_{T(t)} g(x,t)\, dx$ is smooth inside (t_*^j, t_*^{j+1}) if $g(\cdot)$ is smooth.

- Applying quadrature in time yields

$$\int_{t_*^j}^{t_*^{j+1}} \int_{T(t)} g(x,t)\, dx\, dt \approx \sum_l \omega_l \int_{T(t_l)} g(x,t_l)\, dx \tag{5.1}$$

  with appropriate $t_l \in [t_*^j, t_*^{j+1}]$. The remaining spatial integrals over $T(t_l)$ are treated according to the cut topology on $[t_*^j, t_*^{j+1}]$. If the element is not cut between these times then $T(t_l) = T$ or $T(t_l) = \emptyset$ and the integral can be approximated by a standard quadrature rule in space. In the other case, so if a cut occurs, the integral over $T(t_l)$ can for example be computed by the tesselation approach. This is possible since the cut is described by the piecewise linear level set function $\hat{\phi}_h(\cdot, t_l)$.

  The description above only deals with the integration on parts of the space-time prisms where $\{\hat{\phi}_h < 0\}$. For other boundary conditions or interface problems also the integration on $\{\hat{\phi}_h > 0\}$ and $\{\hat{\phi}_h = 0\}$ is needed. For these cases one proceeds similarly as above.

  In the end, all the integrals that need to be computed in the implementation of the isoparametric method can be reduced to the reference configuration described by $\hat{\phi}_h \in V_h^{k_t,1}$. Thus, it should be possible to integrate the isoparametric space-time method into CutFEM codes which provide spatial integration rules for elements which are cut by a piecewise linear approximation of a level set function. Additionally, the mesh deformation is required. However, as mentioned in [LR17] this is also easy to implement.

Remark 20 (Numerical Integration on Hyperrectangles in Isoparametric Unfitted Finite Elements)**.** *In this thesis only simplicial elements are used. The low oder approximation of the level set function is then piecewise linear on each element. This allows for a tesselation of cut elements into simpler geometries on which standard integration rules can be applied. For quadrilateral and hexahedral elements the corresponding low order approximation of the level set function is not piecewise linear anymore. This renders the numerical integration on such elements more challenging. An approach that also takes the isoparametric mapping into account is proposed in [HL17]. The basic principle for the integration is similar to the case of space-time prisms as described in this section.*

Remark 21 (Integration on space-time level set domains by quadrature in time)**.** *There is an alternative approach for computing the integrals $\int_{Q^n} f\, dx\, dt$ over the time slabs Q^n that is used in [HLZ16] and [Zah18]. These papers consider stabilized space-time cut finite element methods for solving PDEs on moving domains. The arising space-time integrals*

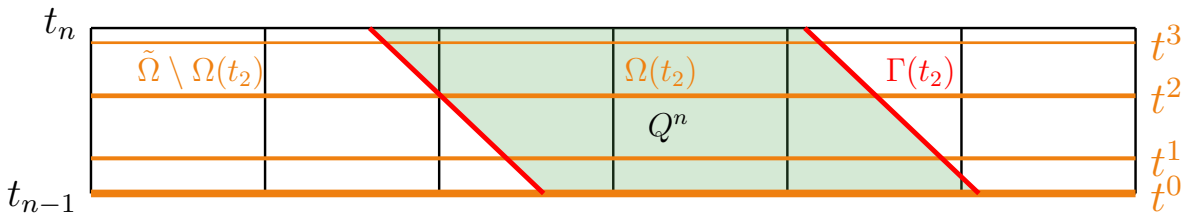

Figure 5.3: Integration on the time slab by quadrature in time.

are approximated by first applying quadrature in time. One chooses a temporal quadrature rule with weights ω_l and corresponding times $t^l \in [t_{n-1}, t_n]$, e.g. the Gauss-Radau rule as illustrated in Figure 5.3. The integral over Q^n is computed by applying quadrature in time first:

$$\int_{Q^n} f(x,t)\, dx\, dt \approx \sum_{l=0}^{3} \omega_l \int_{\Omega(t^l)} f(x,t^l)\, dx.$$

Now it only remains to treat integrals over spatial cut configurations $\Omega(t^l)$. Hence, the quadrature in time approach basically reduces the quadrature problem on space-time level set domains to the purely spatial situation.

This method has the advantage of being simple to implement into codes that can deal with stationary problems on unfitted meshes. Moreover, it can easily be combined with the isoparametric mapping at the quadrature points t^l. Since the mesh transformation is only applied at these quadrature points, the problem of introducing a discontinuity through the space-time mesh transformation, as described in section 4.3, is avoided. Hence, it is not necessary to apply a projection step and conservation of mass can be guaranteed (cf. Remark 19). Also, this method performed very well in our numerical tests.

However, we do not follow this approach here. Instead, we opt for the more involved space-time quadrature as described in this chapter. By computing the cut positions t_*^j as seen in Figure 5.2 on each space-time prism, we can guarantee that the cut topology does not change in the interval $[t_*^j, t_*^{j+1}]$. Hence, the integrand has enough regularity to ensure that the integral in (5.1) can be computed with high accuracy. We question whether this also holds true for the quadrature in time approach. Here, one applies a standard quadrature rule in time without taking the cut positions into account. Due to this reason, we favor our space-time quadrature approach as it appears more promising for a future analysis.

Chapter 6

Numerical experiments for a moving domain problem

In this chapter it will be investigated how the method performs for two different numerical examples. The aim is to compare the numerical results with the error bounds derived in Theorem 3.27. In the implementation we always use the alternative version of the bilinear form (2.9), obtained via integration by parts.

6.1 Moving circle

6.1.1 Description of test case

The moving domain (see Figure 6.1) for this test problem is a circle

$$\Omega(t) = \{(x, y) \in \mathbb{R}^2 \mid \sqrt{x^2 + (y - \rho(t))^2} < r_0\}$$

with $r_0 = \frac{1}{2}$ and $\rho(t) = \frac{1}{\pi}\sin(2\pi t)$. Consider a convection of the form $\mathbf{w} = \big(0, \dot{\rho}\big)$. The right hand side is computed so that the exact solution is given by $u(x, y, t) = \chi(\sqrt{x^2 + (y - \rho(t))^2})$ with $\chi(r) = \cos^2(\frac{\pi r}{2r_0})$.

At $t = 0$ the center of the circle is at $(x, y) = (0, 0)$. It moves in the positive y-direction so that at $t = 1/4$ the center lies at $(x, y) = (0, 1/\pi)$. Then it stops and returns to its original position which it reaches at $t = T$ with $T = 1/2$. We perform the convergence studies over this time interval $[0, T]$. The stabilization parameter for the ghost penalty is chosen as $\gamma_J = 5 \cdot 10^{-2}$.

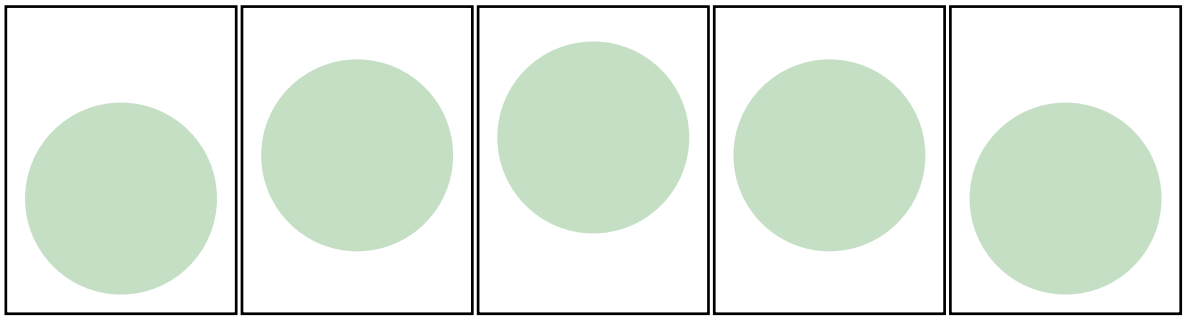

Figure 6.1: Moving circle: The domain $\Omega(t)$ for $t \in \{0, 1/8, \ldots, 4/8\}$.

6.1.2 Convergence tables

This section contains the results of the convergence studies for the test case of the moving circle in the form of tables. First we explain how to read these tables and what quantities are measured.

The errror $u - u_h$ is measured in five different (semi-)norms. The first two are the L^2-norm $\|(u-u_h)(\cdot,T)\|_{L^2(\Omega)}$ and the H^1 seminorm $\|\nabla(u-u_h)(\cdot,T)\|_{L^2(\Omega)}$ at the final time point. To be precise one would need to write $\|\cdot\|_{L^2(\Omega(T))}$ instead of $\|\cdot\|_{L^2(\Omega)}$. The other three measured quantities are $\|\nabla(u-u_h)\|_{L_t^\infty(0,T;\, L_x^2(\Omega))}$, $\|\nabla(u-u_h)\|_{L_t^\infty(0,T;\, L_x^2(\Omega))}$ and $\|\partial_t(u-u_h)\|_{L_t^\infty(0,T;\, L_x^2(\Omega))}$. Here $\|\cdot\|_{L_t^\infty(0,T;\, L_x^2(\Omega))}$ denotes the L^∞-norm in time for functions taking values in $L^2(\Omega(t))$. The L^∞-norm in time is approximated by considering ten equally spaced sample points inside each time interval I_n for $1 \leq n \leq N$ (similar to section 4.2.3).

The results are given in form of tables. The columns correspond to different refinement levels n_s of the spatial mesh. The rows show the error for different timesteps $\Delta t = T/n_t$. The last column contains the estimated order of convergence with respect to refinements in time on the finest spatial mesh (usually $n_s = 6$). Similarly, the estimated order of convergence in space for the smallest time step is shown in the second to last row. Finally, the very last row shows the estimated order of convergence when the spatial mesh and the time step are both refined on each level. The relevant values for computing the rate for this space-time refinement can be found on the diagonal of the tables.

First we pick a fixed $k_s = k_t = k$ with $k \in \{1, 2, 3\}$ and show the behavior of the error in all five described norms. Then selected results for $k_s \neq k_t$ are given. In the end, we also consider the case where the polynomial orders $k_s^{\text{geom}}, k_t^{\text{geom}}$ for the approximation of the geometry are different from the orders k_s, k_t of the approximate solution u_h. This means that the high-order accurate approximation of the level set ϕ_h and the space-time mapping Θ_h are elements of the space $V_h^{k_t^{\text{geom}},k_s^{\text{geom}}}$ respectively its vector valued version.

The results are discussed in the next section.

$k_s = 1, k_t = 1$**:**

$n_t \setminus n_s$	0	1	2	3	4	5	6	eoc_t
1	1.26	1.12	1.12	1.12	1.12	1.12	1.12	
2	0.22	0.3	0.31	0.31	0.31	0.31	0.31	1.87
4	0.15	$8.77 \cdot 10^{-2}$	$9.08 \cdot 10^{-2}$	$9.13 \cdot 10^{-2}$	$9.15 \cdot 10^{-2}$	$9.15 \cdot 10^{-2}$	$9.15 \cdot 10^{-2}$	1.74
8	0.2	$4.29 \cdot 10^{-2}$	$2.60 \cdot 10^{-2}$	$2.39 \cdot 10^{-2}$	$2.39 \cdot 10^{-2}$	$2.39 \cdot 10^{-2}$	$2.39 \cdot 10^{-2}$	1.94
16	0.21	$4.24 \cdot 10^{-2}$	$1.42 \cdot 10^{-2}$	$6.91 \cdot 10^{-3}$	$6.08 \cdot 10^{-3}$	$6.00 \cdot 10^{-3}$	$5.99 \cdot 10^{-3}$	1.99
32	0.22	$4.33 \cdot 10^{-2}$	$1.34 \cdot 10^{-2}$	$3.89 \cdot 10^{-3}$	$1.79 \cdot 10^{-3}$	$1.52 \cdot 10^{-3}$	$1.50 \cdot 10^{-3}$	2.00
64	0.22	$4.36 \cdot 10^{-2}$	$1.34 \cdot 10^{-2}$	$3.62 \cdot 10^{-3}$	$1.02 \cdot 10^{-3}$	$4.49 \cdot 10^{-4}$	$3.82 \cdot 10^{-4}$	1.97
eoc_s		2.32	1.7	1.89	1.83	1.18	0.24	
eoc_{st}		2.06	1.73	1.92	1.98	2	1.99	

Table 6.1: Moving circle problem: The error $\|(u-u_h)(\cdot,T)\|_{L^2(\Omega)}$ for $k_s = 1, k_t = 1$.

$n_t \setminus n_s$	0	1	2	3	4	5	6	eoc_t
1	3.98	3.77	3.74	3.74	3.74	3.74	3.74	
2	1.33	1.01	0.84	0.77	0.75	0.74	0.74	2.34
4	1.1	0.72	0.44	0.29	0.23	0.21	0.21	1.85
8	1.08	0.69	0.39	0.21	0.11	$6.88 \cdot 10^{-2}$	$5.09 \cdot 10^{-2}$	2.01
16	1.08	0.69	0.39	0.21	0.11	$5.40 \cdot 10^{-2}$	$2.82 \cdot 10^{-2}$	0.85
32	1.08	0.69	0.39	0.21	0.11	$5.31 \cdot 10^{-2}$	$2.67 \cdot 10^{-2}$	0.08
64	1.08	0.69	0.39	0.21	0.11	$5.30 \cdot 10^{-2}$	$2.66 \cdot 10^{-2}$	0.01
eoc_s		0.64	0.83	0.93	0.96	0.99	0.99	
eoc_{st}		1.97	1.2	1.07	0.99	1	1	

Table 6.2: Moving circle problem: The error $\|\nabla(u - u_h)(\cdot, T)\|_{L^2(\Omega)}$ for $k_s = 1, k_t = 1$.

$n_t \setminus n_s$	0	1	2	3	4	5	6	eoc_t
1	1.14	1.1	1.11	1.12	1.12	1.12	1.12	
2	0.28	0.32	0.32	0.32	0.32	0.32	0.32	1.79
4	0.15	0.11	0.1	0.1	0.1	0.1	0.1	1.66
8	0.19	$5.08 \cdot 10^{-2}$	$2.93 \cdot 10^{-2}$	$2.65 \cdot 10^{-2}$	$2.68 \cdot 10^{-2}$	$2.70 \cdot 10^{-2}$	$2.70 \cdot 10^{-2}$	1.92
16	0.2	$4.76 \cdot 10^{-2}$	$1.54 \cdot 10^{-2}$	$7.57 \cdot 10^{-3}$	$7.21 \cdot 10^{-3}$	$7.41 \cdot 10^{-3}$	$7.47 \cdot 10^{-3}$	1.86
32	0.21	$4.75 \cdot 10^{-2}$	$1.39 \cdot 10^{-2}$	$4.18 \cdot 10^{-3}$	$1.99 \cdot 10^{-3}$	$1.91 \cdot 10^{-3}$	$1.97 \cdot 10^{-3}$	1.93
64	0.21	$4.76 \cdot 10^{-2}$	$1.38 \cdot 10^{-2}$	$3.69 \cdot 10^{-3}$	$1.09 \cdot 10^{-3}$	$5.03 \cdot 10^{-4}$	$4.92 \cdot 10^{-4}$	2.00
eoc_s		2.12	1.79	1.9	1.76	1.12	$3.12 \cdot 10^{-2}$	
eoc_{st}		1.83	1.65	1.94	1.88	1.92	1.95	

Table 6.3: Moving circle problem: The error $\|u - u_h\|_{L_t^\infty(0,T;\, L_x^2(\Omega))}$ for $k_s = 1, k_t = 1$.

$n_t \setminus n_s$	0	1	2	3	4	5	6	eoc_t
1	3.73	3.73	5.52	8.52	11.86	16.11	22.3	
2	1.43	1.34	1.26	1.23	1.22	1.46	2.41	3.21
4	1.08	0.78	0.55	0.44	0.41	0.4	0.59	2.03
8	1.05	0.71	0.41	0.24	0.16	0.14	0.13	2.17
16	1.05	0.71	0.4	0.21	0.11	$6.44 \cdot 10^{-2}$	$4.57 \cdot 10^{-2}$	1.52
32	1.1	0.72	0.4	0.21	0.11	$5.41 \cdot 10^{-2}$	$2.84 \cdot 10^{-2}$	0.69
64	1.16	0.74	0.4	0.21	0.11	$5.31 \cdot 10^{-2}$	$2.68 \cdot 10^{-2}$	0.09
eoc_s		0.64	0.9	0.95	0.97	0.99	0.99	
eoc_{st}		1.47	1.3	1.19	1.09	1.05	1.02	

Table 6.4: Moving circle problem: The error $\|\nabla(u - u_h)\|_{L_t^\infty(0,T;\, L_x^2(\Omega))}$ for $k_s = 1, k_t = 1$.

$n_t \setminus n_s$	0	1	2	3	4	5	6	eoc_t
1	3.91	3.8	3.81	3.81	3.82	3.82	3.82	
2	2.67	2.83	2.86	2.86	2.86	2.86	2.86	0.42
4	2.02	1.81	1.86	1.91	1.93	1.94	1.94	0.56
8	1.72	1.3	1.23	1.22	1.23	1.23	1.24	0.65
16	1.68	1.1	0.83	0.72	0.69	0.69	0.69	0.83
32	2.35	1.24	0.67	0.44	0.38	0.37	0.37	0.92
64	3.9	1.89	0.66	0.3	0.21	0.19	0.19	0.96
eoc_s		1.04	1.53	1.13	0.49	0.14	$3.05 \cdot 10^{-2}$	
eoc_{st}		0.47	0.6	0.61	0.81	0.91	0.96	

Table 6.5: Moving circle problem: The error $\|\partial_t(u - u_h)\|_{L_t^\infty(0,T;\, L_x^2(\Omega))}$ for $k_s = 1, k_t = 1$.

$k_s = 2, k_t = 2$**:**

$n_t \setminus n_s$	0	1	2	3	4	5	6	eoc_t
1	0.69	0.29	0.2	0.2	0.2	0.2	0.2	
2	0.49	$9.36 \cdot 10^{-2}$	$3.16 \cdot 10^{-2}$	$2.88 \cdot 10^{-2}$	$2.89 \cdot 10^{-2}$	$2.89 \cdot 10^{-2}$	$2.89 \cdot 10^{-2}$	2.79
4	0.47	$8.15 \cdot 10^{-2}$	$8.97 \cdot 10^{-3}$	$2.92 \cdot 10^{-3}$	$2.84 \cdot 10^{-3}$	$2.83 \cdot 10^{-3}$	$2.82 \cdot 10^{-3}$	3.35
8	0.47	$8.10 \cdot 10^{-2}$	$7.60 \cdot 10^{-3}$	$2.51 \cdot 10^{-4}$	$1.80 \cdot 10^{-4}$	$1.77 \cdot 10^{-4}$	$1.77 \cdot 10^{-4}$	4.00
16	0.47	$8.09 \cdot 10^{-2}$	$7.40 \cdot 10^{-3}$	$1.14 \cdot 10^{-4}$	$1.50 \cdot 10^{-5}$	$1.06 \cdot 10^{-5}$	$1.04 \cdot 10^{-5}$	4.09
32	0.47	$8.07 \cdot 10^{-2}$	$7.39 \cdot 10^{-3}$	$1.04 \cdot 10^{-4}$	$9.00 \cdot 10^{-6}$	$1.38 \cdot 10^{-6}$	$7.08 \cdot 10^{-7}$	3.87
64	0.47	$8.07 \cdot 10^{-2}$	$7.36 \cdot 10^{-3}$	$1.00 \cdot 10^{-4}$	$8.91 \cdot 10^{-6}$	$1.13 \cdot 10^{-6}$	$1.53 \cdot 10^{-7}$	2.21
eoc_s		2.54	3.45	6.2	3.49	2.97	2.89	
eoc_{st}		2.89	3.38	5.16	4.07	3.44	3.17	

Table 6.6: Moving circle problem: The error $\|(u - u_h)(\cdot, T)\|_{L^2(\Omega)}$ for $k_s = 2, k_t = 2$.

$n_t \setminus n_s$	0	1	2	3	4	5	6	eoc_t
1	0.76	0.68	0.69	0.71	0.72	0.73	0.73	
2	0.44	0.23	0.2	0.2	0.2	0.2	0.2	1.90
4	0.48	0.14	$4.05 \cdot 10^{-2}$	$2.06 \cdot 10^{-2}$	$1.88 \cdot 10^{-2}$	$1.86 \cdot 10^{-2}$	$1.86 \cdot 10^{-2}$	3.40
8	0.45	0.14	$3.61 \cdot 10^{-2}$	$9.19 \cdot 10^{-3}$	$2.72 \cdot 10^{-3}$	$1.56 \cdot 10^{-3}$	$1.46 \cdot 10^{-3}$	3.67
16	0.45	0.14	$3.68 \cdot 10^{-2}$	$9.38 \cdot 10^{-3}$	$2.38 \cdot 10^{-3}$	$6.15 \cdot 10^{-4}$	$2.10 \cdot 10^{-4}$	2.80
32	0.45	0.14	$3.73 \cdot 10^{-2}$	$9.45 \cdot 10^{-3}$	$2.40 \cdot 10^{-3}$	$6.06 \cdot 10^{-4}$	$1.53 \cdot 10^{-4}$	0.46
64	0.45	0.14	$3.74 \cdot 10^{-2}$	$9.52 \cdot 10^{-3}$	$2.41 \cdot 10^{-3}$	$6.09 \cdot 10^{-4}$	$1.53 \cdot 10^{-4}$	-0.01
eoc_s		1.7	1.89	1.98	1.98	1.99	1.99	
eoc_{st}		1.7	2.52	2.14	1.95	1.97	1.98	

Table 6.7: Moving circle problem: The error $\|\nabla(u - u_h)(\cdot, T)\|_{L^2(\Omega)}$ for $k_s = 2, k_t = 2$.

$n_t \setminus n_s$	0	1	2	3	4	5	6	eoc_t
1	0.69	0.29	0.21	0.21	0.2	0.2	0.2	
2	0.49	$9.36 \cdot 10^{-2}$	$6.47 \cdot 10^{-2}$	$6.37 \cdot 10^{-2}$	$6.33 \cdot 10^{-2}$	$6.31 \cdot 10^{-2}$	$6.30 \cdot 10^{-2}$	1.68
4	0.47	$8.15 \cdot 10^{-2}$	$1.35 \cdot 10^{-2}$	$1.25 \cdot 10^{-2}$	$1.25 \cdot 10^{-2}$	$1.25 \cdot 10^{-2}$	$1.25 \cdot 10^{-2}$	2.33
8	0.47	$8.10 \cdot 10^{-2}$	$7.60 \cdot 10^{-3}$	$2.01 \cdot 10^{-3}$	$2.02 \cdot 10^{-3}$	$2.02 \cdot 10^{-3}$	$2.02 \cdot 10^{-3}$	2.63
16	0.47	$8.09 \cdot 10^{-2}$	$7.40 \cdot 10^{-3}$	$2.94 \cdot 10^{-4}$	$2.80 \cdot 10^{-4}$	$2.80 \cdot 10^{-4}$	$2.80 \cdot 10^{-4}$	2.85
32	0.47	$8.08 \cdot 10^{-2}$	$7.39 \cdot 10^{-3}$	$1.13 \cdot 10^{-4}$	$3.79 \cdot 10^{-5}$	$3.69 \cdot 10^{-5}$	$3.68 \cdot 10^{-5}$	2.93
64	0.47	$8.07 \cdot 10^{-2}$	$7.36 \cdot 10^{-3}$	$1.03 \cdot 10^{-4}$	$1.01 \cdot 10^{-5}$	$4.87 \cdot 10^{-6}$	$4.73 \cdot 10^{-6}$	2.96
eoc_s		2.55	3.45	6.16	3.35	1.05	$4.04 \cdot 10^{-2}$	
eoc_{st}		2.89	2.79	2.75	2.84	2.93	2.96	

Table 6.8: Moving circle problem: The error $\|u - u_h\|_{L_t^\infty(0,T;\, L_x^2(\Omega))}$ for $k_s = 2, k_t = 2$.

$n_t \setminus n_s$	0	1	2	3	4	5	6	eoc_t
1	0.86	0.84	0.87	0.9	0.92	0.92	1.75	
2	0.54	0.4	0.39	0.39	0.4	0.4	0.4	2.13
4	0.48	0.17	$8.09 \cdot 10^{-2}$	$7.35 \cdot 10^{-2}$	$7.33 \cdot 10^{-2}$	$7.34 \cdot 10^{-2}$	$7.34 \cdot 10^{-2}$	2.44
8	0.47	0.16	$3.95 \cdot 10^{-2}$	$1.43 \cdot 10^{-2}$	$1.12 \cdot 10^{-2}$	$1.10 \cdot 10^{-2}$	$1.10 \cdot 10^{-2}$	2.74
16	0.45	0.16	$3.81 \cdot 10^{-2}$	$9.61 \cdot 10^{-3}$	$2.85 \cdot 10^{-3}$	$1.66 \cdot 10^{-3}$	$1.56 \cdot 10^{-3}$	2.82
32	0.45	0.16	$3.81 \cdot 10^{-2}$	$9.60 \cdot 10^{-3}$	$2.94 \cdot 10^{-3}$	$6.53 \cdot 10^{-4}$	$2.64 \cdot 10^{-4}$	2.56
64	0.45	0.17	$3.82 \cdot 10^{-2}$	$9.59 \cdot 10^{-3}$	$2.44 \cdot 10^{-3}$	$6.72 \cdot 10^{-4}$	$1.60 \cdot 10^{-4}$	0.72
eoc_s		1.41	2.15	1.99	1.98	1.86	2.07	
eoc_{st}		1.12	2.3	2.5	2.32	2.13	2.03	

Table 6.9: Moving circle problem: The error $\|\nabla(u - u_h)\|_{L_t^\infty(0,T;\, L_x^2(\Omega))}$ for $k_s = 2, k_t = 2$.

$n_t \setminus n_s$	0	1	2	3	4	5	6	eoc_t
1	3.58	3.75	3.77	3.79	3.79	3.79	3.79	
2	2.83	2.19	2.09	2.1	2.11	2.11	2.11	0.84
4	2.43	0.98	0.93	0.94	0.95	0.95	0.95	1.16
8	1.9	0.43	0.3	0.3	0.3	0.3	0.3	1.65
16	2.46	0.41	0.1	$8.27 \cdot 10^{-2}$	$8.30 \cdot 10^{-2}$	$8.31 \cdot 10^{-2}$	$8.31 \cdot 10^{-2}$	1.86
32	3.3	0.42	$5.64 \cdot 10^{-2}$	$2.27 \cdot 10^{-2}$	$2.17 \cdot 10^{-2}$	$2.17 \cdot 10^{-2}$	$2.17 \cdot 10^{-2}$	1.94
64	4.01	0.59	$5.91 \cdot 10^{-2}$	$6.22 \cdot 10^{-3}$	$5.75 \cdot 10^{-3}$	$5.57 \cdot 10^{-3}$	$5.52 \cdot 10^{-3}$	1.97
eoc_s		2.76	3.32	3.25	0.11	$4.45 \cdot 10^{-2}$	$1.39 \cdot 10^{-2}$	
eoc_{st}		0.71	1.23	1.63	1.86	1.94	1.97	

Table 6.10: Moving circle problem: The error $\|\partial_t(u - u_h)\|_{L_t^\infty(0,T;\, L_x^2(\Omega))}$ for $k_s = 2, k_t = 2$.

$k_s = 3, k_t = 3$**:**

$n_t \setminus n_s$	0	1	2	3	4	5	6	eoc_t
1	0.35	$7.36 \cdot 10^{-2}$	$5.06 \cdot 10^{-2}$	$5.22 \cdot 10^{-2}$	$5.24 \cdot 10^{-2}$	$5.25 \cdot 10^{-2}$	$5.25 \cdot 10^{-2}$	
2	0.35	$6.67 \cdot 10^{-2}$	$8.08 \cdot 10^{-3}$	$3.84 \cdot 10^{-3}$	$3.68 \cdot 10^{-3}$	$3.65 \cdot 10^{-3}$	$3.64 \cdot 10^{-3}$	3.85
4	0.35	$6.47 \cdot 10^{-2}$	$6.19 \cdot 10^{-3}$	$3.99 \cdot 10^{-4}$	$2.75 \cdot 10^{-4}$	$2.60 \cdot 10^{-4}$	$2.57 \cdot 10^{-4}$	3.82
8	0.35	$6.43 \cdot 10^{-2}$	$5.76 \cdot 10^{-3}$	$1.03 \cdot 10^{-4}$	$1.93 \cdot 10^{-5}$	$1.13 \cdot 10^{-5}$	$1.06 \cdot 10^{-5}$	4.60
16	0.35	$6.43 \cdot 10^{-2}$	$5.57 \cdot 10^{-3}$	$4.85 \cdot 10^{-5}$	$4.53 \cdot 10^{-6}$	$9.94 \cdot 10^{-7}$	$4.15 \cdot 10^{-7}$	4.68
32	0.34	$6.42 \cdot 10^{-2}$	$5.56 \cdot 10^{-3}$	$3.38 \cdot 10^{-5}$	$1.46 \cdot 10^{-6}$	$2.79 \cdot 10^{-7}$	$5.78 \cdot 10^{-8}$	2.84
64	0.35	$6.41 \cdot 10^{-2}$	$5.54 \cdot 10^{-3}$	$2.66 \cdot 10^{-5}$	$4.95 \cdot 10^{-7}$	$1.44 \cdot 10^{-7}$	$2.01 \cdot 10^{-8}$	1.53
eoc_s		2.43	3.53	7.7	5.75	1.78	2.84	
eoc_{st}		2.38	3.43	5.92	4.5	4.02	3.79	

Table 6.11: Moving circle problem: The error $\|(u - u_h)(\cdot, T)\|_{L^2(\Omega)}$ for $k_s = 3, k_t = 3$.

$n_t \setminus n_s$	0	1	2	3	4	5	6	eoc_t
1	0.49	0.39	0.39	0.39	0.39	0.39	0.39	
2	0.38	$7.22 \cdot 10^{-2}$	$3.64 \cdot 10^{-2}$	$3.29 \cdot 10^{-2}$	$3.21 \cdot 10^{-2}$	$3.20 \cdot 10^{-2}$	$3.19 \cdot 10^{-2}$	3.60
4	0.6	$7.77 \cdot 10^{-2}$	$1.08 \cdot 10^{-2}$	$4.46 \cdot 10^{-3}$	$3.54 \cdot 10^{-3}$	$3.38 \cdot 10^{-3}$	$3.35 \cdot 10^{-3}$	3.25
8	0.25	$5.48 \cdot 10^{-2}$	$5.65 \cdot 10^{-3}$	$8.59 \cdot 10^{-4}$	$3.00 \cdot 10^{-4}$	$2.17 \cdot 10^{-4}$	$2.07 \cdot 10^{-4}$	4.02
16	0.24	$5.78 \cdot 10^{-2}$	$5.15 \cdot 10^{-3}$	$4.60 \cdot 10^{-4}$	$6.04 \cdot 10^{-5}$	$2.62 \cdot 10^{-5}$	$1.31 \cdot 10^{-5}$	3.98
32	0.23	$6.15 \cdot 10^{-2}$	$4.89 \cdot 10^{-3}$	$2.97 \cdot 10^{-4}$	$6.53 \cdot 10^{-5}$	$2.06 \cdot 10^{-5}$	$7.53 \cdot 10^{-6}$	0.80
64	0.24	$5.27 \cdot 10^{-2}$	$4.81 \cdot 10^{-3}$	$2.76 \cdot 10^{-4}$	$5.52 \cdot 10^{-5}$	$5.80 \cdot 10^{-5}$	$1.32 \cdot 10^{-5}$	−0.81
eoc_s		2.16	3.45	4.12	2.32	$-7.09 \cdot 10^{-2}$	2.13	
eoc_{st}		2.75	2.74	3.65	3.83	1.55	0.64	

Table 6.12: Moving circle problem: The error $\|\nabla(u - u_h)(\cdot, T)\|_{L^2(\Omega)}$ for $k_s = 3, k_t = 3$.

$n_t \setminus n_s$	0	1	2	3	4	5	6	eoc_t
1	0.35	$9.88 \cdot 10^{-2}$	0.1	0.1	0.1	0.1	0.1	
2	0.35	$6.67 \cdot 10^{-2}$	$2.06 \cdot 10^{-2}$	$2.03 \cdot 10^{-2}$	$2.01 \cdot 10^{-2}$	$2.01 \cdot 10^{-2}$	$2.01 \cdot 10^{-2}$	2.34
4	0.35	$6.47 \cdot 10^{-2}$	$6.19 \cdot 10^{-3}$	$2.06 \cdot 10^{-3}$	$2.01 \cdot 10^{-3}$	$2.01 \cdot 10^{-3}$	$2.00 \cdot 10^{-3}$	3.33
8	0.35	$6.43 \cdot 10^{-2}$	$5.76 \cdot 10^{-3}$	$1.62 \cdot 10^{-4}$	$1.59 \cdot 10^{-4}$	$1.60 \cdot 10^{-4}$	$1.60 \cdot 10^{-4}$	3.65
16	0.35	$6.43 \cdot 10^{-2}$	$5.57 \cdot 10^{-3}$	$4.85 \cdot 10^{-5}$	$1.22 \cdot 10^{-5}$	$1.18 \cdot 10^{-5}$	$1.18 \cdot 10^{-5}$	3.77
32	0.34	$6.42 \cdot 10^{-2}$	$5.56 \cdot 10^{-3}$	$3.38 \cdot 10^{-5}$	$1.48 \cdot 10^{-5}$	$1.51 \cdot 10^{-6}$	$7.99 \cdot 10^{-7}$	3.88
64	0.34	$6.41 \cdot 10^{-2}$	$5.54 \cdot 10^{-3}$	$2.88 \cdot 10^{-5}$	$3.43 \cdot 10^{-6}$	$2.41 \cdot 10^{-6}$	$4.79 \cdot 10^{-7}$	0.74
eoc_s		2.43	3.53	7.59	3.07	0.51	2.33	
eoc_{st}		2.37	3.43	5.26	3.73	3.02	1.65	

Table 6.13: Moving circle problem: The error $\|u - u_h\|_{L_t^\infty(0,T;\, L_x^2(\Omega))}$ for $k_s = 3, k_t = 3$.

$n_t \setminus n_s$	0	1	2	3	4	5	6	eoc_t
1	0.73	0.72	0.74	0.74	0.75	0.75	0.75	
2	0.59	0.13	0.11	0.11	0.11	0.11	0.11	2.73
4	0.6	$9.18 \cdot 10^{-2}$	$2.44 \cdot 10^{-2}$	$1.38 \cdot 10^{-2}$	$1.39 \cdot 10^{-2}$	$1.40 \cdot 10^{-2}$	$1.40 \cdot 10^{-2}$	3.00
8	0.45	$8.54 \cdot 10^{-2}$	$9.73 \cdot 10^{-3}$	$1.89 \cdot 10^{-3}$	$1.55 \cdot 10^{-3}$	$1.31 \cdot 10^{-3}$	$1.30 \cdot 10^{-3}$	3.43
16	0.31	$7.32 \cdot 10^{-2}$	$7.77 \cdot 10^{-3}$	$9.71 \cdot 10^{-4}$	$4.41 \cdot 10^{-4}$	$6.29 \cdot 10^{-4}$	$3.74 \cdot 10^{-4}$	1.80
32	0.31	0.14	$7.78 \cdot 10^{-3}$	$3.02 \cdot 10^{-3}$	$3.29 \cdot 10^{-3}$	$7.03 \cdot 10^{-4}$	$3.72 \cdot 10^{-4}$	0.01
64	0.28	$7.62 \cdot 10^{-2}$	$7.78 \cdot 10^{-3}$	$3.40 \cdot 10^{-4}$	$9.83 \cdot 10^{-4}$	$1.12 \cdot 10^{-3}$	$3.76 \cdot 10^{-4}$	−0.02
eoc_s		1.86	3.29	4.52	−1.53	−0.19	1.58	
eoc_{st}		2.43	2.47	3.69	2.1	−0.67	0.9	

Table 6.14: Moving circle problem: The error $\|\nabla(u - u_h)\|_{L_t^\infty(0,T;\, L_x^2(\Omega))}$ for $k_s = 3, k_t = 3$.

$n_t \setminus n_s$	0	1	2	3	4	5	6	eoc_t
1	3.37	3.47	3.44	3.45	3.45	3.45	3.46	
2	2.96	1.35	1.35	1.35	1.35	1.35	1.35	1.36
4	2.82	0.35	0.29	0.28	0.28	0.28	0.28	2.27
8	4.02	0.35	$7.23 \cdot 10^{-2}$	$4.34 \cdot 10^{-2}$	$4.37 \cdot 10^{-2}$	$4.38 \cdot 10^{-2}$	$4.39 \cdot 10^{-2}$	2.67
16	3.85	0.42	$4.88 \cdot 10^{-2}$	$7.86 \cdot 10^{-3}$	$6.13 \cdot 10^{-3}$	$6.22 \cdot 10^{-3}$	$6.24 \cdot 10^{-3}$	2.81
32	6.72	0.83	$4.87 \cdot 10^{-2}$	$2.54 \cdot 10^{-2}$	$1.81 \cdot 10^{-2}$	$2.04 \cdot 10^{-3}$	$8.29 \cdot 10^{-4}$	2.91
64	7.17	0.8	$4.91 \cdot 10^{-2}$	$2.01 \cdot 10^{-3}$	$8.31 \cdot 10^{-3}$	$6.96 \cdot 10^{-3}$	$1.38 \cdot 10^{-3}$	−0.73
eoc_s		3.17	4.02	4.61	−2.05	0.26	2.34	
eoc_{st}		1.33	2.23	2.72	2.82	1.58	0.57	

Table 6.15: Moving circle problem: The error $\|\partial_t(u - u_h)\|_{L_t^\infty(0,T;\, L_x^2(\Omega))}$ for $k_s = 3, k_t = 3$.

Selected results for $k_t \neq k_s$

$n_t \setminus n_s$	0	1	2	3	4	5	6	eoc_t
1	2.73	2.87	3.22	3.38	3.44	3.46	3.46	
2	1.75	1.13	1.21	1.35	1.36	1.36	1.35	1.36
4	2.08	0.92	0.37	0.32	0.3	0.28	0.29	2.24
8	3.1	1.48	0.53	0.13	$8.55 \cdot 10^{-2}$	$7.06 \cdot 10^{-2}$	$5.31 \cdot 10^{-2}$	2.42
16	5.56	2.59	0.69	0.19	$4.93 \cdot 10^{-2}$	$2.86 \cdot 10^{-2}$	$2.23 \cdot 10^{-2}$	1.25
32	8.51	4.57	0.94	0.21	$5.56 \cdot 10^{-2}$	$1.60 \cdot 10^{-2}$	$9.87 \cdot 10^{-3}$	1.18
64	10.67	7.5	1.58	0.3	$6.64 \cdot 10^{-2}$	$1.80 \cdot 10^{-2}$	$5.11 \cdot 10^{-3}$	0.95
eoc_s		0.51	2.25	2.37	2.2	1.88	1.82	
eoc_{st}		1.27	1.59	1.52	1.41	1.62	1.65	

Table 6.16: Moving circle problem: The error $\|\partial_t(u - u_h)\|_{L_t^\infty(0,T;\, L_x^2(\Omega))}$ for $k_s = 1, k_t = 3$.

$n_t \setminus n_s$	0	1	2	3	4	5	6	eoc_t
1	0.64	0.59	0.58	0.58	0.58	0.58	0.58	
2	0.53	0.36	0.34	0.34	0.34	0.34	0.34	0.75
4	0.42	0.1	$7.03 \cdot 10^{-2}$	$7.06 \cdot 10^{-2}$	$7.09 \cdot 10^{-2}$	$7.09 \cdot 10^{-2}$	$7.09 \cdot 10^{-2}$	2.27
8	0.35	$7.22 \cdot 10^{-2}$	$1.38 \cdot 10^{-2}$	$1.10 \cdot 10^{-2}$	$1.11 \cdot 10^{-2}$	$1.11 \cdot 10^{-2}$	$1.11 \cdot 10^{-2}$	2.67
16	0.29	$7.29 \cdot 10^{-2}$	$8.22 \cdot 10^{-3}$	$1.59 \cdot 10^{-3}$	$1.56 \cdot 10^{-3}$	$1.56 \cdot 10^{-3}$	$1.57 \cdot 10^{-3}$	2.83
32	0.3	0.14	$7.77 \cdot 10^{-3}$	$3.93 \cdot 10^{-4}$	$2.19 \cdot 10^{-4}$	$2.16 \cdot 10^{-4}$	$2.16 \cdot 10^{-4}$	2.86
64	0.27	$7.45 \cdot 10^{-2}$	$7.78 \cdot 10^{-3}$	$3.47 \cdot 10^{-4}$	$4.56 \cdot 10^{-5}$	$2.92 \cdot 10^{-5}$	$2.89 \cdot 10^{-5}$	2.90
eoc_s		1.87	3.26	4.49	2.93	0.64	$1.80 \cdot 10^{-2}$	
eoc_{st}		0.83	2.36	2.67	2.82	2.86	2.9	

Table 6.17: Moving circle problem: The error $\|\nabla(u - u_h)\|_{L_t^\infty(0,T;\, L_x^2(\Omega))}$ for $k_s = 3, k_t = 2$ and $k_s^{\mathrm{geom}} = 3, k_t^{\mathrm{geom}} = 4$.

$n_t \setminus n_s$	1	2	3	4	5	6	eoc_t
1	0.22	0.22	0.22	0.22	0.22	0.22	
2	$5.29 \cdot 10^{-2}$	$4.29 \cdot 10^{-2}$	$4.37 \cdot 10^{-2}$	$4.44 \cdot 10^{-2}$	$4.45 \cdot 10^{-2}$	$4.46 \cdot 10^{-2}$	2.31
4	$4.08 \cdot 10^{-2}$	$1.72 \cdot 10^{-2}$	$1.76 \cdot 10^{-2}$	$1.87 \cdot 10^{-2}$	$1.91 \cdot 10^{-2}$	$1.92 \cdot 10^{-2}$	1.22
8	$4.24 \cdot 10^{-2}$	$1.18 \cdot 10^{-2}$	$3.61 \cdot 10^{-3}$	$3.64 \cdot 10^{-3}$	$3.96 \cdot 10^{-3}$	$4.06 \cdot 10^{-3}$	2.24
16	$4.35 \cdot 10^{-2}$	$1.31 \cdot 10^{-2}$	$3.26 \cdot 10^{-3}$	$7.64 \cdot 10^{-4}$	$5.68 \cdot 10^{-4}$	$6.39 \cdot 10^{-4}$	2.67
32	$4.37 \cdot 10^{-2}$	$1.34 \cdot 10^{-2}$	$3.54 \cdot 10^{-3}$	$8.69 \cdot 10^{-4}$	$1.94 \cdot 10^{-4}$	$8.22 \cdot 10^{-5}$	2.96
64	$4.37 \cdot 10^{-2}$	$1.34 \cdot 10^{-2}$	$3.58 \cdot 10^{-3}$	$9.14 \cdot 10^{-4}$	$2.26 \cdot 10^{-4}$	$5.23 \cdot 10^{-5}$	0.65
eoc_s		1.7	1.9	1.97	2.02	2.11	
eoc_{st}		1.62	2.25	2.24	1.97	1.89	

Table 6.18: Moving circle problem: The error $\|(u - u_h)(\cdot, T)\|_{L^2(\Omega)}$ for $k_s = k_t = k_s^{\mathrm{geom}} = 1$ and $k_t^{\mathrm{geom}} = 2$.

$n_t \setminus n_s$	1	2	3	4	5	6	eoc_t
1	0.18	0.17	0.18	0.18	0.18	0.18	
2	$8.75 \cdot 10^{-2}$	$4.95 \cdot 10^{-2}$	$5.12 \cdot 10^{-2}$	$5.21 \cdot 10^{-2}$	$5.24 \cdot 10^{-2}$	$5.24 \cdot 10^{-2}$	1.75
4	$7.59 \cdot 10^{-2}$	$1.75 \cdot 10^{-2}$	$1.79 \cdot 10^{-2}$	$1.91 \cdot 10^{-2}$	$1.95 \cdot 10^{-2}$	$1.96 \cdot 10^{-2}$	1.42
8	$7.56 \cdot 10^{-2}$	$1.23 \cdot 10^{-2}$	$3.34 \cdot 10^{-3}$	$3.62 \cdot 10^{-3}$	$3.97 \cdot 10^{-3}$	$4.07 \cdot 10^{-3}$	2.27
16	$7.68 \cdot 10^{-2}$	$1.34 \cdot 10^{-2}$	$3.00 \cdot 10^{-3}$	$6.88 \cdot 10^{-4}$	$5.60 \cdot 10^{-4}$	$6.38 \cdot 10^{-4}$	2.67
32	$7.68 \cdot 10^{-2}$	$1.36 \cdot 10^{-2}$	$3.31 \cdot 10^{-3}$	$8.08 \cdot 10^{-4}$	$1.77 \cdot 10^{-4}$	$7.95 \cdot 10^{-5}$	3.00
64	$7.68 \cdot 10^{-2}$	$1.37 \cdot 10^{-2}$	$3.36 \cdot 10^{-3}$	$8.58 \cdot 10^{-4}$	$2.11 \cdot 10^{-4}$	$4.84 \cdot 10^{-5}$	0.72
eoc_s		2.49	2.03	1.97	2.02	2.13	
eoc_{st}		2.32	2.39	2.28	1.96	1.87	

Table 6.19: Moving circle problem: The error $\|(u-u_h)(\cdot,T)\|_{L^2(\Omega)}$ for $k_s = 1, k_t = 1$ and $k_s^{\mathrm{geom}} = 3, k_t^{\mathrm{geom}} = 3$.

$n_t \setminus n_s$	0	1	2	3	4	5	eoc_t
1	0.38	0.18	0.18	0.18	0.18	0.18	
2	0.35	$8.35 \cdot 10^{-2}$	$5.24 \cdot 10^{-2}$	$5.23 \cdot 10^{-2}$	$5.24 \cdot 10^{-2}$	$5.24 \cdot 10^{-2}$	1.75
4	0.34	$6.71 \cdot 10^{-2}$	$2.02 \cdot 10^{-2}$	$1.96 \cdot 10^{-2}$	$1.96 \cdot 10^{-2}$	$1.96 \cdot 10^{-2}$	1.42
8	0.35	$6.42 \cdot 10^{-2}$	$6.95 \cdot 10^{-3}$	$4.09 \cdot 10^{-3}$	$4.10 \cdot 10^{-3}$	$4.10 \cdot 10^{-3}$	2.26
16	0.35	$6.43 \cdot 10^{-2}$	$5.59 \cdot 10^{-3}$	$6.70 \cdot 10^{-4}$	$6.71 \cdot 10^{-4}$	$6.72 \cdot 10^{-4}$	2.61
32	0.34	$6.42 \cdot 10^{-2}$	$5.56 \cdot 10^{-3}$	$1.05 \cdot 10^{-4}$	$1.00 \cdot 10^{-4}$	$1.00 \cdot 10^{-4}$	2.74
64	0.35	$6.41 \cdot 10^{-2}$	$5.54 \cdot 10^{-3}$	$3.02 \cdot 10^{-5}$	$1.42 \cdot 10^{-5}$	$1.43 \cdot 10^{-5}$	2.81
128	0.34	$6.41 \cdot 10^{-2}$	$5.52 \cdot 10^{-3}$	$2.32 \cdot 10^{-5}$	$2.01 \cdot 10^{-6}$	$1.98 \cdot 10^{-6}$	2.85
256	0.34	0.26	$5.53 \cdot 10^{-3}$	$2.17 \cdot 10^{-5}$	$4.95 \cdot 10^{-7}$	$2.75 \cdot 10^{-7}$	2.85

Table 6.20: Moving circle problem: The error $\|(u-u_h)(\cdot,T)\|_{L^2(\Omega)}$ for $k_s = 3, k_t = 1$ and $k_s^{\mathrm{geom}} = 3, k_t^{\mathrm{geom}} = 3$.

6.1.3 Discussion of results

In chapter 3 we have derived error estimates for our method. The aim of this section is to compare the analytical predictions with the numerical observations from the test problem. An overview of the results is given in Table 6.21. It will now be discussed how the results given in the column 'numerical observation' are concluded from the data in the previous section. Consider the different (semi-)norms one after another.

- $\|\partial_t \cdot\|_Q$:

  In the numerical experiment the strong (semi-)norm $\|\partial_t \cdot\|_{L_t^\infty(0,T;\, L_x^2(\Omega))}$ was measured. The Tables 6.5,6.10 and 6.15 show $\|\partial_t(u-u_h)\|_{L_t^\infty(0,T;\, L_x^2(\Omega))}$ for $k_t = k_s = 1, 2, 3$ respectively. The convergence in time is of order k_t. For $k_t = k_s = 2, 3$ we observe a spatial convergence of order $k_s + 1$. However, for $k_t = k_s = 1$ the highest spatial rate measured is merely 1.53. To investigate this case more closely we have increased the polynomial degree in time to $k_t = 3$. The results are shown in Table 6.16. Now a second order spatial convergence is clearly visible. Hence, the poor spatial convergence for $k_t = 1$ is due to the fact that the overall error is dominated by the temporal error. Overall, it is numericall observed that

  $$\|\partial_t(u-u_h)\|_{L_t^\infty(0,T;\, L_x^2(\Omega))} \lesssim \Delta t^{k_t} + h^{k_s+1},$$

  which is optimal with respect to the approximation error estimate. With regard to the spatial convergence this is also better than the discretization error estimate.

(semi-)norm $\lvert\cdot\rvert = \dots$	approximation error $\inf_{w_h \in W_h} \lvert u - w_h\rvert \leq C \cdot \dots$	discretization error $\lvert u - u_h\rvert \leq C \cdot \dots$	numerical observation $\lvert u - u_h\rvert$
$\lVert\partial_t \cdot\rVert_Q$	$\Delta t^{k_t} + h^{k_s+1}$	$\Delta t^{k_t} + \sqrt{(1+\frac{\Delta t}{h})}\frac{h^{k_s}}{\Delta t^{1/2}}$	$\Delta t^{k_t} + h^{k_s+1}$
$\lVert\nabla \cdot\rVert_Q$	$\Delta t^{k_t+1} + h^{k_s}$	$\Delta t^{k_t+1/2} + \sqrt{(1+\frac{\Delta t}{h})}h^{k_s}$	$\Delta t^{k_t+1} + h^{k_s}$
$\lVert\cdot\rVert_Q$	$\Delta t^{k_t+1} + h^{k_s+1}$	-	$\Delta t^{k_t+1} + h^{k_s+1}$
$\lVert\nabla \cdot\rVert_{\Omega(T)}$	$\Delta t^{k_t+1/2} + \Delta t^{-1/2} h^{k_s}$	-	$\Delta t^{k_t+1} + h^{k_s}$
$\lVert\cdot\rVert_{\Omega(T)}$	$\Delta t^{k_t+1/2} + \Delta t^{-1/2} h^{k_s+1}$	$\Delta t^{k_t+1/2} + \sqrt{(1+\frac{\Delta t}{h})}h^{k_s}$	$\Delta t^{k_t+1+\alpha(k_t)} + h^{k_s+1}$ $\alpha(k_t) = 1$ for $k_t = 1, 2$ $\alpha(k_t = 3) > 1/2$

Table 6.21: Moving circle problem: Comparing the approximation and discretization error estimate with the numerical observations.

- $\lVert\nabla \cdot\rVert_Q$:

  The results for the stronger norm $\lVert\nabla \cdot\rVert_{L_t^\infty(0,T;\, L_x^2(\Omega))}$ are given in Tables 6.4,6.9 and 6.14. For $k_t = k_s = 1$ the error certainly behaves as $\mathcal{O}(\Delta t^2 + h)$. For $k_t = k_s = 2$ a second order spatial convergence is clearly visible. According to the approximation error estimate one would expect a rate of three for refinements in time. But the three highest values for eoc_t gathered from Table 6.9 are only $2.83, 2.74$ and 2.56. This is due to the influence of the spatial errors. When the polynomial degree k_s is increased to $k_s = 3$, as shown in Table 6.17, the three highest values for eoc_t improve to $2.90, 2.86$ and 2.83. The situation for $k_t = k_s = 3$ seems to be similar. We conclude that

  $$\lVert\nabla(u - u_h)\rVert_{L_t^\infty(0,T;\, L_x^2(\Omega))} \lesssim \Delta t^{k_t+1} + h^{k_s}$$

  is observed.

- $\lVert\cdot\rVert_Q$:

  Tables 6.3,6.8 and 6.13 show the results for the stronger norm $\lVert\cdot\rVert_{L_t^\infty(0,T;\, L_x^2(\Omega))}$. For $k_t = k_s \in \{1, 2\}$ the error behaves as

  $$\lVert u - u_h\rVert_{L_t^\infty(0,T;\, L_x^2(\Omega))} \lesssim \Delta t^{k_t+1} + h^{k_s+1}.$$

  To conlude that this rate also holds true for $k_t = k_s = 3$ one would need to observe a spatial convergence of order four. This value does actually not occur in Table 6.13, which is due to a kick at refinement level 3. However, the mean of the three highest values for eoc_s is 4.73. Hence, the overall rate seems to be four.

- $\lVert\nabla \cdot\rVert_{\Omega(T)}$:

  The results for the H^1 semi-norm at the final time are given in Tables 6.2,6.7 and 6.12. It is observed that

  $$\lVert\nabla(u - u_h)(\cdot, T)\rVert_{\Omega(T)} \lesssim \Delta t^{k_t+1} + h^{k_s}.$$

  Actually this is half an order in time better than the approximation error estimate.

- $\|\cdot\|_{\Omega(T)}$:

  The L^2-error at the final time point for $k_t = k_s \in \{1, 2, 3\}$ is shown in Tables 6.1,6.6 and 6.11. For $k_t = k_s = 2$ we have also plotted the results in Figure 6.3. This highlights the saturation of the error which occurs on a mesh of a given gridsize or for a fixed time step. With respect to spatial refinements a rate of k_s+1 is observed.

  For refinements in time we make an interesting observation:

  - For $k_t = 1$, $k_s = 1$ and a piecewise linear approximation of the geometry ($k_s^{\text{geom}} = k_t^{\text{geom}} = 1$) Table 6.1 shows a second order rate of convergence for refinements in time. But if the polynomial order of the geometry approximation in time is increased to $k_t^{\text{geom}} = 2$, as shown in Table 6.18, then the rate improves to three. Thus, for $k_t^{\text{geom}} = 1$ the convergence rate was limited by the low-order approximation of the geometry with respect to time. Increasing the polynomial degrees of the geometry approximation even further to $k_s^{\text{geom}} = k_t^{\text{geom}} = 3$, as shown in Table 6.19, does only lead to a small additional improvement of the rate. More precisely, we observe the the estimated orders of convergence: $2.27, 2.67$ and 3.00. Then the rate drops to 0.72 in the last refinement as the spatial error begins to dominate. In order to reduce the impact of the spatial error we can increase k_s to three. The results are shown in Table 6.20 and Figure 6.2. A third order rate of convergence is observed.
  - For $k_t = 2$ it can be seen in Table 6.6 and Figure 6.3 that $\|(u - u_h)(\cdot, T)\|_{\Omega(T)}$ converges at a rate of four with respect to refinements in time. Increasing k_t^{geom} did not lead to a further improvement of the rate in our numerical experiments.
  - For $k_t = 3$ a maximal estimated order of convergence of 4.68 can be seen in Table 6.11. We expect that it should also be possible to improve this rate to five by means of a better approximation of the geometry and an increase of k_s to mitigate the influence of the spatial error.

  Hence, the numerical experiment shows that

$$\|(u - u_h)(\cdot, T)\|_{\Omega(T)} \lesssim \Delta t^{k_t+1+\alpha(k_t)} + h^{k_s+1},$$

  where $\alpha(k_t) = 1$ for $k_t = 1, 2$ and $\alpha(k_t = 3) > 1/2$. That is, we observe superconvergence with respect to refinements in time.

In this example the numerical error in all considered norms converges at least as good as the bound for the approximation error. At the fixed time T it even converges better than the approximation error estimate in $\|\cdot\|_{\Omega(T)}$ and $\|\nabla\cdot\|_{\Omega(T)}$. Hence, the estimates for the discretization error derived in chapter 3 are definetely suboptimal for this example.

Another interesting observation is the superconvergence at the time level T with respect to refinements in time. It has been shown in Theorem 12.7 of [Tho97] that the space-time DG FEM with $k_s = k_t = 1$ applied to the fitted heat equation admits an error bound of the form

$$\|(u - u_h)(\cdot, T)\|_{\Omega} \leq C(\Delta t^3 + h^2).$$

Based on this analysis (see Theorem 12.3 in [Tho97]), one would expect an error bound of the form

$$\|(u - u_h)(\cdot, T)\|_{\Omega} \leq C(\Delta t^{2k_t+1} + h^{k_s+1}) \tag{6.1}$$

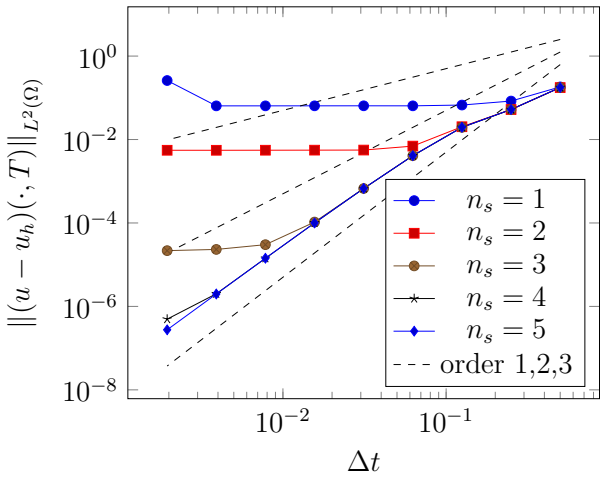

Figure 6.2: Moving circle problem $k_s = 3, k_t = 1, k_s^{\text{geom}} = 3, k_t^{\text{geom}} = 3$: The error $\|(u-u_h)(\cdot,T)\|_{L^2(\Omega)}$ for refinements in time on different meshes (spatial refinement levels $n_s = 1$ to $n_s = 5$).

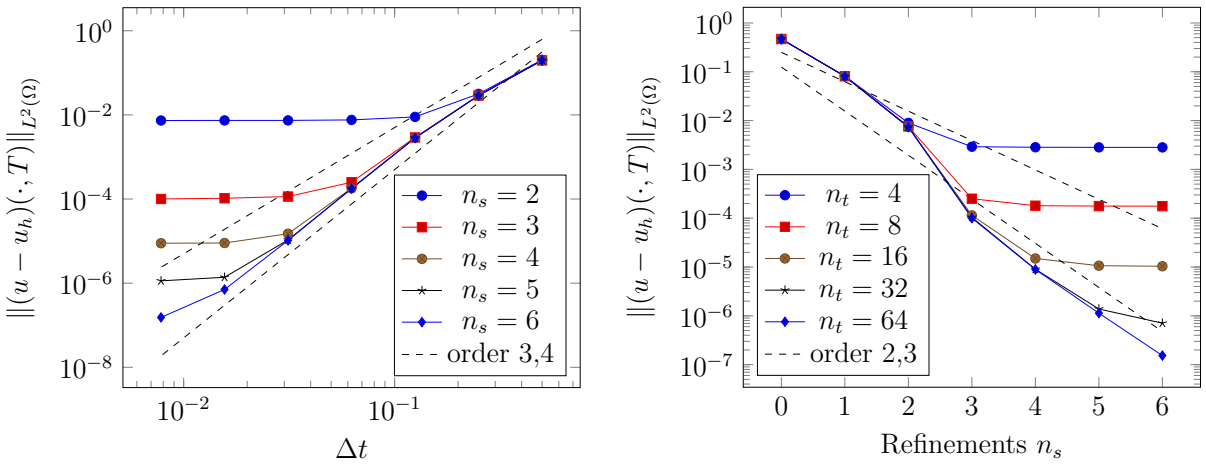

Figure 6.3: Moving circle problem $k_s = 2, k_t = 2$: The error $\|(u-u_h)(\cdot,T)\|_{L^2(\Omega)}$ for refinements in time and space.

to hold true for general polynomial orders provided that the solution is sufficiently smooth.

In section 3.4.2 of [Leh15] a similar method as discussed here has been applied to a moving interface problem. The considered geometry was a moving sphere. For $k_s = k_t = 1$ an order of around 2.5 for the convergence in time has been observed. Moreover, it was expected that for finer spatial resolutions and a better approximation of the geometry the rate can be improved to three. The results of this section confirm this expectation for the simpler two dimensional test problem considered here.

For $k_t = 2$ one would expect to see a rate of five with respect to refinements in time based on (6.1). In our numerical experiments, a rate of four has been observed. This is one and a half orders higher than expected by the approximation error estimate, but not sufficient to speak of full superconvergence. Therefore, we conclude that we see some effects of superconvergence, but do not fully understand the phenomenon yet.

6.2 Moving and deforming ellipse

6.2.1 Description of test case

The domain in the last example was moving but did not change its shape. Now we consider the more challenging case of a moving domain which is additionally deforming. The level set function is given by

$$\phi(x, y, t) = \sqrt{[\xi(x - x_0 - \rho_x)]^2 + [\eta(y - y_0 - \rho_y)]^2} - r_0,$$

with

$$\rho_x(t) = \frac{1}{2}\sin(4\pi t), \qquad \rho_y(t) = \sin(2\pi t)$$

and

$$\xi(t) = 1 - \frac{1}{2}\sin^2(4\pi t) \qquad \eta(t) = 1 - \frac{1}{2}\sin^2(2\pi t).$$

The constants are chosen as $x_0 = 1, y_0 = 1/2$ and $r_0 = 1/3$. As the background domain we take $\tilde{\Omega} = [-0.5, 2.5] \times [0.0, 2.5]$.

The resulting domain $\Omega(t) = \{(x, y) \in \tilde{\Omega} \mid \phi(x, y, t) < 0\}$ is a moving and deforming ellipse. The center of the ellipse is translated through the domain by the velocity field $\mathbf{w}(t) = \big(\dot{\rho_x}(t), \dot{\rho_y}(t)\big)$. The scaling factors ξ and η lead to an additional deformation of the ellipse. In particular, the velocity of the boundary in normal direction $\mathcal{V}_n$ does not need to coincide with the value of the convection field in normal direction $\mathbf{w} \cdot \mathbf{n}$. Note that this violates an assumption that was needed for deriving Lemma 2.1.

At $t = 0$ the domain starts as a circle. It then undergoes quite strong deformations while travelling in circular motion in the background domain. At $t = T = 1/2$ it has completed a full revolution. Half of this motion is shown in Figure 6.4.

The right hand side is computed so that the solution is given by

$$u(x, y, t) = \chi(\phi(x, y, t) + r_0),$$

with $\chi(r) = \cos^2(\frac{\pi r}{2r_0})$. The convergence studies are performed over the time interval $[0, T]$. The stabilization parameter for the ghost penalty is chosen as $\gamma_J = 5 \cdot 10^{-2}$.

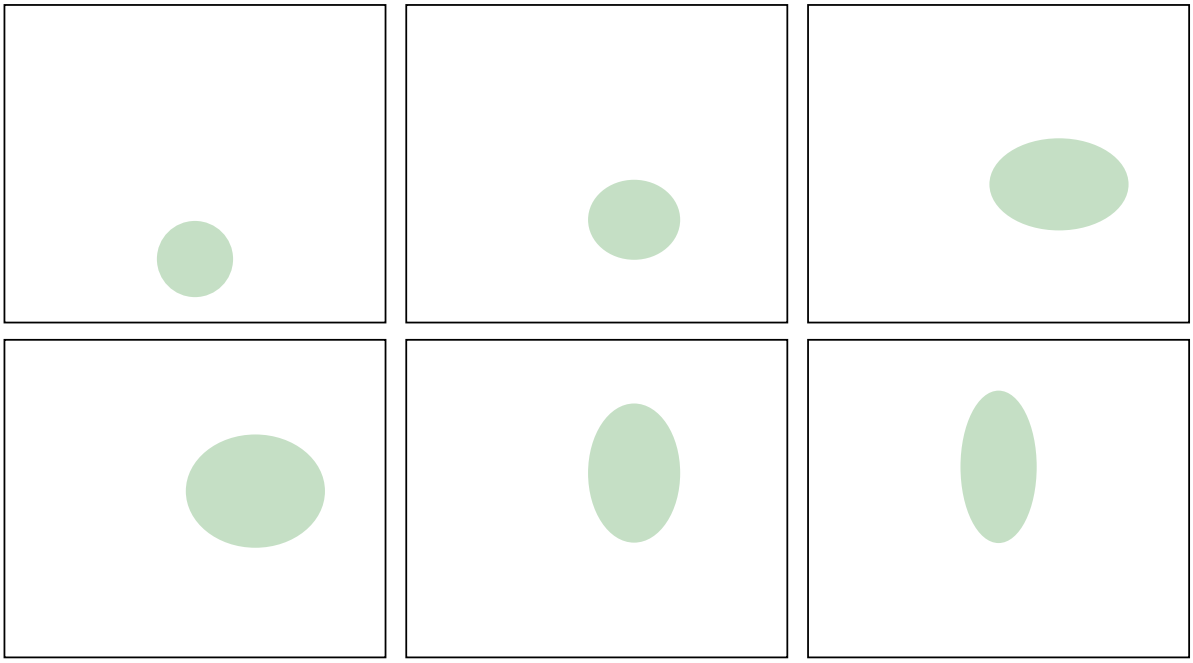

Figure 6.4: Moving and deforming ellipse: The domain $\Omega(t)$ for $t \in \{0, 1/20, 2/20, 3/20, 4/20, 5/20\}$.

6.2.2 Discussion of results

We consider the case of quadratic elements in time and space: $k_s = k_t = 2$. The polynomial degrees of the geometry approximation are chosen accordingly: $k_s^{\text{geom}} = k_s$ and $k_t^{\text{geom}} = k_t$. The error is measured in the (semi-)norms: $\|\cdot\|_{L^2(\Omega)}$, $\|\partial_t \cdot\|_{L_t^\infty(0,T;\, L_x^2(\Omega))}$ and $\|\nabla \cdot\|_{L_t^\infty(0,T;\, L_x^2(\Omega))}$.

- $\|\cdot\|_{\Omega(T)}$:
  Figure 6.5 shows that the error behaves as
  $$\|(u - u_h)(\cdot, T)\|_{\Omega(T)} \lesssim \Delta t^4 + h^3.$$
  Again the convergence with respect to refinements in time is at least an order better than expected.

- $\|\partial_t \cdot\|_{L_t^\infty(0,T;\, L_x^2(\Omega))}$:
  It can be seen in Figure 6.6 that $\|\partial_t(u - u_h)\|_{L_t^\infty(0,T;\, L_x^2(\Omega))}$ converges with a quadratic rate for refinements in time. For investigating the convergence in space we have increased the polynomial degree in time to four. This reduces the effect of temporal errors. Then a cubic rate of convergence in space is observed.

- $\|\nabla \cdot\|_{L_t^\infty(0,T;\, L_x^2(\Omega))}$:
  Figure 6.7 shows the results for $\|\nabla(u - u_h)\|_{L_t^\infty(0,T;\, L_x^2(\Omega))}$. We observe a second order rate of convergence in space and a rate of nearly three in time.

As in the previous experiment the observed rate of convergence is again much better than the derived error estimate

$$|||u - u_h||| \lesssim \Delta t^{k_t+1/2} + \sqrt{\left(1 + \frac{\Delta t}{h}\right)} h^{k_s}$$

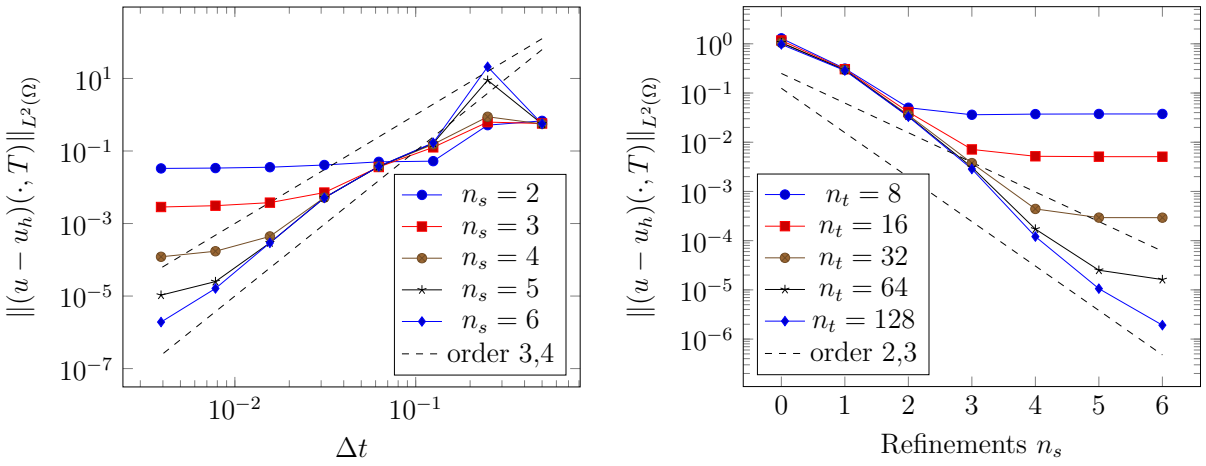

Figure 6.5: Moving and deforming ellipse, $k_s = 2, k_t = 2$: The error $\|(u-u_h)(\cdot,T)\|_{L^2(\Omega)}$ for refinements in time and space.

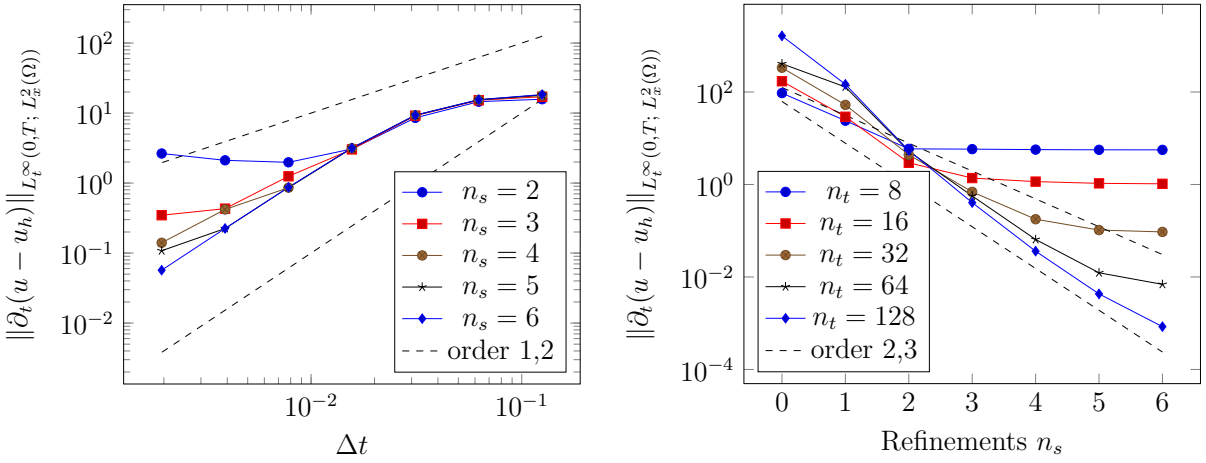

Figure 6.6: Moving and deforming ellipse: The error $\|\partial_t(u-u_h)\|_{L_t^\infty(0,T;\, L_x^2(\Omega))}$ for refinements in time (with $k_s = k_t = 2$) and space (with $k_s = 2, k_t = 4$).

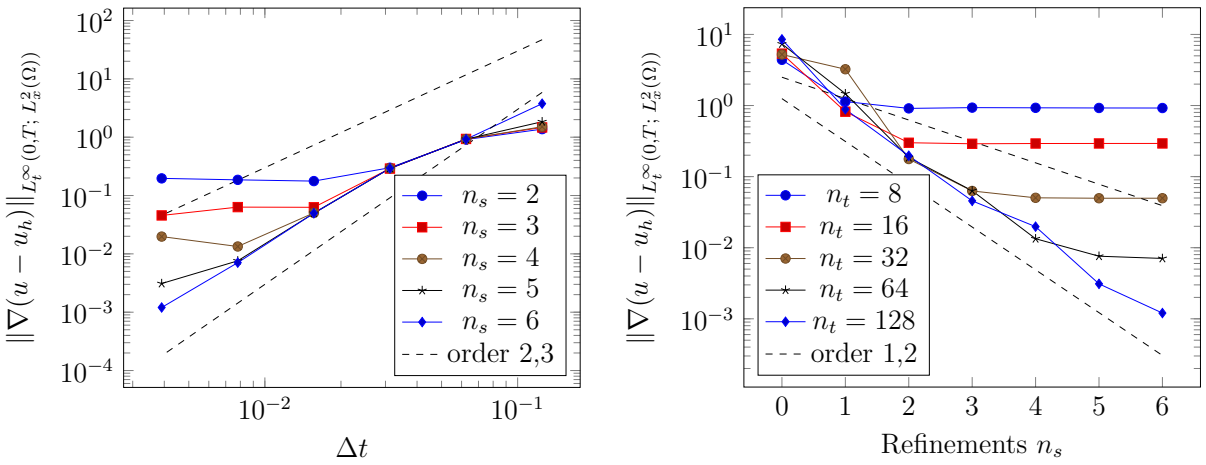

Figure 6.7: Moving and deforming ellipse, $k_s = k_t = 2$: The error $\|\nabla(u-u_h)\|_{L_t^\infty(0,T;\, L_x^2(\Omega))}$ for refinements in time and space.

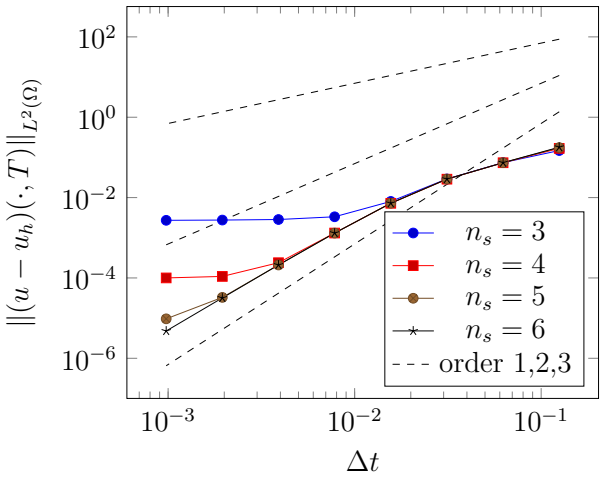

,

$n_t \setminus n_s$	6	eoc_t
4	0.18	
8	$7.39 \cdot 10^{-2}$	1.28
16	$2.88 \cdot 10^{-2}$	1.36
32	$7.24 \cdot 10^{-3}$	1.99
64	$1.31 \cdot 10^{-3}$	2.47
128	$2.10 \cdot 10^{-4}$	2.64
256	$3.18 \cdot 10^{-5}$	2.72
512	$4.78 \cdot 10^{-6}$	2.73

Figure 6.8: Moving and deforming ellipse $k_t = 1$: The error $\|(u - u_h)(\cdot, T)\|_{\Omega(T)}$ for refinements in time, where $k_s = 2$ and $k_t^{\text{geom}} = k_s^{\text{geom}} = 2$.

suggests.

In the last example it was observed that the error in the $\|\cdot\|_{\Omega(T)}$-norm for $k_t = 1$ converges at a rate of about three with respect to refinements in time provided that the approximation of the geometry is sufficiently accurate. Since the evolution of the domain is more complicated in this example it is interesting to investiate whether the superconvergence can still be observed. Figure 6.2 shows the results for refinements in time with $k_t = 1$. We have chosen $k_t^{\text{geom}} = k_s^{\text{geom}} = 2$ to provide a better approximation of the geometry and $k_s = 2$ to alleviate the effects of spatial errors. On the finest mesh a highest rate of 2.73 is observed. This is slightly worse than for the moving circle problem (Tables 6.19 and 6.20). Nevertheless, the observed rate is definitely higher than 2.0 so that one can still speak of superconvergence.

Chapter 7

Isoparametric unfitted space-time FEM for a two-phase interface problem

This chapter deals with the application of the isoparametric unfitted space-time DG method to a mass transport problem in two-phase flows. First we introduce the PDE that needs to be solved and provide some information on the physical background. For further details on the modelling we refer to section 1.2 of [Leh15] and references therein. Then we derive an isoparametric space-time discretization for this problem. It is based on the Space-Time-DG Nitsche-XFEM method that has been introduced and analyzed in [LR13] and [Leh15] for linear finite elements in time and space.

Compared to the moving domain problem from the previous chapters, the two-phase interface problem poses some additional challenges. Firstly, the problem now consists of two PDEs given inside the bulk phases instead of just one. Secondly, there are additional conditions at the interface separating the two fluids which need to be taken care of. To this end, the Nitsche technique can be used.

7.1 Introduction

We are interested in computing the concentration of a soluble species u inside the two fluids. The fluids are assumed to be immiscible, incompressible and contained in the background domain Ω. A phase transition is not allowed. We consider the situation that one of the phases $\Omega_1(t)$ is completely surrounded by the other phase $\Omega_2(t)$. The interface $\Gamma(t) \coloneqq \bar{\Omega}_1(t) \cap \bar{\Omega}_2(t)$ is assumed to have thickness zero. I.e. it is sharp and separates Ω into two disjoint regions as shown in Figure 7.1.

Furthermore, we assume that species conservation across the interface holds. In particular, the species do not adhere to the interface and no chemical reactions take place there. The transport of the species through the interface is then caused by diffusion and modelled by Fick's law. Conservation of mass across the interface then leads to the first interface condition:

$$\alpha_1 \nabla u_1 \cdot \mathbf{n} = \alpha_2 \nabla u_2 \cdot \mathbf{n},$$

where α_i are the diffusivities of the fluids and u_i denotes the solution inside the phase $\Omega_i(t)$ for $i = 1, 2$. The normal $\mathbf{n}$ points from Ω_1 to Ω_2, i.e. $\mathbf{n} = \mathbf{n_1}$ is the outer normal of

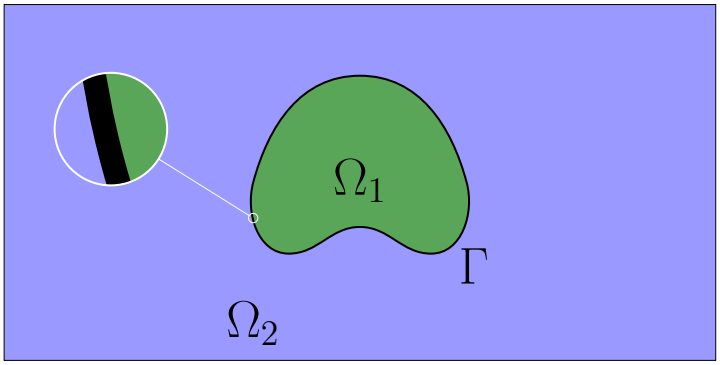

Figure 7.1: Sketch of the two phases.

Ω_1. Using the jump operator $[\![\cdot]\!]$ at the interface defined by

$$[\![v(x)]\!] := \lim_{s\to 0+} v(x + s\cdot\mathbf{n}) - \lim_{s\to 0+} v(x - s\cdot\mathbf{n}),\ x \in \Gamma(t), t \in (0,T],$$

this condition can be written as $[\![\alpha\nabla u\cdot\mathbf{n}]\!] = 0$ on $\Gamma(t)$.

The second interface condition stems from chemical reasons. We assume that the chemical potentials from both sides of the interface are in balance so that Henry's law

$$\beta_1 u_1 = \beta_2 u_2$$

holds true on $\Gamma(t)$. Here $\beta_i, i = 1,2$ are the Henry coefficients describing the solvability of the species in the fluid.

Inside the phases we use the same convection diffusion equation as treated in the previous chapters:

$$\partial_t u_i + \mathbf{w}\cdot\nabla u_i - \operatorname{div}(\alpha_i\nabla u_i) = f_i \text{ in } \Omega_i(t),\ i = 1,2.$$

The model has to be complemented by suitable initial conditions at $\Omega_i(0)$ and boundary conditions on $\partial\Omega$. Here only homogeneous Dirichlet boundary conditions will be considered:

$$u_2(\cdot,t) = 0 \text{ on } \partial\Omega,\ t \in (0,T].$$

We arrive at:

$$\begin{aligned}
\partial_t u_i + \mathbf{w}\cdot\nabla u_i - \operatorname{div}(\alpha_i\nabla u_i) &= f_i && \text{in } \Omega_i(t), && t\in[0,T] && (7.1)\\
[\![-\alpha\nabla u\cdot\mathbf{n}]\!] &= 0 && \text{on } \Gamma(t), && t\in[0,T], && (7.2)\\
[\![\beta u]\!] &= 0 && \text{on } \Gamma(t), && t\in[0,T], && (7.3)\\
u_i(\cdot,t=0) &= u_0^i && \text{in } \Omega_i(0), && && (7.4)\\
u_2(\cdot,t) &= 0 && \text{on } \partial\Omega, && t\in(0,T]. && (7.5)
\end{aligned}$$

The problem is visualized in Figure 7.2.

Similar to the discretization from chapter 2 for the moving domain problem, the following assumptions are made:

- The velocity field $\mathbf{w}$ shall originate from an incompressible flow: $\operatorname{div}(\mathbf{w}) = 0$ and is assumed to be bounded: $\|\mathbf{w}\|_\infty < \infty$.

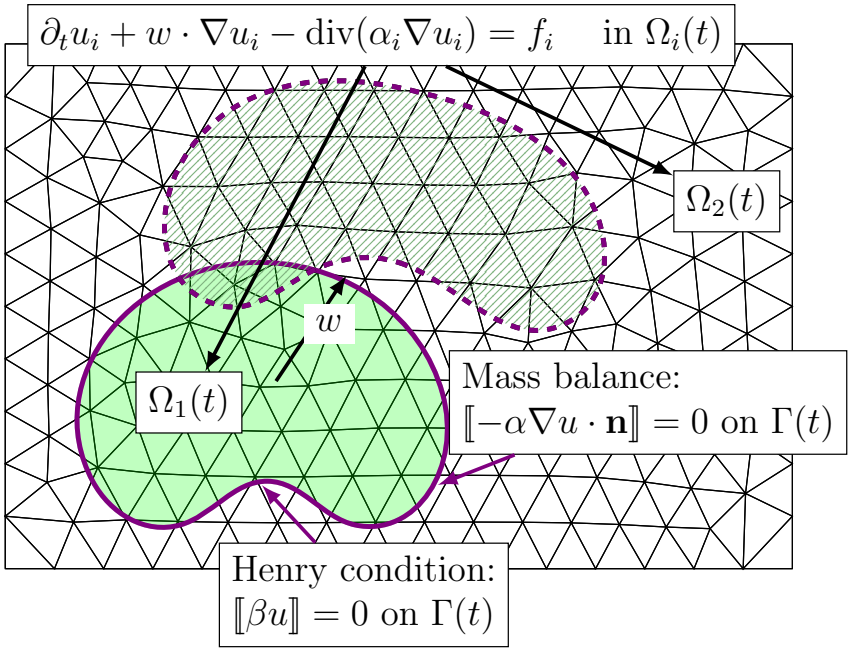

Figure 7.2: Mass transport problem in two-phase flows.

- The velocity of the interface in normal direction $\mathcal{V}_n$ shall coincide with the value of the convection field in normal direction: $\mathcal{V}_n = \mathbf{w} \cdot \mathbf{n}$.

Compared to the moving domain problem from the previous chapters, the problem considered here now poses the additional challenge of having to respect the interface conditions. In general, it holds that $\beta_1 \neq \beta_2$ and $\alpha_1 \neq \alpha_2$, so that the solution exhibits jumps and kinks across the interface. Due to the motions of the interface, these discontinuities travel in time. Thus, an unfitted discretization has to be able to approximate functions that have a discontinuity whose position moves inside the discretization elements. An optimal approximation can be achieved by using twice the degrees of freedom of a standard finite element space in the interface region.

7.2 Derivation of the method

Notation

To formulate the variational formulation it is necessary to generalize the notation from chapter 2 to the setting of a two-phase problem. This is easily done by introducing an additional index $i \in \{1, 2\}$ which indicates the domain $\Omega_i(t)$. As before, let $0 < t_1 < \ldots < t_{N-1} < t_N$ be a partition of the time domain into time intervals $I_n = (t_{n-1}, t_n]$ with constant size $\Delta t = t_n - t_{n-1}$. The space-time slabs are given by $Q_i^n := \cup_{t \in I_n} \Omega_i(t) \times \{t\}$ for $i = 1, 2$. These are contained in the tensor product domain $Q^n = \Omega \times I_n$. We denote the union over all time slabs by $Q_i = \cup_{n=1}^N Q_i^n$ and $Q = \cup_{n=1}^N Q^n$. The spatial domain at a fixed time $\Omega_i(t_n)$ will again be abbreviated by $\Omega_i^n = \Omega_i(t_n)$. Further, we define the space-time interface $\Gamma_* := \cup_{t \in (0,T]} \Gamma(t) \times \{t\}$ and its restriction to the time slab $\Gamma_*^n := \cup_{t \in I_n} \Gamma(t) \times \{t\}$.

Further, let $\mathcal{T}_h$ be a shape-regular triangulation of the background domain. Let $V_h^{k_s}$ be a standard finite element space of order k_s on this mesh. We define an extension

operator $\mathcal{E}$ that extends the domains Q_i^n onto a domain with a tensor product structure within each time slab

$$\mathcal{E}(Q_i^n) \coloneqq \{x \in T \text{ for some } T \in \mathcal{T}_h \text{ with } Q_T^n \cap Q_i^n \neq \emptyset\},$$

where we recall that the space-time prisms are defined by $Q_T^n = T \times I_n$. Let then $\mathcal{E}(Q_i) = \cup_{n=1}^N (\mathcal{E}(Q_i^n))$. The restriction is given by

$$\mathcal{I}(Q_i^n) \coloneqq Q_i^n \setminus \mathcal{E}(Q^n \setminus Q_i^n).$$

Then we introduce purely spatial counterparts

$$\mathcal{I}(\Omega_i^n) \text{ such that } \mathcal{I}(\Omega_i^n) \times I_n = \mathcal{I}(Q_i^n),$$

$$\mathcal{E}(\Omega_i^n) \text{ such that } \mathcal{E}(\Omega_i^n) \times I_n = \mathcal{E}(Q_i^n),$$

for $i = 1, 2$.

The space-time finite element spaces on the time slab are defined by:

$$W_n^i \coloneqq \{v : \mathcal{E}(Q_i^n) \to \mathbb{R} \mid v(x,t) = \sum_{m=0}^{k_t} t^m \phi_m,\ \phi_m \in V_h^{k_s}(\mathcal{E}(\Omega_i^n))\}. \tag{7.6}$$

We combine these into the space $W_n^\Gamma \coloneqq W_n^1 \oplus W_n^2$. The space on the complete space-time domain is defined by restriction to the time slabs: $W_h^\Gamma \coloneqq \{v : Q \to \mathbb{R} \mid v_{\restriction Q^n} \in W_n^\Gamma\}$.

Remark 22 (CutFEM vs XFEM)**.** *The space W_n^Γ is basically contructed by piecing together two standard space-time finite element spaces which have been cut-off at the space-time interface. Such an approach is known as CutFEM in the literature. It is possible to give an equivalent description of W_n^Γ which may be more intuitive. Let W_n be the standard space-time finite element space on the tensor product Q^n defined in (3.13). The space W_n^Γ is obtained by enriching W_n by new basis functions which capture the discontinuity of the solution across the space-time interface Γ_*^n. We have $W_n^\Gamma = W_n \oplus W_n^x$, where the part W_n^x contains basis functions that are discontinuous across the space-time interface. A precise definition can be found in section 3.2.3 of [Leh15], where such a characterization of W_n^Γ has been used. Splitting W_n^Γ into a standard space W_n and a so called XFEM-part W_n^x, including the enrichments functions, might be advantageous for preconditioning purposes (cf. section 3.5 of [Leh15]).*

In the derivation of the variational formulation we will multiply by a test function $\beta v = (\beta_1 v_1, \beta_2 v_2) \in W_h^\Gamma$. It is convenient to introduce β -weighted scalar products that allow to absorb the Henry coefficient. To this end, define

$$(u_i, v_i)_{Q_i^n} \coloneqq \int_{Q_i^n} \beta_i u_i v_i \, dx \, dt$$

and

$$(u_i, v_i)_{\Omega_i^n} \coloneqq \int_{\Omega_i^n} \beta_i u_i v_i \, dx.$$

Derivation of the variational formulation

We start by multiplying the equation (7.1) by a test function $\beta v \in W_h^\Gamma$ and integrate over the space-time domain:

$$\sum_{i=1,2}\sum_{n=1}^{N}(\partial_t u_i + \mathbf{w}\cdot\nabla u_i - \operatorname{div}(\alpha_i\nabla u_i), v_i)_{Q_i^n} = \sum_{i=1,2}\sum_{n=1}^{N}(f_i, v_i)_{Q_i^n}.$$

Denote the right hand side by $f(v) = \sum_{i=1,2}\sum_{n=1}^{N}(f_i, v_i)_{Q_i^n}$.

Now an integration by parts is performed on the space-time convection (∇, ∂_t). First consider Q_1^n. For the time derivative one obtains

$$(\partial_t u_1, v_1)_{Q_1^n} = -(u_1, \partial_t v_1)_{Q_1^n} + \big((u_1)_-^n, (v_1)_-^n\big)_{\Omega_1^n} - \big((u_1)_-^{n-1}, (v_1)_+^{n-1}\big)_{\Omega_1^{n-1}} - \int_{t_{n-1}}^{t_n}\int_{\partial\Omega_1(t)} \beta_1 \mathcal{V}_n u_1 v_1 \, ds dt,$$

where $\mathcal{V}_n$ denotes the velocity of the interface in normal direction and $(u_1)_-^{n-1}$ is the upwind flux.

For the convection term one has

$$\begin{aligned}(\mathbf{w}\cdot\nabla u_1, v_1)_{Q_1^n} &= -(u_1, \nabla\cdot(\mathbf{w}v_1))_{Q_1^n} + \int_{t_{n-1}}^{t_n}\int_{\partial\Omega_1(t)} \beta_1 \mathbf{w}\cdot\mathbf{n} u_1 v_1 \, ds dt \\ &= -(u_1, \mathbf{w}\cdot\nabla v_1)_{Q_1^n} + \int_{t_{n-1}}^{t_n}\int_{\partial\Omega_1(t)} \beta_1 \mathbf{w}\cdot\mathbf{n} u_1 v_1 \, ds dt,\end{aligned}$$

where it was used that $\nabla\cdot(\mathbf{w}v_1) = v_1\nabla\cdot\mathbf{w} + \mathbf{w}\cdot\nabla v_1 = w\cdot\nabla v_1$ since $\mathbf{w}$ is divergence free.

Now one has that the velocity of the interface in normal direction coincides with the convection field: $\mathbf{w}\cdot\mathbf{n} - \mathcal{V}_n = 0$. So these two terms cancel and we obtain:

$$(\partial_t u_1 + \mathbf{w}\cdot\nabla u_1, v_1)_{Q_1^n} = -(u_1, \partial_t v_1 + \mathbf{w}\cdot\nabla v_1)_{Q_1^n} + \big((u_1)_-^n, (v_1)_-^n\big)_{\Omega_1^n} - \big((u_1)_-^{n-1}, (v_1)_+^{n-1}\big)_{\Omega_1^{n-1}}.$$

Using that $u_2 = v_2 = 0$ on $\partial\Omega$ we obtain that the same formula holds when Q_1^n is replaced by Q_2^n. Summing up over the time slabs leads to:

$$\begin{aligned}&\sum_{i=1,2}\sum_{n=1}^{N}(\partial_t u_i + \mathbf{w}\cdot\nabla u_i, v_i)_{Q_i^n} \\ &= -\sum_{i=1,2}\sum_{n=1}^{N}(u_i, \partial_t v_i + \mathbf{w}\cdot\nabla v_i)_{Q_i^n} + \sum_{i=1,2}\sum_{n=1}^{N}\{\big((u_i)_-^n, (v_i)_-^n\big)_{\Omega_i^n} - \big((u_i)_-^{n-1}, (v_i)_+^{n-1}\big)_{\Omega_i^{n-1}}\} \\ &= -\sum_{i=1,2}\sum_{n=1}^{N}(u_i, \partial_t v_i + \mathbf{w}\cdot\nabla v_i)_{Q_i^n} - \sum_{i=1,2}\sum_{n=1}^{N-1}\big((u_i)_-^n, [\![v_i]\!]^n\big)_{\Omega_i^n} + \big((u_i)_-^N, (v_i)_-^N\big)_{\Omega_i^N} - (u_0^i, (v_i)_+^0)_{\Omega_i^0}.\end{aligned}$$

Now defining

$$d'(u,v) \coloneqq \sum_{n=1}^{N} d'^n(u,v),$$

where

$$d'^{n}(u,v) \coloneqq -\sum_{i=1,2} (u_i, \partial_t v_i + \mathbf{w}\cdot\nabla v_i)_{Q_i^n} \quad \text{for } 1 \le n \le N, \tag{7.7}$$

$$b'(u,v) \coloneqq \sum_{n=1}^{N-1} b'^{n}(u,v) + \sum_{i=1,2} \left((u_i)_-^N, (v_i)_-^N\right)_{\Omega_i^N},$$

where

$$b'^{n}(u,v) \coloneqq -\sum_{i=1,2} \left((u_i)_-^n, [\![v_i]\!]^n\right)_{\Omega_i^n} \quad \text{for } 1 \le n \le N-1,$$

and $c(w,v) \coloneqq \sum_{i=1,2} \left(w^i, (v_i)_+^0\right)_{\Omega_i^0}$, one has

$$\sum_{i=1,2}\sum_{n=1}^{N} (\partial_t u + \mathbf{w}\cdot\nabla u, v)_{Q_i^n} = d'(u,v) + b'(u,v) - c(u_0,v).$$

Next the diffusion term will be treated. An integration by parts leads to:

$$\begin{aligned}
\sum_{i=1,2} (-\operatorname{div}(\alpha_i\nabla u_i), v_i)_{Q_i^n} &= \sum_{i=1,2} (\alpha_i\nabla u_i, \nabla v_i)_{Q_i^n} - \int_{t_{n-1}}^{t_n}\int_{\Gamma(t)} \sum_{i=1,2} \alpha_i\nabla u_i \mathbf{n}_i \beta_i v_i \, d\mathbf{s}\, dt \\
&= \sum_{i=1,2} (\alpha_i\nabla u_i, \nabla v_i)_{Q_i^n} - \int_{t_{n-1}}^{t_n}\int_{\Gamma(t)} [\![\alpha\nabla u\cdot\mathbf{n}\beta v]\!] \, d\mathbf{s}\, dt \\
&= \sum_{i=1,2} (\alpha_i\nabla u_i, \nabla v_i)_{Q_i^n} - \int_{t_{n-1}}^{t_n}\int_{\Gamma(t)} \{\!\{\alpha\nabla u\cdot\mathbf{n}\}\!\} [\![\beta v]\!] \, d\mathbf{s}\, dt.
\end{aligned}$$

Here the weighted average $\{\!\{\cdot\}\!\}$ is defined by

$$\{\!\{\alpha\nabla u\cdot\mathbf{n}\}\!\} \coloneqq (\kappa_1\alpha_1\nabla u_1 + \kappa_2\alpha_2\nabla u_2)\cdot\mathbf{n}_1,$$

for a convex combination of $\kappa_i \in [0,1]$, $\kappa_1+\kappa_2 = 1$. To rewrite the jump term in this way we used that the normal flux is univalued at the interface due to conservation of mass (7.2). Further, we can transform the iterated integrals to integrals on the space-time interface by means of the following formula:

$$\int_{t_{n-1}}^{t_n}\int_{\Gamma(t)} f(\mathbf{s}) d\mathbf{s}\, dt = \int_{\Gamma_*^n} f(\mathbf{s})\nu(\mathbf{s})\, d\mathbf{s},$$

where $\nu(s) = (1+(w\cdot\mathbf{n}))^{-1/2}$ and w is the (interface) velocity. Here $d\mathbf{s}$ denotes both the surface measure on $\Gamma(t)$ as well as on Γ_*. Employing this formula we can write

$$-\int_{t_{n-1}}^{t_n}\int_{\Gamma(t)} \{\!\{\alpha\nabla u\cdot\mathbf{n}\}\!\} [\![\beta v]\!] d\mathbf{s}\, dt = -(\nu\{\!\{\alpha\nabla u\mathbf{n}\}\!\}, [\![\beta v]\!])_{\Gamma_*^n} \coloneqq N_c^n(u,v).$$

The full Nitsche form $N^n(\cdot,\cdot)$ on the time slab is then obtained by adding additional symmetry and stabilization terms.

$$N^n(u,v) \coloneqq N_c^n(u,v) + N_c^n(v,u) + N_s^n(u,v),$$

where $N_s^n(u,v) \coloneqq \left(\nu\bar{\alpha}\frac{\lambda}{h}[\![\beta u]\!],[\![\beta v]\!]\right)_{\Gamma_*^n}$. Due to the Henry condition (7.3) the additional terms vanish for the exact solution. In other words, the stabilization is consistent. So, defining

$$a(u,v) \coloneqq \sum_{n=1}^{N} a^n(u,v), \text{ where } a^n(u,v) \coloneqq \sum_{i=1,2} (\alpha_i \nabla u_i, \nabla v_i)_{Q_i^n} \text{ for } 1 \leq n \leq N,$$

and $N(u,v) \coloneqq \sum_{n=1}^{N} N^n(u,v)$ yields:

$$\sum_{i=1,2}\sum_{n=1}^{N} -(\operatorname{div}(\alpha_i \nabla u_i), v_i)_{Q_i^n} = a(u,v) + N(u,v).$$

Finally, we need to add an analogue to the ghost penalty stabilization term from chapter 2. Let $\mathcal{F} = \{F\}$ be the set of spatial facets of $\mathcal{T}_h$. The relevant facets for the stabilization on Q_i^n are then given by

$$\mathcal{F}_{R_i}^{*,n} = \{F \in \mathcal{F} \ : \ F = T_1 \cap T_2,\ T_1 \in \mathcal{E}(\Omega_i^n) \setminus \mathcal{I}(\Omega_i^n),\ T_2 \in \mathcal{E}(\Omega_i^n)\}.$$

The corresponding facet-patches are defined as before

$$\omega_F = T_1 \cup T_2,\ F \subset \partial T_j,\ j = 1,2.$$

Then we define the stabilization term

$$j_h^n(u,v) \coloneqq \sum_{i=1,2} \int_{t_{n-1}}^{t_n} \gamma_J \left(1 + \frac{\Delta t}{h}\right) \sum_{F \in \mathcal{F}_{R_i}^{*,n}} \int_{\omega_F} \frac{1}{h^2} [\![u_i]\!]_{\omega_F} [\![v_i]\!]_{\omega_F} \, dx \, dt$$

and

$$J(u,v) \coloneqq \sum_{n=1}^{N} j_h^n(u,v).$$

Finally, we arrive at the discrete variational formulation

Find $u_h \in W_h^\Gamma$ such that

$$B(u_h, v_h) + J(u_h, v_h) = f(v_h) + c(u_0, v_h) \text{ for all } v_h \in W_h^\Gamma, \tag{7.8}$$

where $B(u_h, v_h) = a(u_h, v_h) + b'(u_h, v_h) + d'(u_h, v_h) + N(u_h, v_h)$.

Isoparametric adaptations to discretization

The variational formulation derived so far assumes an exact handling of the geometry. The changes that are necessary for the extension to an isoparametric discretization are analogous to the moving domain problem (cf. section 4.3). Let Θ_h denote the space-time

mapping corresponding to the time slabs Q^n. The space-time finite element spaces W_n^i from (7.6) then need to be replaced by the isoparametric spaces

$$W_{n,\Theta_h}^i := \{v \mid v(t,\Theta_h(t,\hat{x})) = \hat{v}(t,\hat{x}) \text{ for } \hat{x} \in \Omega_i^{\text{lin}}(t), \text{ with } \hat{v} \in W_n^i\}.$$

Accordingly, W_n^Γ is replaced by $W_{n,\Theta_h}^1 \oplus W_{n,\Theta_h}^2$.

The changes to the terms in the variational formulation are analogous to section 4.3 as well. In the bilinear form $d'^n(\cdot,\cdot)$ we need to add an additional term $\frac{\partial_t \Theta_h}{\partial_t} \cdot \nabla v_i$ that accounts for the mesh velocity. Moreover, a projection step is necessary when the solution from the top of the time slab Q_i^{n-1} is passed on as an initial condition to the variational formulation on the next time slab Q_i^n. The projection is computed separately for each Q_i^n for $i = 1, 2$.

Remark 23 ((space-time) surface integrals)**.** *In contrast to the fictitious domain problem in the previous chapters, we have to consider and implement also (space-time) surface integrals stemming from the Nitsche terms. This can be done with similar techniques as explained in section 5.2. Thanks to the explicit geometry description provided by the space-time mapping, it is again sufficient to consider the situation of a space-time interface described by a level set function which is piecewise linear with respect to the spatial variable. Furthermore, the space-time integrals over the space-time surface can be written as iterated integrals over spatial surface integrals.*

Chapter 8

Numerical experiments for a two-phase interface problem

In this chapter we investigate the performance of the method introduced in chapter 7 for two test problems. The interface in the first problem is a (curved) plane. In the second problem we consider again the case of a moving circle.

8.1 Moving (curved) plane

We start with a two-dimensional adaptation of an example from section 3.4.1 of [Leh15]. It easily allows to switch between a planar and a curved interface. To this end, consider the domains $\Omega_1(t) = \{(x, y) \in \Omega \mid |x - q(y) - \rho(t)| < \frac{D}{2}\}$ and $\Omega_2(t) = \Omega \setminus \Omega_1(t)$ with $D = 1/3$ and q and ρ to be determined. The background domain is chosen as a box $\Omega = [0, 2]^2$. This example assumes periodic boundary conditions: $u(x = 0) = u(x = 2)$ and $u(y = 0) = u(y = 2)$. The data is prescribed so that the exact solution is given by $u(x, y, t) = \sin(\pi t)u_i(x - q(y) - \rho(t))$ where

- $u_1(y) = ay + by^3$,
- $u_2(y) = \sin(\pi y)$.

The convection field is given by $\mathbf{w} = \big(\dot{\rho}, 0\big)$. The diffusivities are chosen as $(\alpha_1, \alpha_2) = (1, 2)$ and the Henry weights $(\beta_1, \beta_2) = (1.5, 1)$. To make the interface conditions hold in an approximate sence we choose $a \approx 1.02728$ and $b \approx 6.34294$. The freedom to pick ρ and q offers the possibility to construct different kinds of interfaces:

- The easiest case is a planar interface $q(y) = 1$ in a linear motion $\rho(t) = 0.25t$.
- To build a non-planar interface one can chose $q(y) = \frac{7}{8} + \frac{1}{4}y^2(2 - y)^2$. Further, $\rho(t) = \frac{1}{4\pi}\sin(2\pi t)$ leads to a harmonic motion.

The convergence studies are performed over the interval $[0, T]$ with $T = 1$. We consider quadratic elements in space and time and measure the L^2-norm at the final time T. The stabilization parameter for the ghost penalty is chosen as $\gamma_J = 10^3$.

Planar interface: Since the interface is planar, the space-time mesh transformation was not used in this case. The results for the planar interface are shown in Figure 8.1. We observe a spatial rate of convergence which is at least three. The rate with respect to refinements in time is somewhere between three and four.

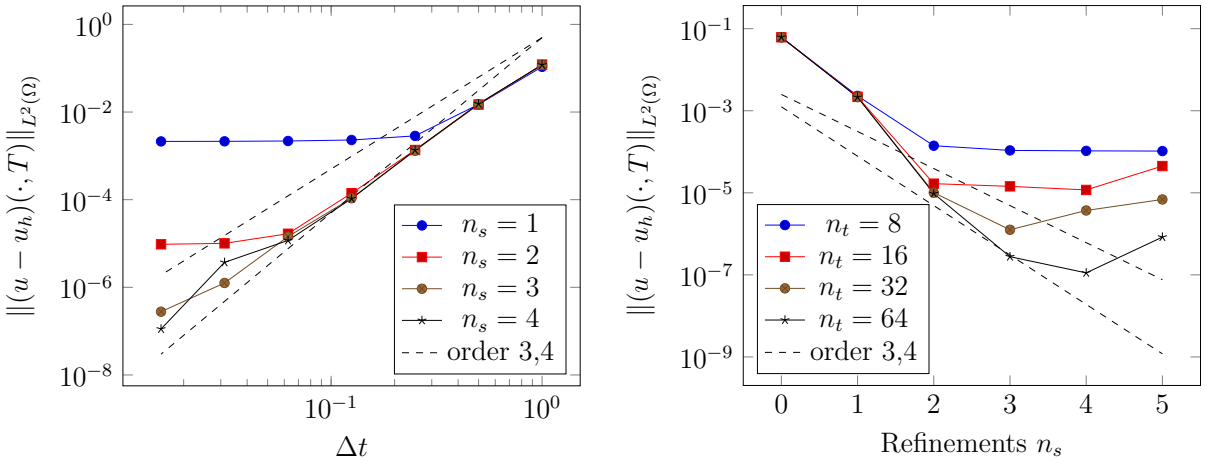

Figure 8.1: Moving plane - planar interface, $k_s = 2, k_t = 2$: The error $\|(u-u_h)(\cdot,T)\|_{L^2(\Omega)}$ for refinements in time and space.

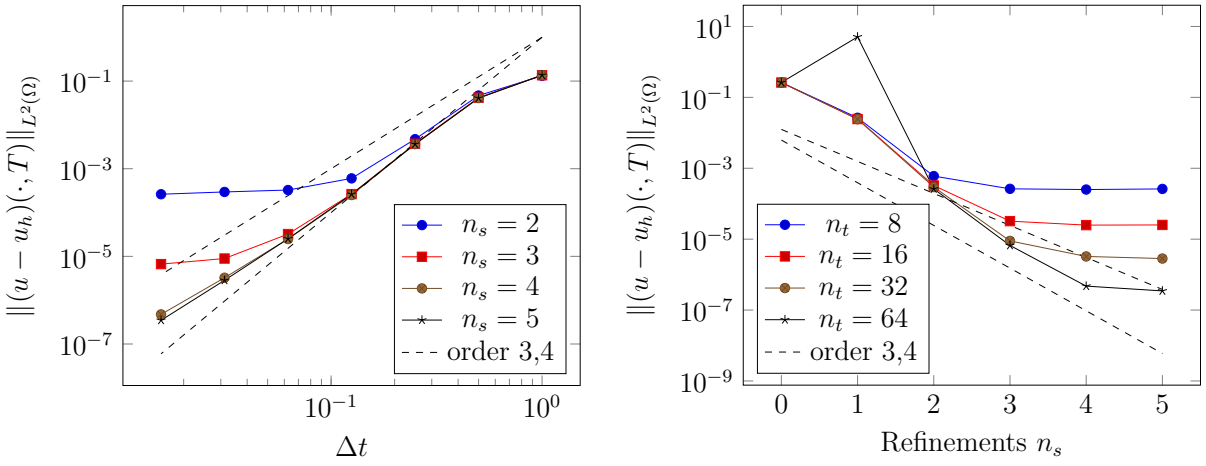

Figure 8.2: Moving plane - curved interface, $k_s = 2, k_t = 2$: The error $\|(u-u_h)(\cdot,T)\|_{L^2(\Omega)}$ for refinements in time and space.

Curved interface: For the curved case we use the mesh transformation to deal with the more complicated geometry of the interface. Figure 8.2 shows the results for the curved case. The observed spatial rate of convergence is again at least three. Likewise, the rate of convergence with respect to refinements in time is between three and four. In the third refinement the rate is quite close to four but it deteriorates in the later refinements.

The results for the planar and curved case are quite similar thanks to the higher order accurate geometry description provided by the isoparametric space-time mapping.

8.2 Moving circle

The geometry for this example is again a moving circle as shown in Figure 8.3. But this time we consider an interface problem. Let

$$\Omega_1(t) = \{(x,y) \in \mathbb{R}^2 \mid \sqrt{(x-0.5-\rho(t))^2 + (y-1)^2} < 1/3\},$$

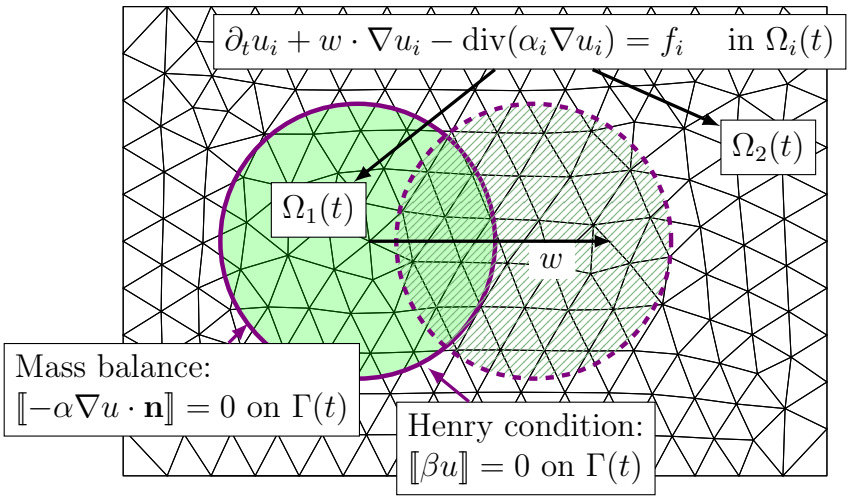

Figure 8.3: Mass transport problem in two-phase flows: Moving circle.

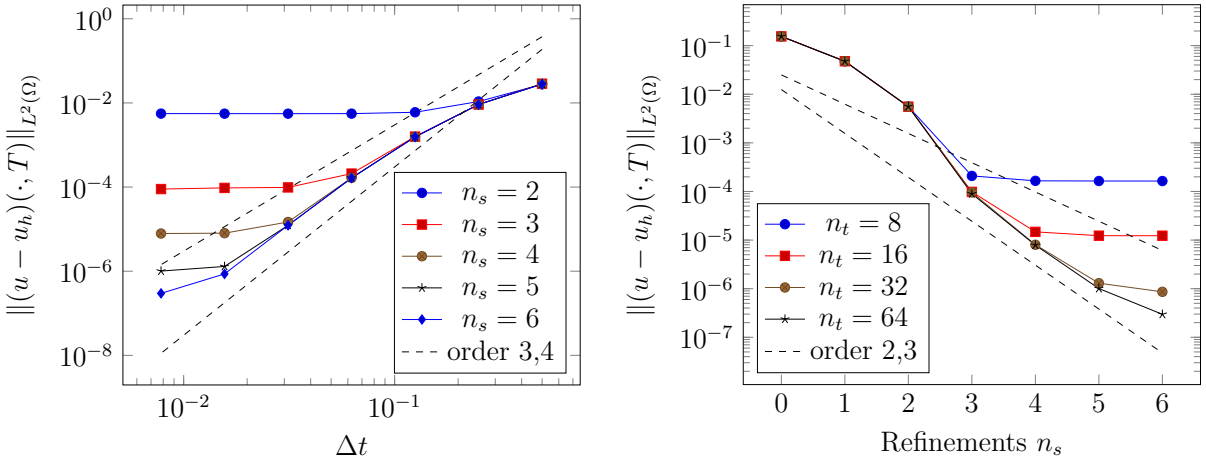

Figure 8.4: Moving circle problem $k_s = 2, k_t = 2$: The error $\|(u-u_h)(\cdot,T)\|_{L^2(\Omega)}$ for refinements in time and space.

where $\rho(t) = \frac{1}{4\pi}\sin(2\pi t)$ and $\Omega_2(t) = [0,2]^2 \setminus \Omega_1(t)$. The data is chosen so that the exact solution is given by

$$u(x,y,t) = \sin(\pi t) u_i(\sqrt{(x-0.5-\rho(t))^2 + (y-1)^2})$$

with $u_1(y) = a + by^2$ and $u_2(y) = \cos(\pi y)$. The evolution of the geometry is driven by the convection field $w = \big(0, \dot{\rho}\big)$ with $\rho(t) = \frac{1}{4\pi}\sin(2\pi t)$. Choose $(\alpha_1, \alpha_2) = (10, 20)$ and $(\beta_1, \beta_2) = (2, 1)$. To fulfill the interface conditions approximately we set $a \approx 1.1569$ and $b \approx -8.1621$.

The convergence studies are performed over the time interval $[0, T]$ with $T = 1/2$. The stabilization parameter for the ghost penalty is chosen as $\gamma_J = 10^{-1}$.

The results for $\|(u-u_h)(\cdot,T)\|_{L^2(\Omega)}$ with quadratic elements in time and space are shown in Figure 8.4. The observed spatial rate of convergence is three. With respect to convergence in time we see a rate between three and four.

In this example, time-dependent Dirichlet data has been used for the boundary condition. We notice that this already prohibits superconvergence behavior if not chosen with care, cf. [VR18].

Chapter 9

Conclusion

9.1 Summary

In this thesis we have investigated a higher order unfitted finite element method for moving domain problems. As a model problem, a simple convection-diffusion equation on a moving domain was considered. For this equation we first derived a space-time DG formulation which assumes an exact handling of the geometry. Under this assumption, an a priori error analysis was carried out. We arrived at an error estimate in a discrete norm that is anisotropic in the time step and the spatial mesh width. To the best of our knowledge, this is the first higher order (order greater-than two) error bound proven for an Eulerian method of a moving domain problem. However, this estimate is suboptimal with respect to the approximation error bounds .

For the implementation of higher order unfitted methods it is essential to carry out the quadrature on the cut elements with sufficient accuracy. To this end, we have generalized an approach introduced in [Leh16] and [LR17] for the stationary case. The general idea is to construct a space-time mapping of the underlying mesh which provides a higher order accurate explicit description of the geometry. All the integrals that need to be computed in an implementation of the method can be reduced to a reference configuration which is piecewise planar with respect to the spatial dimension. We have described the resulting isoparametric finite element method and discussed implementational aspects.

The performance of the proposed method was studied in numerical experiments. The observed rates of convergence are at least as good as the approximation error bounds. Since the method performs better in all our experiments than guaranteed by the a priori estimate, the derived estimate is probably not sharp.

As an application of our method to a physically more interesting problem, we have considered a mass transport problem in two-phase flows. A corresponding variational formulation was derived, but an analysis was not carried out. In numerical experiments similar rates of convergence for the L^2-norm at the final point in time have been observed as for the moving domain problem.

9.2 Open problems and outlook

The development of higher order unfitted finite element methods for moving domain problems is still in its infancy. The approach investigated in this thesis appears to be promising as it is accessible for a rigorous error analysis and performs well in numerical

experiments. Nevertheless, many interesting questions remain for further research. In the following we will sketch some of them.

Improvement of the error analysis assuming exact geometry handling The error estimate derived in the discrete norm that was given in Theorem 3.27 appears to be suboptimal. In the numerical experiments we observe better rates of convergence as guaranteed by the Theorem. One might attempt to improve on this estimate by means of duality arguments. Alternatively, it is possible that a different kind of analysis might lead to better error bounds. However, we note that the analysis of our method method is challenging, since the finite element spaces are time-dependent. Hence, the usual analysis for parabolic problems, which involves an error splitting based on the Ritz projection, cannot be applied directly.

Error analysis of the isoparametric method We have only provided an analysis which assumes that all the arising integrals can be calculated exactly. The next step would be an extension of the analysis to the isoparametric method introduced in chapter 4. A corresponding analysis for a stationary problem, which allows for optimal error bounds, has been given in [LR17] and [LR16]. In this regard, it is important to have suitable space-time interpolation operators at hand which can deal with the discontinuity of the space-time mesh transformation between the time slabs (see section 4.2.2). This is one of the reasons why we have constructed tailor-made interpolation operators in this thesis instead of retreating to nodal interpolation. Overall, an extension of the analysis that takes the isoparametric space-time mapping into account should be possible and might be the subject of a forthcoming paper. In this regard, it is also planned to cover details of the projection operator that is used to treat the discontinuity of the space-time mesh transformation between the time slabs.

Analysis of the two-phase interface problem An application of the method to a mass transport problem in two-phase flows has been presented. Since the method performs well in numerical experiments, it might be interesting to extend our analysis from the moving domain problem to the setting of two-phase flows. The PDEs in the bulk phases coincide for both problems. The additional challenge comes from the Nitsche terms enforcing the interface conditions. The Nitsche terms in the stationary case can be controlled by a special choice of the weights in the averaging operator (cf. [HH02]). This approach has been extended to the instationary case in [LR13]. In this paper the authors show error estimates for a similar method as presented in chapter 7 for the case of piecewise linear finite elements in space and time. Apart from being higher order, our method differs from the one presented in [LR13] by the additional ghost penalty stabilization that we employ. Due to the stabilization term we expect that stability of our variational formulation can be ensured independent of the choice of the weights in the avaraging operator. This might be advantageous for the case that the diffusion coefficients α_i have a large contrast. Furthermore, the conditioning of the arising linear systems is expected to be independent of the cut position even in the higher order case.

Linear solvers for (high-order) unfitted FEM Concerning the linear systems for unfitted finite elements methods one faces a difficult situation. On the one hand, one wants to ensure condition number bounds which are independent of the cut position.

A popular way to guarantee this is by means of a ghost penalty stabilization. On the other hand, the efficient solution of the arising linear systems is desired. To this end, one would like to construct suitable preconditioners. However, the ghost penalty stabilization might complicate this task by introducing additional couplings into the system. For time dependent problems the situation becomes even more complicated as the cut positions move through the mesh. Controlling and solving the linear systems arising in unfitted discretizations efficiently is highly desired for the practical application of these methods.

Extension to spatially three-dimensional problems The numerical examples treated in this thesis are all spatially two-dimensional. With a view towards applications it is clearly desired to treat the spatially three-dimensional case as well. Hence, the extension of the implementation in `ngsxfem` to three spatial dimensions and the treatment of challenging test cases are interesting tasks for the future.

Extension to more complicated problems The moving domain problem considered in chapters 2-6 is rather simple. To treat physically realistic problems it might be necessary to take couplings and nonlinear effects into account. Constructing higher-order discretizations for such problems is challenging. Other members of our working group tackle such tasks. We hope that part of this thesis might be useful for their work.

Bibliography

[BB01] R. Becker and M. Braack. A finite element pressure gradient stabilization for the Stokes equations based on local projections. *Calcolo*, 38(4):173–199, 2001.

[Ber89] C. Bernardi. Optimal finite-element interpolation on curved domains. *SIAM J. Numer. Anal.*, 26(5):1212–1240, 1989.

[BH12] E. Burman and P. Hansbo. Fictitious domain finite element methods using cut elements: II. A stabilized Nitsche method. *Appl. Numer. Math.*, 62(4):328–341, 2012.

[BH14] E. Burman and P. Hansbo. Fictitious domain methods using cut elements: III. A stabilized Nitsche method for Stokes' problem. *ESAIM Math. Model. Numer. Anal.*, 48(3):859–874, 2014.

[BHL15] E. Burman, P. Hansbo, and M. G. Larson. A stabilized cut finite element method for partial differential equations on surfaces: The Laplace-Beltrami operator. *Comput. Methods Appl. Mech. Engrg.*, 285:188–207, 2015.

[BHLZ16] E. Burman, P. Hansbo, M. G. Larson, and S. Zahedi. Cut finite element methods for coupled bulk-surface problems. *Numer. Math.*, 133(2):203–231, 2016.

[BIN78] O. V. Besov, V. P. Il'in, and S. M. Nikol'skiĭ. *Integral representations of functions and imbedding theorems. Vol. I.* V. H. Winston & Sons, Washington, D.C.; Halsted Press [John Wiley & Sons], New York-Toronto, Ont.-London, 1978. Translated from the Russian, Scripta Series in Mathematics, Edited by Mitchell H. Taibleson.

[Bra07] D. Braess. *Finite elements*. Cambridge University Press, Cambridge, third edition, 2007. Theory, fast solvers, and applications in elasticity theory, Translated from the German by Larry L. Schumaker.

[BS08] S. C. Brenner and L. R. Scott. *The mathematical theory of finite element methods*, volume 15 of *Texts in Applied Mathematics*. Springer, New York, third edition, 2008.

[Bur10] E. Burman. Ghost penalty. *C. R. Math. Acad. Sci. Paris*, 348(21-22):1217–1220, 2010.

[DPE12] D. A. Di Pietro and A. Ern. *Mathematical aspects of discontinuous Galerkin methods*, volume 69 of *Mathématiques & Applications (Berlin) [Mathematics & Applications]*. Springer, Heidelberg, 2012.

[GR07] C. Grossmann and H.-G. Roos. *Numerical treatment of partial differential equations*. Universitext. Springer, Berlin, 2007. Translated and revised from the 3rd (2005) German edition by Martin Stynes.

[HH02] A. Hansbo and P. Hansbo. An unfitted finite element method, based on Nitsche's method, for elliptic interface problems. *Comput. Methods Appl. Mech. Engrg.*, 191(47-48):5537–5552, 2002.

[HL17] F. Heimann and C. Lehrenfeld. Numerical integration on hyperrectangles in isoparametric unfitted finite elements. submitted to Proceedings of ENUMATH 2017.

[HLZ16] P. Hansbo, M. G. Larson, and S. Zahedi. A cut finite element method for coupled bulk-surface problems on time-dependent domains. *Comput. Methods Appl. Mech. Engrg.*, 307:96–116, 2016.

[Leh15] C. Lehrenfeld. *On a Space-Time Extended Finite Element Method for the Solution of a Class of Two-Phase Mass Transport Problems*. PhD thesis, RWTH Aachen, February 2015.

[Leh16] C. Lehrenfeld. High order unfitted finite element methods on level set domains using isoparametric mappings. *Computer Methods in Applied Mechanics and Engineering*, 300:716 – 733, 2016.

[Len86] M. Lenoir. Optimal isoparametric finite elements and error estimates for domains involving curved boundaries. *SIAM J. Numer. Anal.*, 23(3):562–580, 1986.

[LR13] C. Lehrenfeld and A. Reusken. Analysis of a Nitsche XFEM-DG discretization for a class of two-phase mass transport problems. *SIAM J. Numer. Anal.*, 51:958–983, 2013.

[LR16] C. Lehrenfeld and A. Reusken. L^2-estimates for a high order unfitted finite element method for elliptic interface problems. *arXiv preprint arXiv:1604.04529*, 2016.

[LR17] C. Lehrenfeld and A. Reusken. Analysis of a high order unfitted finite element method for an elliptic interface problem. *IMA J. Numer. Anal.*, 00:1–37, 2017. first online.

[MGW09] U. M. Mayer, A. Gerstenberger, and W. A. Wall. Interface handling for three-dimensional higher-order XFEM-computations in fluid-structure interaction. *International Journal for Numerical Methods in Engineering*, 79(7):846–869, 2009.

[MLLR14] A. Massing, M. G. Larson, A. Logg, and M. E. Rognes. A stabilized Nitsche fictitious domain method for the Stokes problem. *J. Sci. Comput.*, 61(3):604–628, 2014.

[Nær14] T. A. Nærland. Geometry decomposition algorithms for the Nitsche method on unfitted geometries. Master's thesis, University of Oslo, 2014.

[Nit71] J. Nitsche. über ein Variationsprinzip zur Lösung von Dirichlet-Problemen bei Verwendung von Teilräumen, die keinen Randbedingungen unterworfen sind. *Abh. Math. Sem. Univ. Hamburg*, 36:9–15, 1971. Collection of articles dedicated to Lothar Collatz on his sixtieth birthday.

[RN09] A. Reusken and T. H. Nguyen. Nitsche's method for a transport problem in two-phase incompressible flows. *J. Fourier Anal. Appl.*, 15(5):663–683, 2009.

[RST08] H.-G. Roos, M. Stynes, and L. Tobiska. *Robust numerical methods for singularly perturbed differential equations*, volume 24 of *Springer Series in Computational Mathematics*. Springer-Verlag, Berlin, second edition, 2008. Convection-diffusion-reaction and flow problems.

[Sch97] J. Schöberl. NETGEN An advancing front 2D/3D-mesh generator based on abstract rules. *Computing and Visualization in Science*, 1(1):41–52, 1997.

[Sch10] F. Schieweck. *A*-stable discontinuous Galerkin-Petrov time discretization of higher order. *J. Numer. Math.*, 18(1):25–57, 2010.

[Sch14] J. Schöberl. C++11 implementation of finite elements in NGSolve. Technical report, ASC-2014-30, Institute for Analysis and Scientific Computing, September 2014.

[Sch17] B. Schott. *Stabilized Cut Finite Element Methods for Complex Interface Coupled Flow Problems*. Dissertation, Technische Universität München, München, 2017.

[Tho97] V. Thomée. *Galerkin finite element methods for parabolic problems*, volume 25 of *Springer Series in Computational Mathematics*. Springer-Verlag, Berlin, 1997.

[VR18] I. Voulis and A. Reusken. Discontinuous Galerkin Time Discretization Methods for Parabolic Problems with Constraints. *arXiv:1801.06361*, January 2018.

[WH03] T. Warburton and J. S. Hesthaven. On the constants in *hp*-finite element trace inverse inequalities. *Comput. Methods Appl. Mech. Engrg.*, 192(25):2765–2773, 2003.

[WYW06] Z. Wu, J. Yin, and C. Wang. *Elliptic & parabolic equations*. World Scientific Publishing Co. Pte. Ltd., Hackensack, NJ, 2006.

[Zah18] S. Zahedi. A space-time cut finite element method with quadrature in time. In *Geometrically Unfitted Finite Element Methods and Applications - Proceedings of the UCL Workshop 2016*, Lecture Notes in Computational Science and Engineering. Springer, 2018.